processes

Review

The Review of the Application of the Heat Pipe on Enhancing Performance of the Air-Conditioning System in Buildings

Tianhao Yuan [1], Zeyu Liu [1], Linlin Zhang [1,*], Suiju Dong [2] and Jilong Zhang [3]

[1] School of Environmental and Municipal Engineering, North China University of Water Resources and Electric Power, Zhengzhou 450046, China; y.tianhao@163.com (T.Y.); liuzeyuthr@163.com (Z.L.)
[2] Zhengzhou Heating Qiyuan Technology Co., Ltd., Zhengzhou 450062, China; zzrlsj@163.com
[3] Henan Provincial Academy of Building Research, Zhengzhou 450063, China; jkyzjl@126.com
* Correspondence: zhangll226@163.com

Abstract: An air-conditioning system (ACS), which consumes large amounts of high-grade energy, is essential for maintaining the indoor thermal environment of modern buildings. However, an ACS consumes almost half of the total energy of the building. Therefore, it is necessary to reduce the energy consumption of the ACS to promote energy conservation and emission reduction in the building sector. In fact, there is an abundance of waste heat and low-grade energies with the potential to be utilized in ACS in nature, but many of them are not utilized efficiently or cannot be utilized at all due to the low efficiency of thermal energy conversion. Known as a passive thermal transfer device, the application of a heat pipe (HP) in the ACS has shown explosive growth in recent years. HPs have been demonstrated to be an effective method for reducing building cooling and heating demands and energy consumption in ACS with experimental and simulation methods. This paper summarizes the different HP types applied in the ACS and provides brief insight into the performance enhancement of the ACS integrated with HP. Four types of HPs, namely tubular HP (THP), loop HP (LHP), pulsating HP (PHP) and flat HP (FHP), are presented. Their working principles and scope of applications are reviewed. Then, HPs used in natural cooling system, split air conditioner (SAC), centralized ACS (CACS) and cooling terminal devices are comprehensively reviewed. Finally, the heat transfer characteristics and energy savings of the above systems are critically analyzed. The results show that the performance of the HP is greatly affected by its own structure, working fluid and external environmental conditions. The energy saving of ACS coupled with HP is 3–40.9%. The payback period of this system ranges from 1.9–10 years. It demonstrates that the HP plays a significant role in reducing ACS energy consumption and improving indoor thermal comfort.

Keywords: heat pipe; air-conditioning system; dehumidification; heat recovery; cooling radiator

Citation: Yuan, T.; Liu, Z.; Zhang, L.; Dong, S.; Zhang, J. The Review of the Application of the Heat Pipe on Enhancing Performance of the Air-Conditioning System in Buildings. *Processes* **2023**, *11*, 3081. https://doi.org/10.3390/pr11113081

Academic Editor: Hussein A. Mohammed

Received: 11 September 2023
Revised: 10 October 2023
Accepted: 23 October 2023
Published: 26 October 2023

1. Introduction

Modern buildings provide comfortable, clean and safe shelters for human beings to live and work in at the cost of energy consumption. Building energy consumption, which will further increase with improved indoor thermal comfort levels, accounts for nearly 30% of total social energy consumption in China and more than 40% in Europe and OECD countries [1–3]. Such huge energy consumption caused by buildings makes carbon emissions the primary cause of global warming, climate change and air pollution [4]. Thus, improving the energy efficiency of the building energy consumption system has become the focus of global attention. As the key building energy consumption system, heating, ventilation and air-conditioning (HVAC) systems, sometimes called air-conditioning systems (ACS), are responsible for 40–60% of the total building energy consumption [5,6]. How to reduce this part of energy consumption has become a key issue in promoting energy conservation and emission reduction in the building sector.

ACS is usually classified into two categories, i.e., split air conditioner (SAC) and centralized ACS (CACS) [7]. The SAC, or so-called split ACS [8], plays a major role in air-conditioning requirements of domestic and small office buildings in summer [9]. However, the performance of the SAC drops significantly under the operation condition of high outdoor ambient temperature, and the indoor air quality cannot be guaranteed [10]. Moreover, the condensate water from the SAC is usually discharged on the spot, although the daily production of the condensate water reaches 52.99 kg during the main air-conditioning season for an SAC, resulting in the waste of the cold energy stored in the condensate water [11]. For the CACS, it is commonly serviced for large-scale public buildings [12]. The indoor air quality of the CACS is improved significantly as fresh air is induced into the room, compared with the SAC. However, processes of reheating in the air handling unit (AHU) and the indoor air exhaust bring corresponding additional energy consumption and energy waste for the CACS, such as the air–air system [13,14]. In fact, there is an abundance of waste heat and low-grade energies with the potential to be utilized in ACS in nature. Numerous researchers have optimized the performance of the ACS in terms of the selection of natural cold sources, the application of heat recovery systems and the utilization of high efficiency terminals.

1.1. Application of Natural Cold Sources

Natural cold source cooling technologies, such as direct ground-coupled cooling [5,15], natural ventilation [16,17] and novel radiative sky cooling [18,19], can cut down the running time of electric-driven chillers, thereby achieving the goal of reducing energy consumption of the ACS. Yuan et al. [5] performed thermodynamic and economic analysis for a ground-source heat pump system coupled with borehole free cooling. The results showed that free cooling with borehole water matched the indoor air parameter with the design indoor conditions and also improved the average annual cooling efficiency of the ground source heat pump system to 16.22. The average annual energy consumption and operation costs could be decreased to 55.9% and 56.0%, respectively. Gratia et al. [20] chose a narrow plan building suited for natural ventilation to study the use of night ventilation to cool office buildings in the moderate climate of Belgium. They found that single-sided ventilation was as efficient as cross night ventilation, which reduced the cooling load by approximately 40%. As a natural cooling technology, nocturnal sky cooling follows the principle of objects on the Earth's surface at night giving off heat to the colder sky and becoming colder [21,22]. Cooling air or water produced by nocturnal sky radiators can be used to counteract the building heat gain and maintain building thermal comfort in summer. Aili et al. [18] developed a kW-scale, 24-h continuously operational radiative sky cooling system and experimentally investigated the corresponding heat rejection performance at different flow rates. The results showed that after a 14-h nighttime operation, the storage tank temperature decreased from initial 27 to final 7 °C, with the temperature reduction of 20 °C. This demonstrated that the radiative sky cooling radiator had a cooling capacity of $120 \pm 10\ \mathrm{W/m^2}$ during the nighttime in a typical summer month in Phoenix. Previous studies have confirmed that natural cooling sources can reduce energy consumption in conventional refrigeration systems. However, natural cold sources still need to be transported to the indoor terminals by fans or water pumps corresponding with the energy consumption.

1.2. Application of Dehumidification Heat Recovery Systems

A dew-point air supply system has the advantages of a simple air handling process and energy saving. However, the humidity regulation of the room is poor, as the air stream leaving the cooling coil (CC) is usually too high in relative humidity and too low in temperature, easily causing uncomfortable feelings of the people living in it [23]. Moreover, the risk of illness will increase if people stay in a room with high relative humidity for a long time [24]. In order to create a better, simple air supply control condition and a thermal comfort environment, the cold supply air is always reheated before entering the room. However, this process will consume additional energy.

To maintain indoor air quality at a high level, the ACS always possesses ventilation functions. However, if the outdoor air is taken into the room and indoor air is exhausted to the outside directly, it will increase the demands of the cooling and heating loads for buildings, resulting in the increase in the energy consumption of the ACS. In addition, there is a large amount of low-grade energy in the air exhausted from indoor spaces. This part of energy has great potential to reduce the energy consumption of ACS through heat recovery devices. To reduce the energy consumption of ACS, energy recovery facilities, such as rotary wheel and fixed plate HE, are commonly used in the heat recovery system [25].

1.3. Application of the High Efficiency Terminals

As terminals in the ACS transfer heat to the indoor space and affect the indoor comfort and energy efficiency of the ACS directly, high-efficiency terminals are necessary for the ACS. The conventional terminal, such as the fan coil, has a fast heat exchange performance. However, it cannot avoid mechanical energy consumption. Therefore, more and more scholars are aiming at the research of space radiant heating and cooling terminals, which can improve the performance of the ACS without lowering the desired level of comfort conditions of buildings [26–28]. However, the thermal response speed of radiant terminals is relatively slow due to the high thermal inertia and low heat transfer coefficient compared to that of a convective terminal [29].

As a result of the above problems, most of the waste heat and natural low-grade energies are not utilized efficiently or cannot be utilized at all. Therefore, more and more researchers are focusing on the advantages of a heat pipe (HP) for waste heat recovery and natural low-grade energy applications. The HP, which usually consists of the evaporator, adiabatic and condenser sections, is a passive thermal transfer device based on the internal gas–liquid phase change principle without consuming external mechanical power [30]. The heat transfer coefficient of the HP is hundreds of times that of the copper pipe and the thermal response is very fast [31]. This means that a large quantity of heat can be transported through a small cross-sectional area over a considerable distance. The working principle of an HP is that when the evaporator section is heated, the liquid working medium inside absorbs the heat and evaporates. Then, the vapor travels along the HP to the condenser section and condenses back into liquid, accompanied by the latent heat release. Finally, the working fluid returns to the evaporator section by gravity or capillary force. With the continuous evaporation and condensation processes of the working medium in the HP, heat is continuously transferred from the evaporator to the condenser section. There are four types of HPs commonly used in HVAC systems, such as tubular HP (THP) [32], loop HP (LHP) [33], pulsating HP (PHP) [31] and flat HP (FHP) [34].

In past years, HPs with different forms have been widely applied in engineering applications, such as heat recovery systems [35–38], electronics cooling equipment [39–41], solar water heater systems [42–45], photovoltaic cooling systems [46–48], thermoelectric cooling [49–51], data center cooling systems [52–54] and ACSs [55–57]. The ACS integrated with HP mainly concerns the hot spots of the natural cooling system and performance improvements with respect to the natural cooling system, SAC, CACS and cooling terminal devices.

The goal of this work is to summarize the different HP types applied in the ACS and provide a brief insight into the performance enhancement of the ACS integrated with HP. The rest of this paper is organized as follows: Section 2 presents the conventional HP applied in the ACS. Section 3 provides an overview of the application of the HP applied in the ACS. Finally, the conclusions are provided in Section 4.

2. HP Type Applied in the ACS

2.1. THP

Two types of THPs are usually used to improve the performance of ACS. One is the traditional HP containing a wick structure, named wicked HP, as shown in Figure 1a. The driving power of this HP is the capillary force generated by the wick. The other is gravity (gravity-assisted) HP (GHP) [32], or so-called wickless HP and two-phase closed thermosyphon (TPCT) [58], as shown in Figure 1b. This type of HP has a smooth inner wall and is driven by gravity force [59]. It should be noted that the installation position of the evaporator section of the GHP is lower than that of the condenser section.

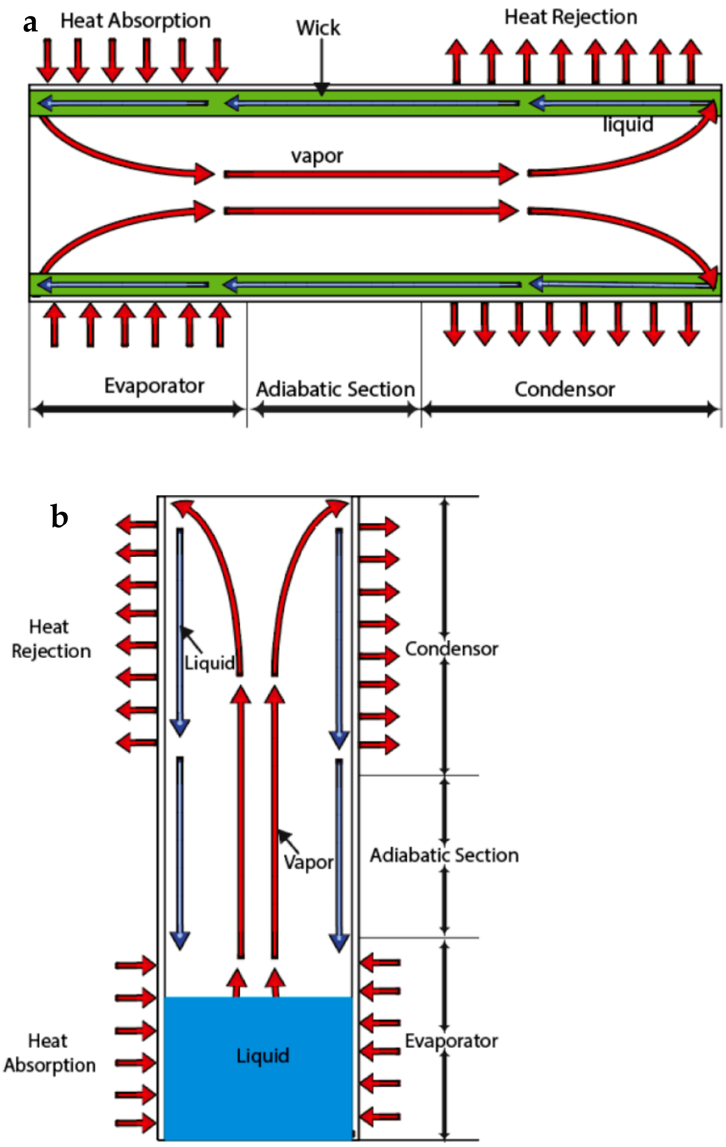

Figure 1. The structure and the heat transfer principle of the cylindrical HP ((**a**) Wicked HP and (**b**) Wickless HP) [60].

2.2. LHP

LHP [33], or so-called separate HP (SHP) [61], and two-phase thermosyphon loop HP (TPTLHP) [62] is a high-performance passive two-phase heat-transfer device, of which the evaporator and condenser sections are connected by the riser (or the vapor line) and downcomer (or the liquid line) end-to-end to form a loop. As shown in Figure 2, there are two types of LHP. One of the LHP has a compensation chamber in the evaporator section (shown in Figure 2a). However, the other type has no compensation chamber (shown in Figure 2b). The working fluid in the LHP is driven by capillary, gravity or join force coming from the capillary and gravity [33,63,64]. The LHP performs better in long-distance heat transfer, design and manufacturing flexibility compared with the traditional THP [64].

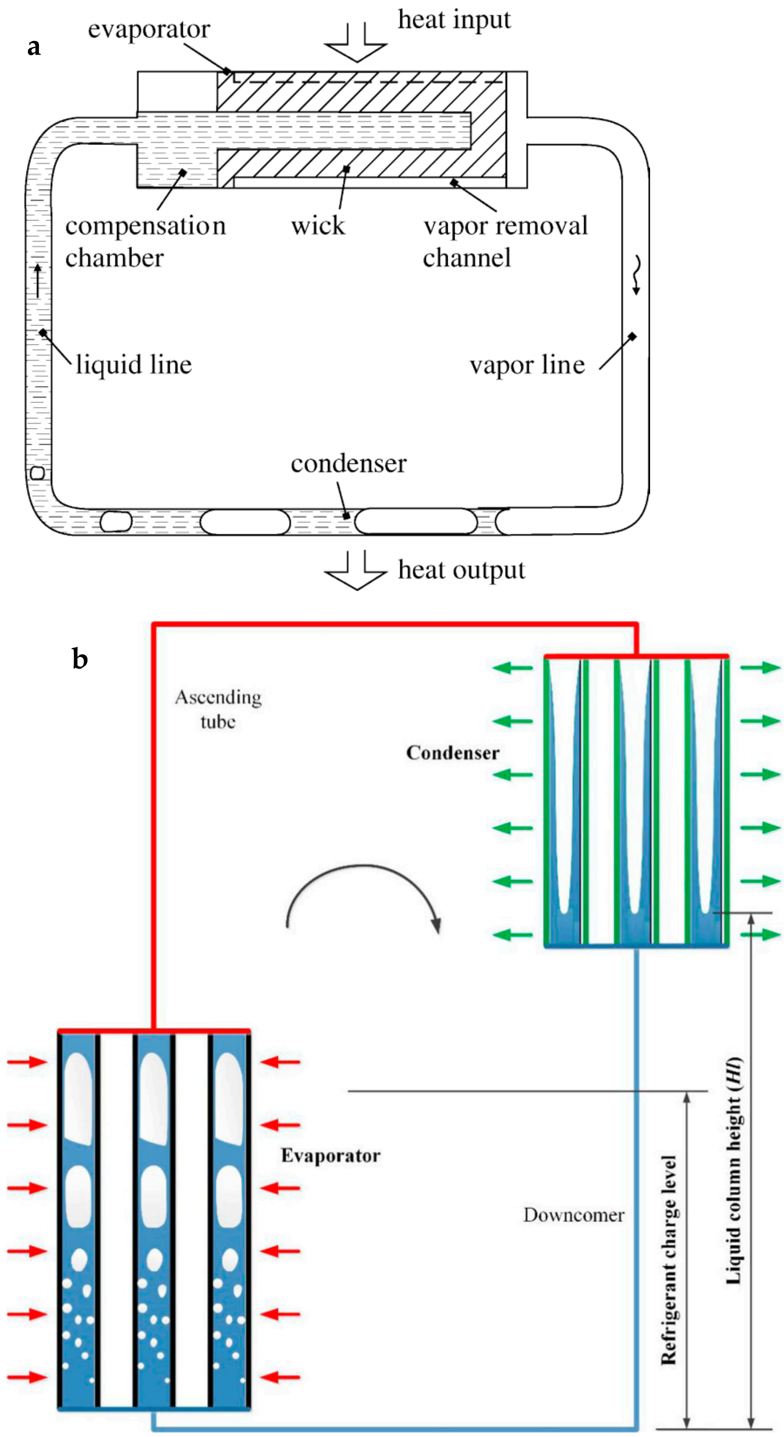

Figure 2. The structure diagram of the LHP ((**a**) LHP with the compensation chamber [33] and (**b**) LHP without the compensation chamber [61]).

2.3. PHP

PHP, or so-called oscillating HP (OHP), invented by Akachi [65] in the 1990s, is made by bending a long capillary tube without the wicking structure into multiple turns. As shown in Figure 3, when PHP is running, the working fluid in the capillary tube has two flow states. One of the flow states is random oscillation (shown in Figure 3a). This will affect the heat transfer of the PHP, especially when the oscillation pause occurs [66]. Thus, some scholars have improved the heat transfer by installing the check valve in the PHP to control the liquid slug flow in one direction, as shown in Figure 3b.

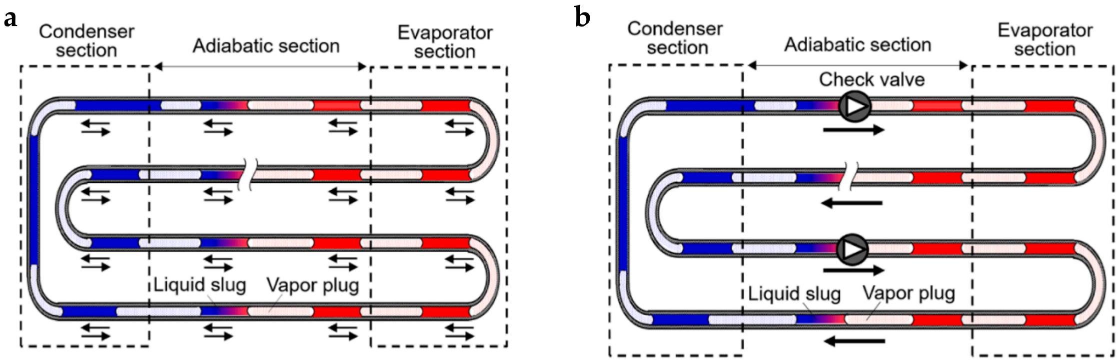

Figure 3. The structure and the heat transfer principle of the PHP ((**a**) PHP without the check valve and (**b**) PHP with the check valve) [67].

2.4. FHP

Flat micro-HP (FMHP) array is a relatively new HP technology relying on gravity and capillary force to drive the circulating flow of the working fluid, which was invented by Zhao et al. [34] in recent years. Sometimes, it is abbreviated as the FHP [68]. As shown in Figure 4, an FMHP array is made of several micro-HPs [45]. Multiple parallel micro HPs solve the problem of low heat transfer capacity caused by micro scale in traditional HPs. Moreover, there are many small ribs (or micro-grooves) in the micro channel to enhance the heat transfer performance of the FHP.

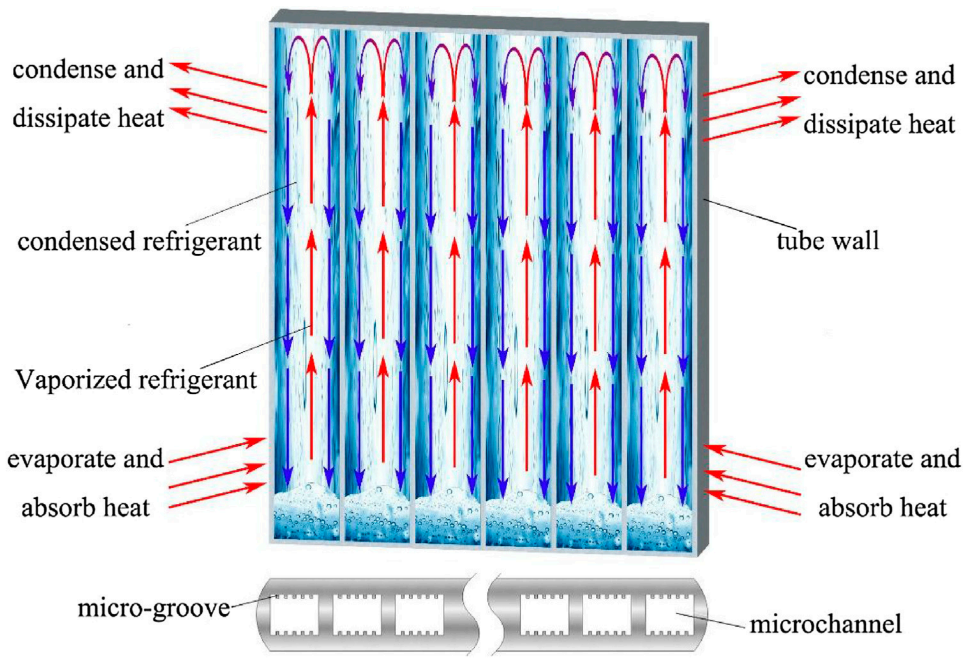

Figure 4. The structure and heat transfer principle of the FHP [45].

The classification of the four types of HPs mentioned above is mainly based on their structures and the driving modes of the working fluid. Each HP has advantages and disadvantages. THP has the advantages of compact structure and low cost, but its efficiency is greatly affected by the installation angle, which limits its application in practical engineering. The structure of the LHP is relatively flexible, and the LHP solves the problem of the short heat transfer distance of the conventional THP. However, the working fluid in the LHP is subjected to multiple forces, and the heat transfer mechanism is relatively complex, resulting in challenges for designers. PHP has the advantage of transmitting both latent and sensible heat simultaneously. It is less affected by gravity force and has a flexible heating mode. However, PHP has the problem of oscillation stagnation, which will seriously affect its heat transfer performance. FHP has the advantage of a flat surface and easy adhesion to the surface of cooled objects. Its heat transfer is relatively large compared with that of conventional THP. However, the disadvantage of the FHP is the same as that of the GHP. Moreover, FHP is more difficult to manufacture.

3. Overview and Discussion of the Application of HP Applied in the ACS

3.1. Natural Cooling System Integrated with HP

Saw et al. [69] proposed an active cool roof system integrated with the PHP for buildings in tropical areas. The evaporator section of the PHP was located below the metal roof to remove the heat flux on the metal roof, while the condenser section was located at the top of the metal roof to release heat to the external cooling water loop. The experimental results showed that the PHP cool roof system could effectively decrease the attic temperature with a reduction of nearly 12.9% compared with the bare metal roof. However, this proposed system relied on external circulating water to discharge the heat from the condenser section of the PHP. In fact, there are many low-grade energy sources in nature, such as night air energy and sky radiation energy, that can be used for cooling or auxiliary cooling. The outdoor ambient temperature at night may be much lower than the indoor temperature in cold and hot summer and cold winter regions in summer. Li and Zhang [70] proposed a new passive cooling system integrated with a wall implanted with the HP (WIHP). The schematic and heat transfer process of the WIHP is shown in Figure 5. When the temperature of the outer surface of the external wall was lower than the temperature of the inner surface in summer, the working fluid in the evaporator section of the HP pasted on the inner surface of the wall absorbed heat and transferred it to the condenser section pasted on the outside of the wall. The above processes enabled the heat to rapidly dissipate from the indoor space to the outdoor ambient. The results showed that passive cooling technology improved the indoor thermal environment. WIHP had a faster thermal response time compared with a conventional wall. The heat transfer capacity of the WIHP was 50.7 kW/m^2 in summer, while the value was 1.1 kW/m^2 for the conventional wall under the same working conditions. The average temperature of the inner surface of the north WIHP was about 2 °C lower than that of the conventional wall.

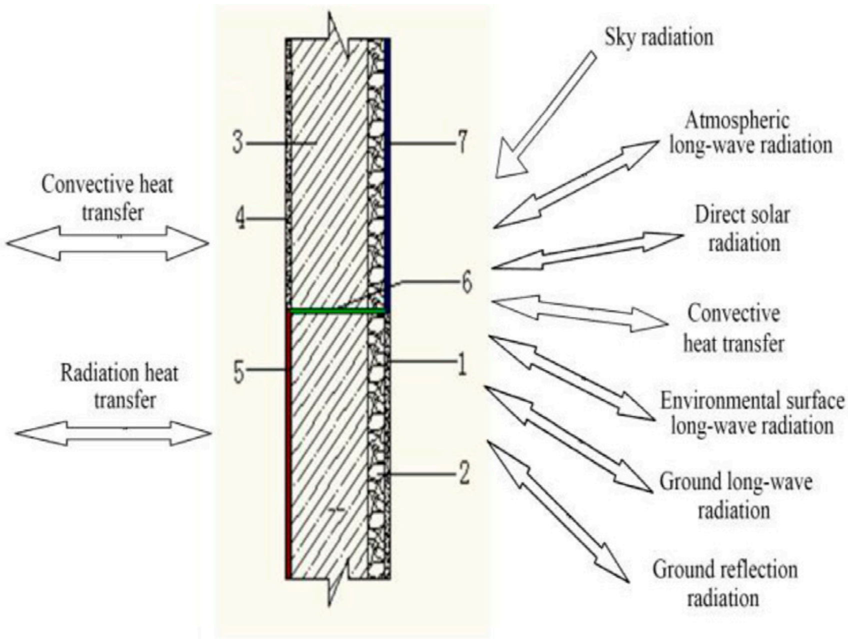

Figure 5. Schematic and heat transfer process of WIHP [70]: (1) Cement mortar of the exterior surface, (2) Insulation board, (3) Wall, (4) Cement mortar of the inner surface, (5) Evaporator section of the HP, (6) Adiabatic section of the HP, (7) Condenser section of the HP.

Turnpenny et al. [71] proposed a cooling system that had latent heat storage equipment coupled with the HP implanted in the phase change material (PCM) to reduce energy consumption of the ACS in buildings, as shown in Figure 6. The proposed system was hung below the ceiling. The working process of the proposed system was that, when shutters were opened during the nighttime, cool outside air was drawn over the condenser section of the HP through the fan, and then heat from the PCM was extracted to the outside. After this heat-changing process, cold energy was stored in the PCM. In contrast, freezing PCM was used to absorb the indoor heat gain through the HP during the daytime. By using testing and theoretical modeling research methods, they found that the heat transfer rate of the proposed PCM unit was about 40 W during the melt period.

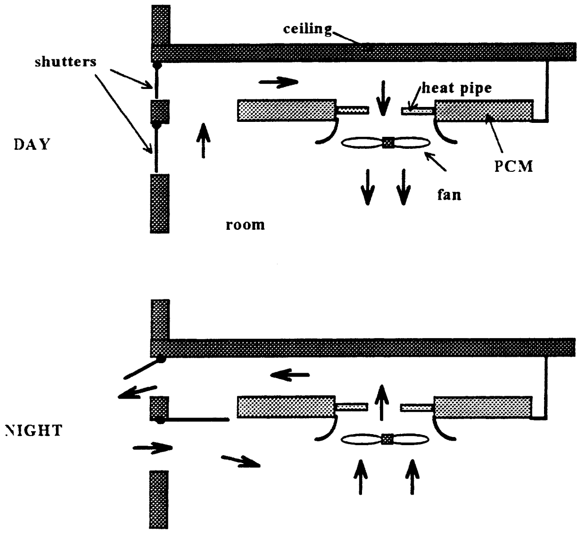

Figure 6. Schematic and working process of the proposed system [71].

Singh et al. [72] utilized unidirectional heat transfer characteristics of the GHP to capture the cold energy from the ambient and store it in the water storage tank for the datacenter energy conservation. As shown in Figure 7, the proposed cooling system consisted of the electric refrigeration subsystem, water cold energy storage subsystem inserted with the HP and heat exchange subsystem. The HP module, made of stainless steel with aluminum fins and R134a as the working fluid, was inserted into the water tank to form the test rig. A thermal resistance-capacitance model and experimental test were used to investigate the performance of the proposed system. As a result, the proposed cooling system could handle 60% of the heat load for the datacenter every year. The payback period for the cooling system was about 3.5 years, which was an acceptable period.

Yan et al. [73] proposed a seasonal cold storage system based on SHP for sustainable building cooling. As shown in Figure 8, the proposed system was mainly comprised of the SHP, underground tank, terminal devices and water pump. All devices were connected through pipelines. The heat transfer process was that when the outdoor temperature was sufficiently low, the cold energy in the outdoor air was transferred through the SHP to the water in the underground tank until all water was frozen in winter. Then, the stored cold energy was released into the indoor space by terminal devices to maintain the thermal environment of the building in the cooling season. R22 was charged into the SHP with a filling ratio of 100% of the evaporator section. The results showed that the ice-stored tank could be fully charged with ice by the end of each March. The proposed system had an annual cooling storage capacity of approximately 31,500 kW and a cooling release capacity of approximately 28,350 kW, which could meet approximately 34% of the building's cooling needs. The payback period of the seasonal cold storage system was about 8–10 years.

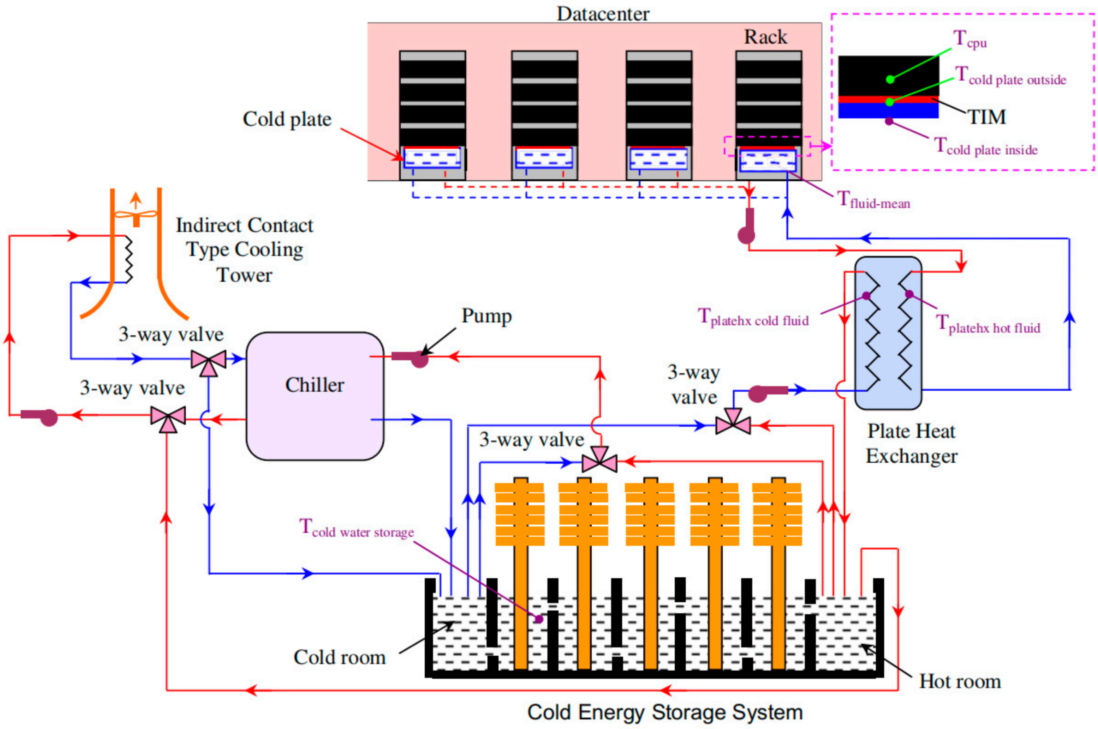

Figure 7. Datacenter cooling system with HP-based cold energy storage system [72].

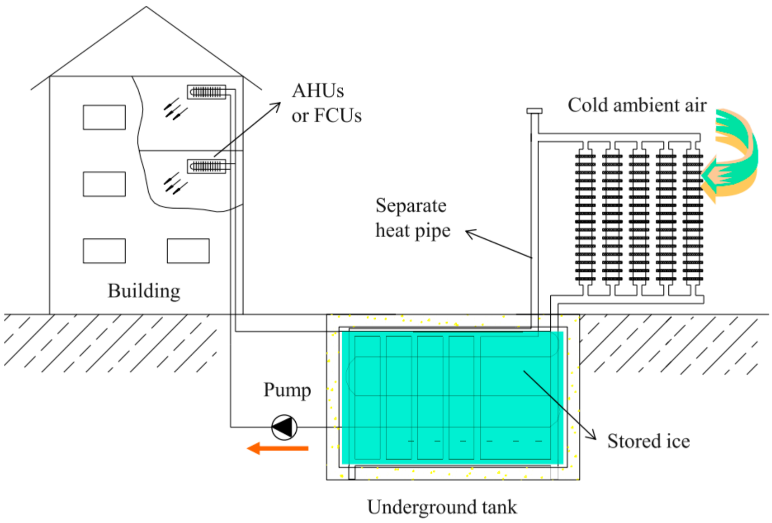

Figure 8. Schematic of a seasonal ice storage system integrated with SHP [73].

Chotivisarut et al. [74,75] proposed a new nocturnal sky cooling system with an HP sky radiator. As shown in Figure 9, the condenser sections of HPs were attached with an aluminum plate and acted as a thermal radiator, which was installed on a pitched roof. The evaporator sections were immersed in a water storage tank. The novel cooling system had no circulating power device between the sky radiator and the water storage tank. This would avoid heat gain of the stored water from the submersible pump. The operation process of the cooling system was that the HP sky radiator extracted heat from the water and transferred it to the ambient environment at night. The stored cold energy was released into the room by an indoor heat exchanger. The simulation and test results indicated that the proposed cooling system had great potential in reducing cooling load in the low temperature and humidity areas. These studies also demonstrated the feasibility of seasonal nocturnal cooling storage using a sky radiation radiator.

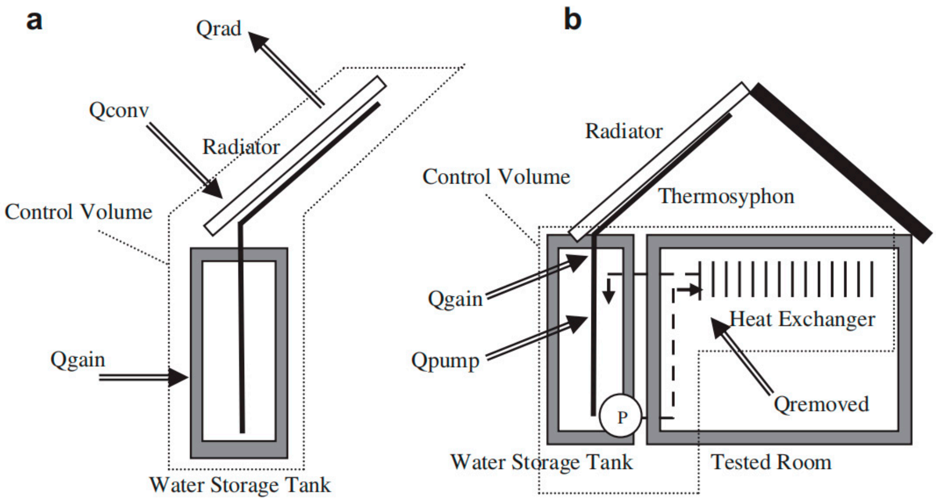

Figure 9. Schematic of the energy flows at the considered boundaries ((**a**) At the radiator and water storage tank and (**b**) At water storage tank and CC) [74].

He et al. [76], Yu et al. [77,78] and Shen et al. [79] improved the structure of the WIHP by combining with the PCM, micro-channel HP (MHP) and radiative cooling (RC) plate and developed a MHP-RC-PCM wall. As shown in Figure 10, the PCMs were packaged in an aluminum box arranged tightly against the inner surface of the south wall. The evaporator sections of the MHPs were dipped in the PCMs, while the condenser sections attached to the radiative plate were extended to the outside surface of the wall. During the daytime, the heat transferred from the outside to the inside of the wall can be stored in the PCMs. This would reduce and delay the rise in indoor temperature. In addition, the heat stored in the PCMs could be rapidly discharged into the outdoor environment via the walls and MHPs. Experimental and numerical methods were used to investigate the performance of the MHP-RC-PCM wall. They found that the inner surface temperature of the south MHP-RC-PCM wall had a minimum value compared with the other two control groups. Moreover, the average time lag of the MHP-RC-PCM was about 4.5 h, which was approximately 80 min longer than that of the traditional brick wall. The cooling loads of the south wall were decreased by over 40% under some conditions compared to the traditional brick wall. They also confirmed that low wind speeds favored lower cooling loads, while reducing the emissivity of the radiative plate exhibited the opposite trend.

Yan et al. [80–84] proposed a novel pipe encapsulated the PCM wall system for self-activated heat removal of the building in the summer season. Different from that proposed by He et al. [76], Yu et al. [77,78] and Shen et al. [79], they improved the combination of the wall, PCM, GHPs and nocturnal sky radiator with upward and downward pipes, as shown in Figure 11. The PCM was encapsulated between the inner pipe and the outer pipe. And the inner pipe was link to the GHP system. The pipes encapsulated in the PCM were embedded into the wall. The working fluid in the GHP system circulated between the wall embedded with HP and the sky radiator through the upward and downward pipes. The authors conducted a series of simulation and experimental studies on the characteristics of the pipe encapsulated PCM wall. The results showed that there was a great energy-saving potential of the proposed system used in buildings. The pipe encapsulated PCM wall system could improve the thermal insulation effect of the wall in the daytime and remove a lot of the indoor heat gain during the nighttime. The cooling loads of buildings with the proposed system in Hong Kong, Wuhan, Beijing, Harbin and Kunming could be reduced by 11.7, 16.1, 21.1, 28.6 and 44.2%, respectively, compared to that of the traditional wall.

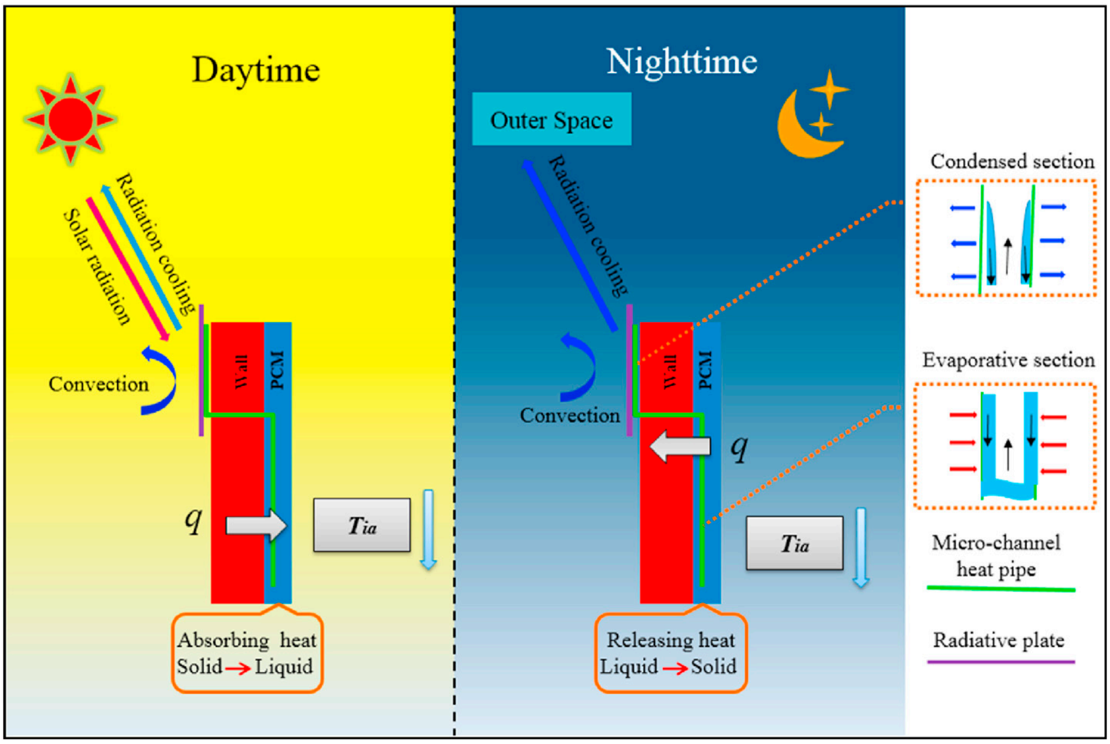

Figure 10. Schematic and working principles of the MHP-RC-PCM wall [76].

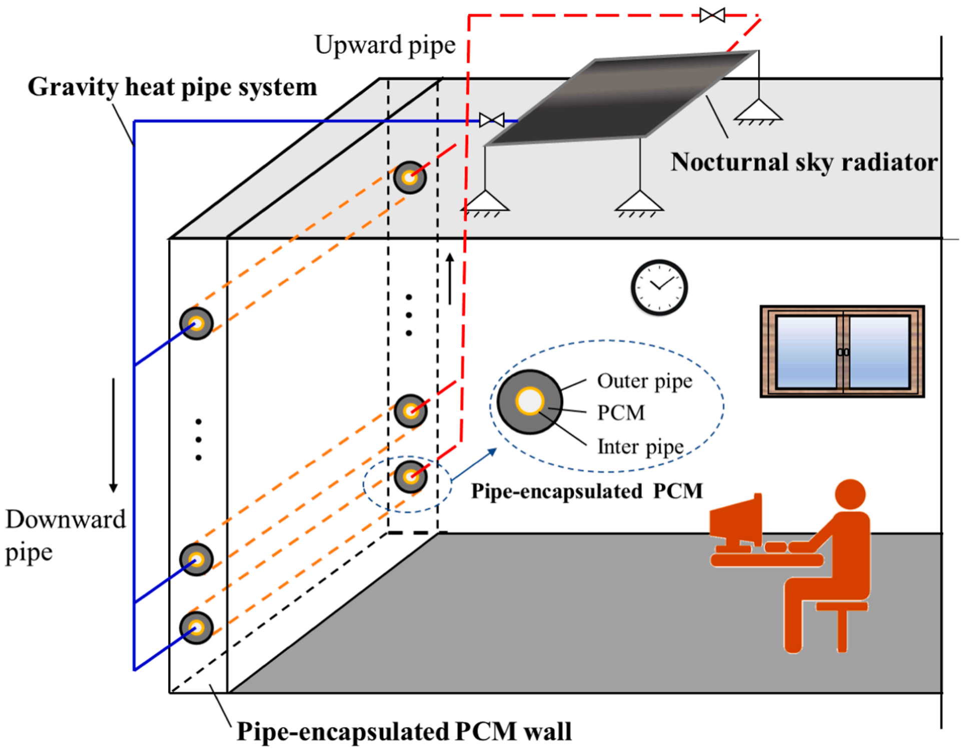

Figure 11. The coupled system of the pipe encapsulated PCM wall and nocturnal sky radiator [80].

3.2. Evaporative Cooling System Integrated with HP

As an environmentally friendly cooling technology, evaporative cooling technology including direct, indirect and combined direct/indirect cooling systems consumes less energy but can transfers the heat from air to water effectively and decreases the indoor temperature [85]. However, such cooling systems are limited by the surrounding ambient wet bulb temperature and perform well only in hot and dry climates, with cooling efficiencies typically below 80% [86]. To improve the behaviors of evaporative cooling systems, Fikri et al. [87] designed a direct-indirect evaporative cooler embedded with the HP. As shown in Figure 12, the HP heat exchanger (HPHE) was set before the direct evaporative cooler (DEC) as an indirect cooling device. The condenser section of the HP was submerged in additional sump, while the evaporator section was installed in the inlet duct. Water was charged into the HP with a filling ratio of 50%. The air handling process was that outdoor air temperature was first indirectly reduced by the HPHE. Then, it was further decreased through the DEC. The test results indicated that the saturation efficiency of the proposed direct-indirect evaporative cooler increased with an increase in the inlet temperature. However, it decreased with an increase in relative humidity and air velocity. The highest value of the saturation efficiency exceeded 1 and reached 1.03 when the DEC was integrated with HP. After that, Fikri et al. [88] proposed a three-stage combined evaporative cooler that consisted of three apparatuses. Two different HP modules (shown in Figure 13) were employed to enhance the performance of the arrangements. The first apparatus was a single DEC. The second apparatus (shown in Figure 14a) was a DEC integrated with the first HP module. The third apparatus (shown in Figure 14b) was a DEC with the second HP module. The results showed that the outlet air relative humidity of the first and second apparatuses was over 80%. However, the outlet relative humidity was reduced to 30.15–55.4% for the third apparatus. This value was suitable for the indoor thermal comfort requirement.

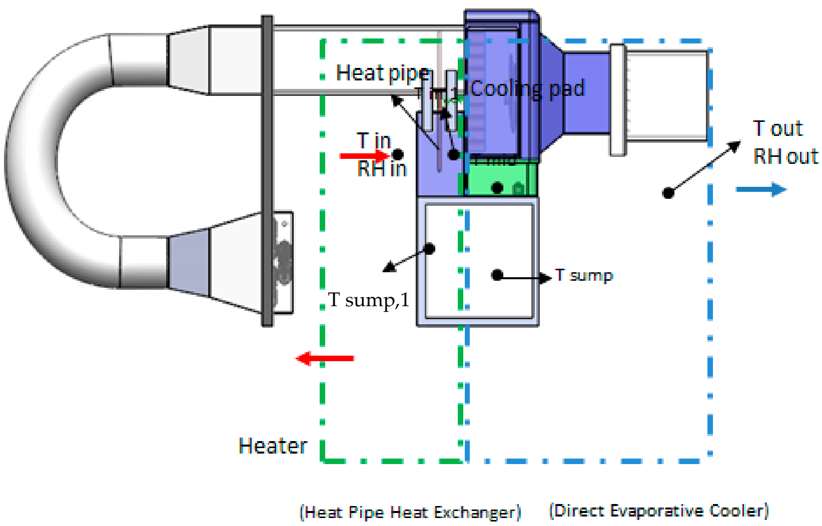

Figure 12. Schematic of the direct-indirect evaporative cooler integrated with HP [87].

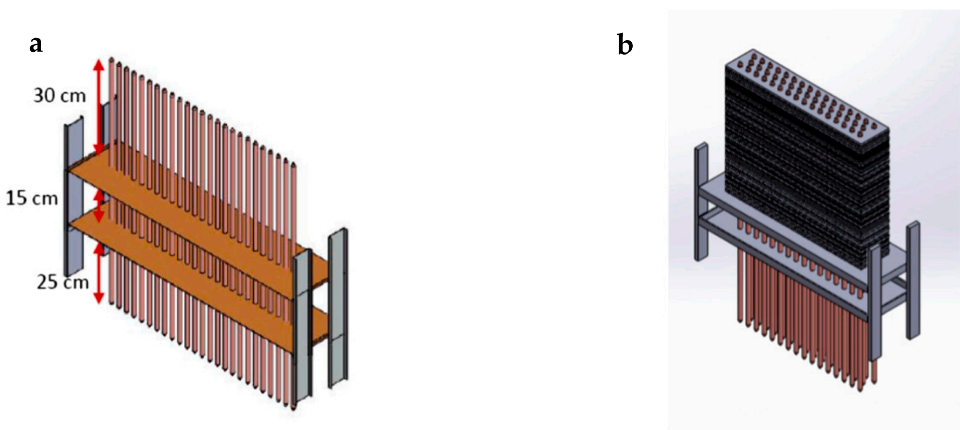

Figure 13. Schematic of the HP modules ((**a**) The first HP module and (**b**) The second HP module) [88].

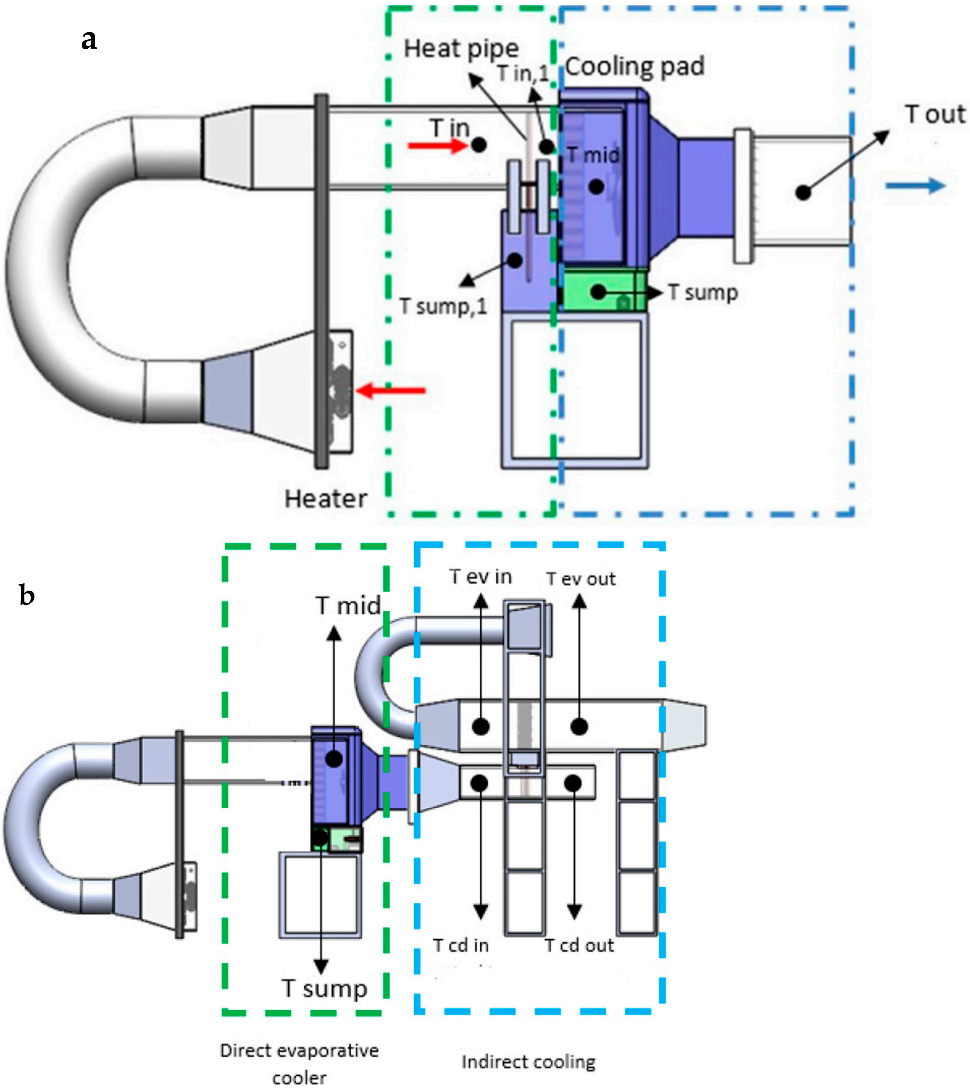

Figure 14. Schematic of the arrangements ((**a**) The second arrangement and (**b**) The third arrangement) [88].

Riffat and Zhu [89] proposed a novel indirect evaporative cooler (IEC) using porous ceramic and horizontal HP and developed a mathematical heat transfer model to investigate its performance. As shown in Figure 15, the HPHE was deployed to create two separate airflow channels, such as a dry air passage for the indoor air and a wet air passage for the outdoor air, through which wet and dry air exchanged sensible heat without mixing. An experimental investigation was employed to verify the simulation results. They found that the mathematical model was fitted to predict the performance of the IEC. The supply air temperature could be reduced by about 1–2.5 °C. The cooling capacity of the IEC ranged from 12.3 to 41.8 W/m^2. It increased as the outdoor air velocity increased, while it decreased as the outdoor air humidity increased. From the perspective of indoor working conditions, the cooling capacity increased with increasing indoor air velocity in a low speed range, but it remained nearly constant at a higher speed. In other research, they applied the new IEC into a chilled ceiling in an environmental chamber [90]. The indoor air temperature reduction was 3.8 °C per square meter of ceramic surface area for the room equipped with a chilled ceiling using the horizontal IEC.

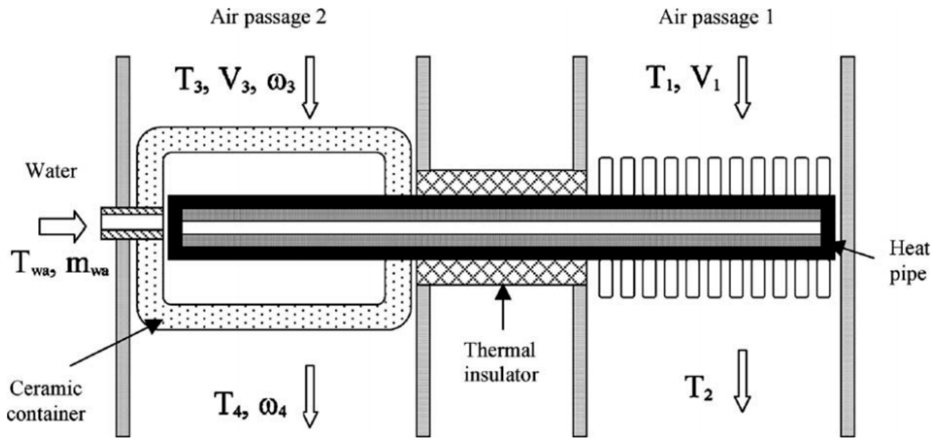

Figure 15. Schematic of the IEC [89].

Amer [91] and Boukhanouf et al. [92] improved the mechanical design of IEC-integrated porous ceramic and HP. Different from the previous literature, HPs were arranged vertically and the partition board between the dry and wet channels was provided with an air vent, through which partial dry and cold air was transported to the wet channel, as shown in Figure 16. Simulation and experimental testing methods were adopted to investigate the thermal performance of the proposed IEC. They found that the cooling capacity of the proposed IEC decreased with a decrease in the inlet air flowrate. In contrast, the wet bulb effectiveness and COP increased as the inlet air flow rate decreased. When the inlet air flowrate was 150 m^3/s, the wet bulb effectiveness of the proposed system increased from 0.7 to 0.84 with the inlet air temperature increasing from 30 to 40 °C. Meanwhile, the in- and out-let temperature difference of the supply air increased from about 7.5 to 10.7 °C, which implied that the cooling capacity increased as the inlet air temperature increased. In contrast, increasing the inlet air relative humidity led to an increase in the wet bulb effectiveness, while the temperature difference between the inlet and outlet of the supply air decreased, which represented that the cooling capacity would decrease as the inlet air humidity increased. In conclusion, an increase in wet bulb effectiveness may not necessarily contribute to an increase in cooling performance. When the ratio of the airflow entering the wet channel to the dry channel was 0.5, the wet bulb effectiveness and cooling capacity would have the optimum values. Under typical operating conditions of 35 °C ambient temperature and 35% relative humidity, the value of the wet bulb effectiveness, specific cooling capacity and COP was 0.8, 140 W/m^2 and 11.43, respectively. Similar results were obtained by Ref. [93].

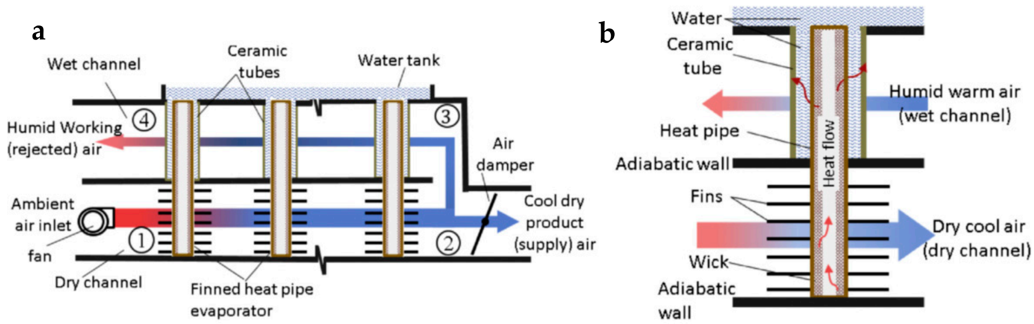

Figure 16. Schematic of the IEC-integrated porous ceramic and HP ((**a**) Schematic of the cooler configuration and (**b**) Structure of HP-ceramic) [92].

Alharbi et al. [94] built a numerical heat and mass transfer model for a hollow porous ceramic cuboid-finned HP evaporative cooling system. An experimental setup was also established and measured under the conditions of the inlet air temperature ranging from

30 to 40 °C with an increment of 5 °C and relative humidity ranging from 35 to 55% with an increment of 5%. The results showed that the cooling capacity of the proposed device increased with the increment in dry bulb temperature. However, it decreased with an increase in relative humidity. This is consistent with the conclusions of Refs. [91,92]. When the inlet air temperature was 35 °C and the relative humidity was 35%, a supply air dry bulb temperature of 22.3 °C was achieved. This value was lower than the air wet bulb temperature. The cooling capacity, wet bulb effectiveness and dew point effectiveness were 196 W/m^2, 1.05 and 0.73, respectively.

3.3. Split Air Conditioner Integrated with HP

Naphon [95] fixed a cooling device consisting of HPs and a water tank in front of the outdoor unit of the SAC to improve the performance of the SAC. The schematic of the SAC integrated with the HP is shown in Figure 17. The length and diameter of the HP were 600 and 10 mm, respectively. R134a was charged as the working fluid with a filling ratio of 50%. HPs with three rows were staggered as the heat exchanger, and the condenser parts were placed into the water tank. Compared with a conventional SAC, the proposed SAC coupling with the HP cooling device provided the highest COP and energy efficiency ratio (EER) with increases of 6.4 and 17.5%, respectively.

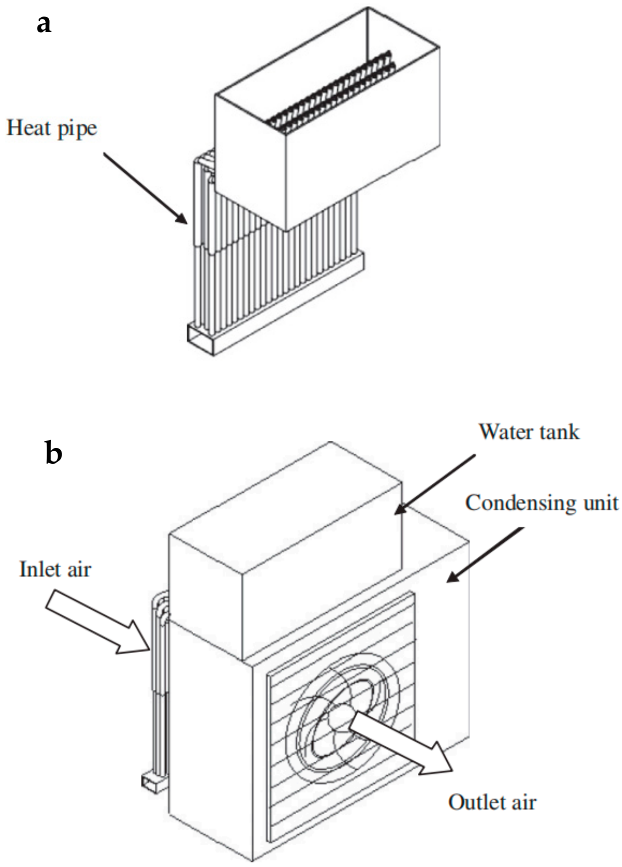

Figure 17. Schematic of the SAC integrated with the THP ((**a**) Condensing unit integrated with HP and (**b**) Installation diagram of the condensing unit) [95].

Alklaibi [96] theoretically evaluated two possible configurations for incorporating the LHP into the SAC to perform the reheat process. The schematic of the SAC coupled with the LHP is shown in Figure 18. For the one configuration, the evaporator section of the LHP was placed in front of the evaporator of the SAC, and the condenser section was placed after the evaporator of the SAC (shown in Figure 18a). This configuration could pre-cool the return air and reheat the supply air. For the other configuration, the LHP condenser was installed after the evaporator of the SAC and the LHP evaporator was installed in front of the condenser of the SAC (shown in Figure 18b). The second configuration could cool down the air entering the condenser of the SAC and reheat the supply air. The results showed that both configurations had the same COP, and the COP could be improved by reducing the compressor energy demand when LHP was used instead of the heating component under a low sensible heat coefficient working condition.

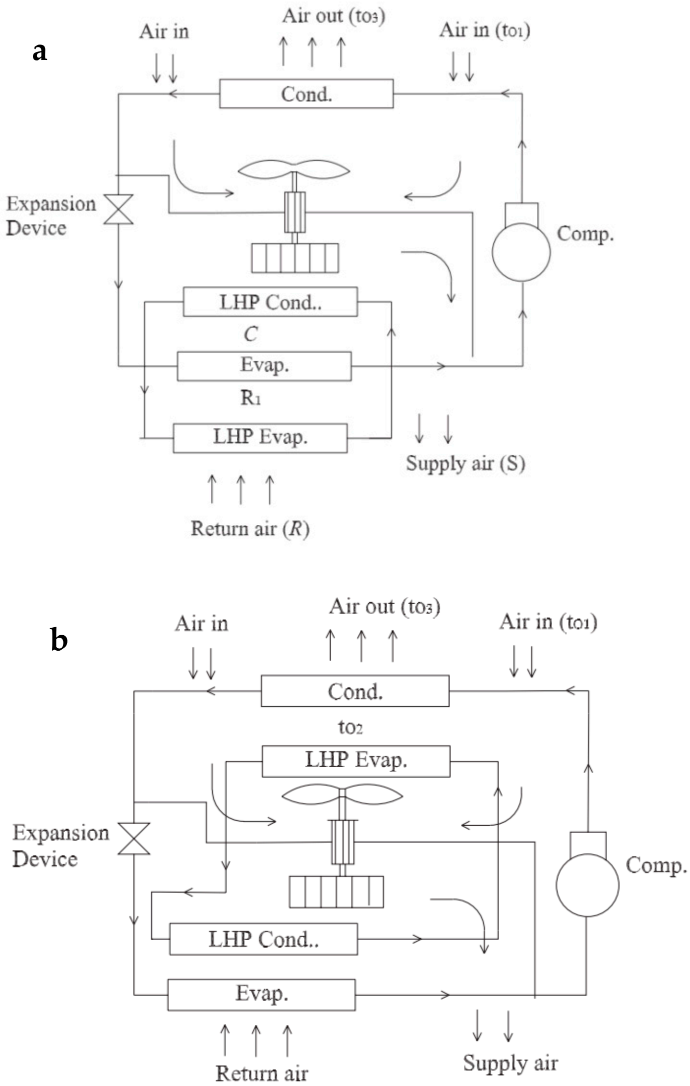

Figure 18. Schematic of the SAC integrated with the LHP ((**a**) LHP set around the evaporator of the SAC and (**b**) LHP set around the evaporator and condenser of the SAC) [96].

Nethaji and Tharves Mohideen [97] experimentally investigated the energy consumption and dehumidification of an SAC coupled with the LHP. Three LHP units made of copper were installed on the CC of the SAC. As shown in Figure 19, the LHP comprised of the compensation chamber, the evaporator and condenser sections, and the vapor and liquid tubes. Ethanol was selected as the working fluid, and the filling ratio was 51.3%. The length of the whole LPH was 2400 mm, of which the length of the evaporator section was 600 mm with a diameter of 12 mm. The length of the compensation chamber set in the evaporator section was 300 mm with a diameter of 24 mm. The length of the condenser section was 900 mm, with a diameter of 20 mm. Both the vapor and liquid tubes had a length of 300 mm with an outside diameter of 3 mm and an inside diameter of 1.5 mm. Under an indoor temperature of 22–26 °C and relative humidity of 50%, they found that the COP of the SAC improved by 18–20%. The dehumidification capability enhanced by 30%. The latent heat recovery was 482 W.

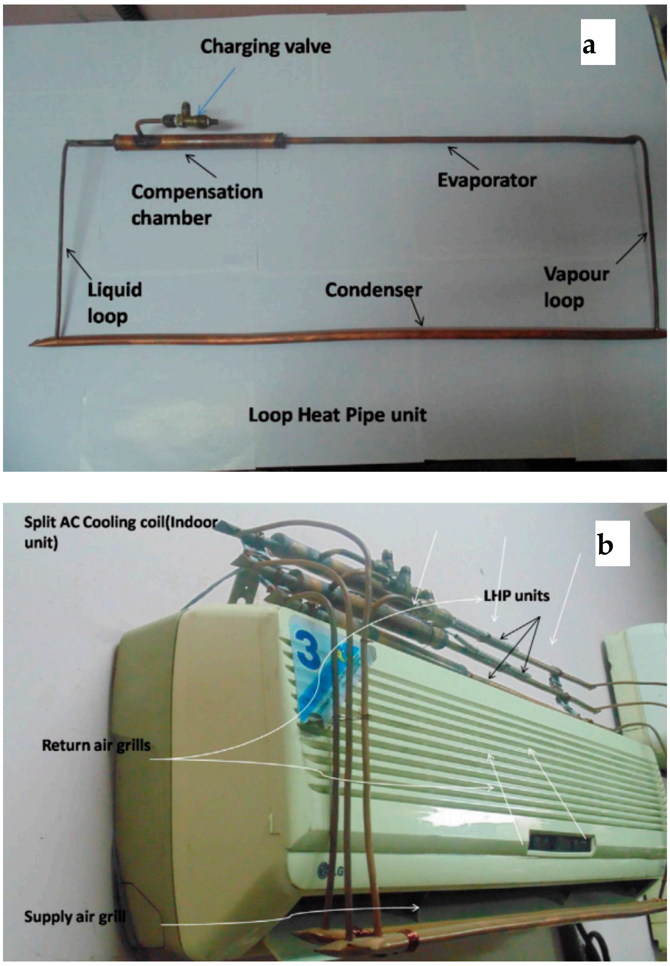

Figure 19. Photograph of the LHP and incorporation of LHP into the SAC ((**a**) Photograph of the LHP and (**b**) Photograph of the incorporation of LHP in the SAC) [97].

Eidan et al. [56] experimentally investigated the thermal characteristics of a window-type air conditioner integrated with a novel HPHE. As shown in Figure 20a, the new HPHE comprised of a vacuum-tight copper pipe, a wicked area and a working fluid. It was used to superheat the refrigerant entering the compressor and supercool the refrigerant from the condenser. Distilled water, acetone and R134a were selected as the working fluids. The filling ratios (volume ratio relative to evaporator) were 50 and 100%. The proposed device is shown in Figure 20b. Experimental tests were conducted at an ambient temperature from 30 to 55 °C. The results showed that the thermal effectiveness of the HPHE remarkably increased with increasing ambient temperature at a filling ratio of 100%. The best thermal effectiveness was achieved when the HPHE was charged with acetone fluid. The refrigeration effect was enhanced by 3.5, 6.03 and 3.97% for 100% filling ratio of R134a, acetone and water, compared to the window-type air conditioner without the HPHE. Meanwhile, the consumed power savings of the window-type air conditioner with the HPHE were 2.01, 2.195 and 1.33% for water, acetone and R134a, respectively.

Xia et al. [98] used an HP heat sink (HPHS) to manage the heat dissipation of the controller for the inverter SAC. The whole controller was encapsulated in a box, and the micro fan was added into the box, as shown in Figure 21. Two types of HPHS (including U-type and L-type) were installed on the chips of the controller, as shown in Figure 22. Water was charged into the HP. Through simulation and experimental data analysis, they found that L-type HPHS was more advantageous in terms of thermal management and had average temperature reductions of 10.0 and 5.9 °C for small power chips and large power chips, respectively.

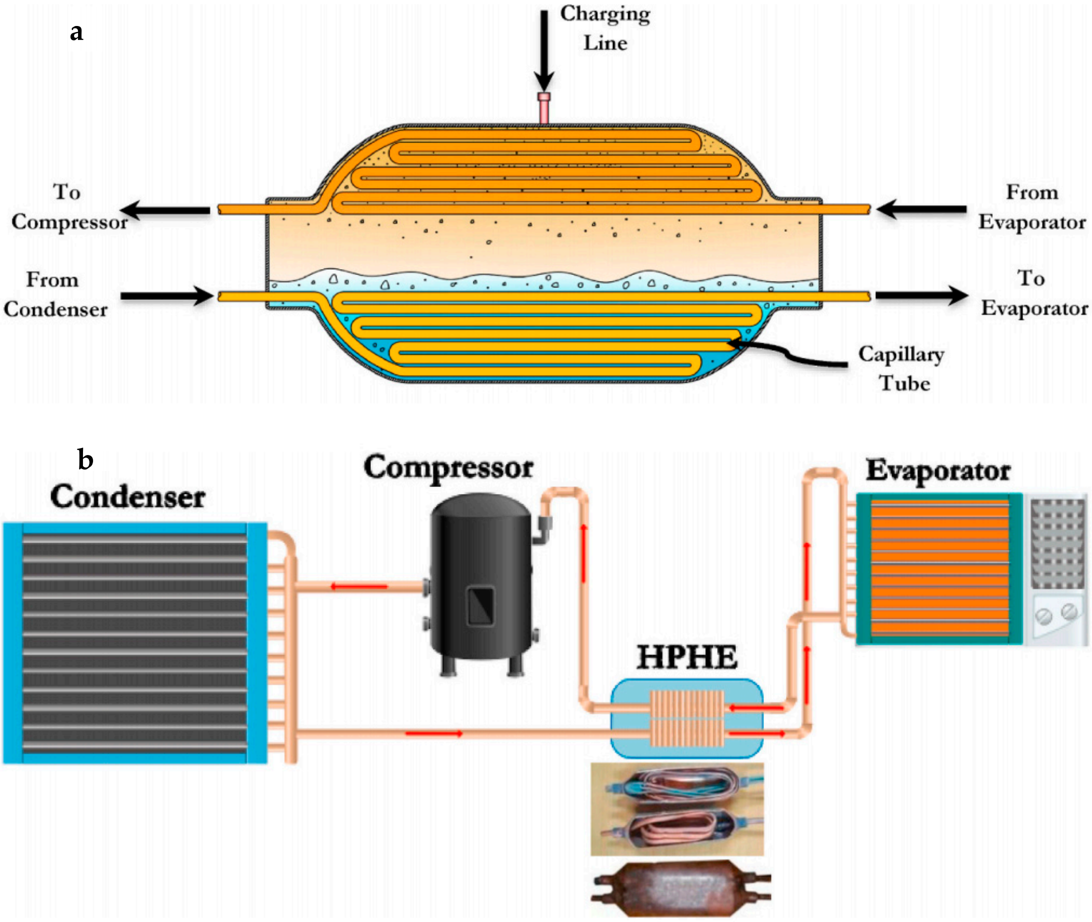

Figure 20. Schematic of the proposed HPHE and window-type air conditioner ((**a**) The novel HPHE and (**b**) Window-type air conditioner equipped with the HPHE) [56].

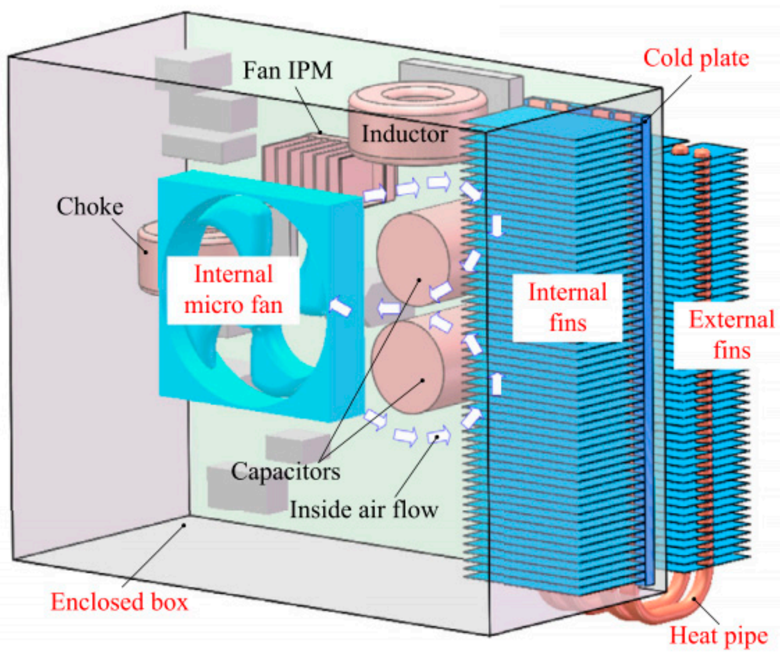

Figure 21. Schematic structure of the enclosed controller [98].

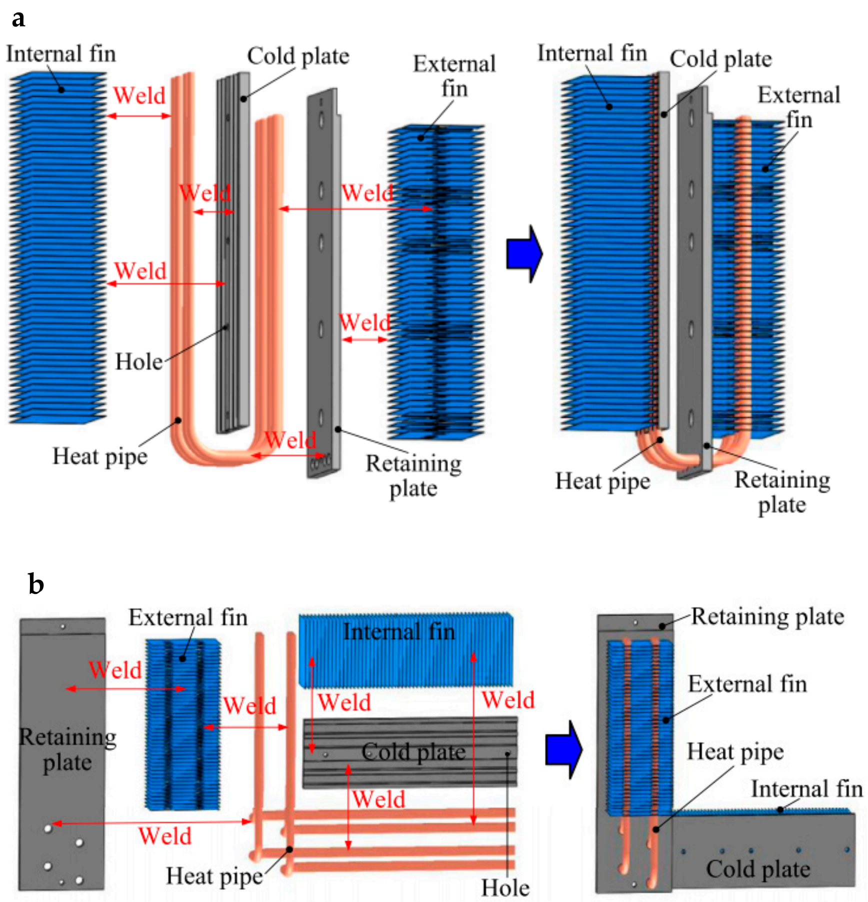

Figure 22. Structures of two types of HPHS ((**a**) U-type HPHS and (**b**) L-type HPHS) [98].

Nakkaew et al. [99] installed an HPHE at the outlet of the compressor to enhance the behavior of the SAC. A HPHE with a size of 300 mm × 108 mm (Length × Height, L × H) was installed in the SAC (shown in Figure 23). As shown in Figure 24, the HPHE was comprised of the HP, holder and plate fins. The HP was made of copper with an outside diameter of 8 mm. The length of the HP was 300 mm, of which the length of the evaporator section was 50 mm. The lengths of the condenser section and adiabatic section were 180 mm and 70 mm, respectively. Deionized water in an amount of 1.21–1.31 cc was used as the working fluid. The experimental results showed that the maximum heat transfer rate of the HPHE was about 240 W at the working conditions of an air velocity of 5 m/s and a heater surface temperature of 70 °C. The EER of the proposed SAC increased by about 3% and was fractionally higher than that of the traditional SAC.

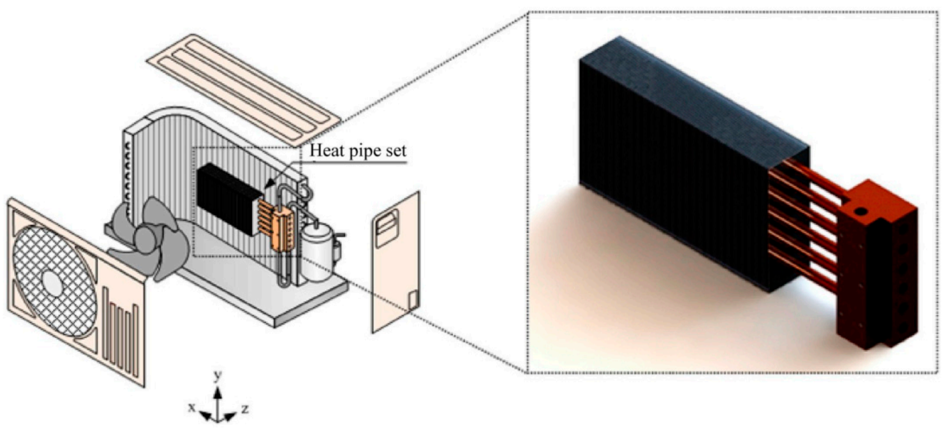

Figure 23. The position of the HPHE in the SAC [99].

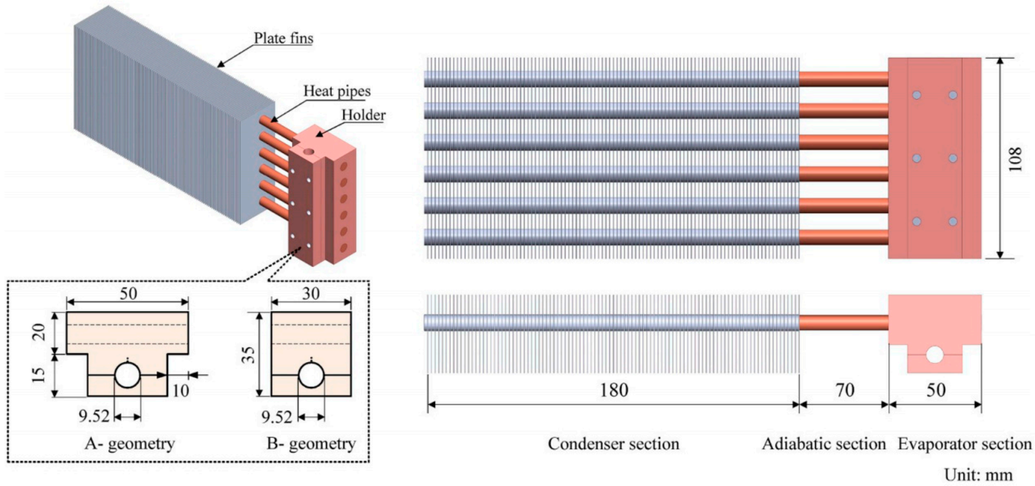

Figure 24. Schematic of the HPHE [99].

3.4. Centralized ACSs Integrated with HP

3.4.1. Dehumidification Based on the HPHE

In the past years, many researchers have attempted to dehumidify the supply air of the ACS through installing an HPHE around the CC. Wu et al. [100] used the vertical HPHE consisting of thermosiphon HPs into a traditional AHU to control the supply air relative humidity. The evaporator section of the HPHE was used as a pre-cooler to precool the inlet air, and the condenser section acted as a re-heater to reheat the cold air passing through the CC, as shown in Figure 25. Air handling processes of the AHU with and without HPHE in the psychrometric plot are shown in Figure 26. The sensible energy effectiveness for the HPHE (calculated by Formula (1) [101]) and for the CC (calculated by Formula (2) [102]) was usually used to evaluate the energy savings and the enhancement of dehumidification of the ACS integrated with HP. Different from the air handling processes of the conventional AHU, the AHU with HPHE had the process of precooling the hot inlet air. The schematic of the HPHE is shown in Figure 27. The HPHE consisted of 3 rows of 24 pure copper thermosyphon tubes with a diameter of 15.88 mm. Refrigerant 22 was charged into the HP with a filling rate of 60% of the evaporator section. The experimental test showed that HPHE could be an advantageous replacement for conventional reheat coils. The relative humidity of the air stream passing through the condenser of the HPHE could be reduced to 70–74% from 92–100%. A heat recovery of 1920–2504.5 kJ/h was obtained. In addition, the cooling capability improved by 20–32.7% was also discovered for the CC. Firouzfar et al. [103] experimentally investigated the effectiveness and the energy savings of the vertical HPHE with silver nanofluid. Methanol-silver nanofluid was filled into the HP with a filling rate of 50% of the evaporator section. The results indicated that when the nanofluid was used as the working fluid, the energy savings by the evaporator and the condenser of the HPHE for precooling and reheating were about 8.8–31.5% and 18–100%, respectively. These values, as well as the sensible energy effectiveness coefficient, were higher than that of the HPHE with pure methanol. This demonstrated that the HPHE using methanol-silver nanofluid had a better performance than that of using pure methanol.

$$\varepsilon_{\mathrm{HP}} = \frac{T_1 - T_2}{T_1 - T_3} \text{ or } \varepsilon_{\mathrm{HP}} = \frac{T_4 - T_3}{T_1 - T_3} \quad (1)$$

$$\varepsilon_{\mathrm{CC}} = \frac{C_{\mathrm{p23}}(T_2 - T_3)}{h_1 - h_3} \quad (2)$$

where $\varepsilon_{\mathrm{HP}}$ represents the sensible energy effectiveness of the HPHE; $\varepsilon_{\mathrm{CC}}$ is the sensible energy effectiveness of the CC; T_1 is the inlet air temperature, °C; T_2 is the air temperature after passing through the evaporator section of the HPGE, °C; T_3 is the air temperature after passing through the CC, °C; T_4 is the air temperature after passing through the condenser section of the HPHE, °C. C_{p23} is the specific heat of the dry air component in the process of 2–3. h_1 is the enthalpy value of air state point 1, kJ/kg; h_3 is the enthalpy value of air state point 3, kJ/kg.

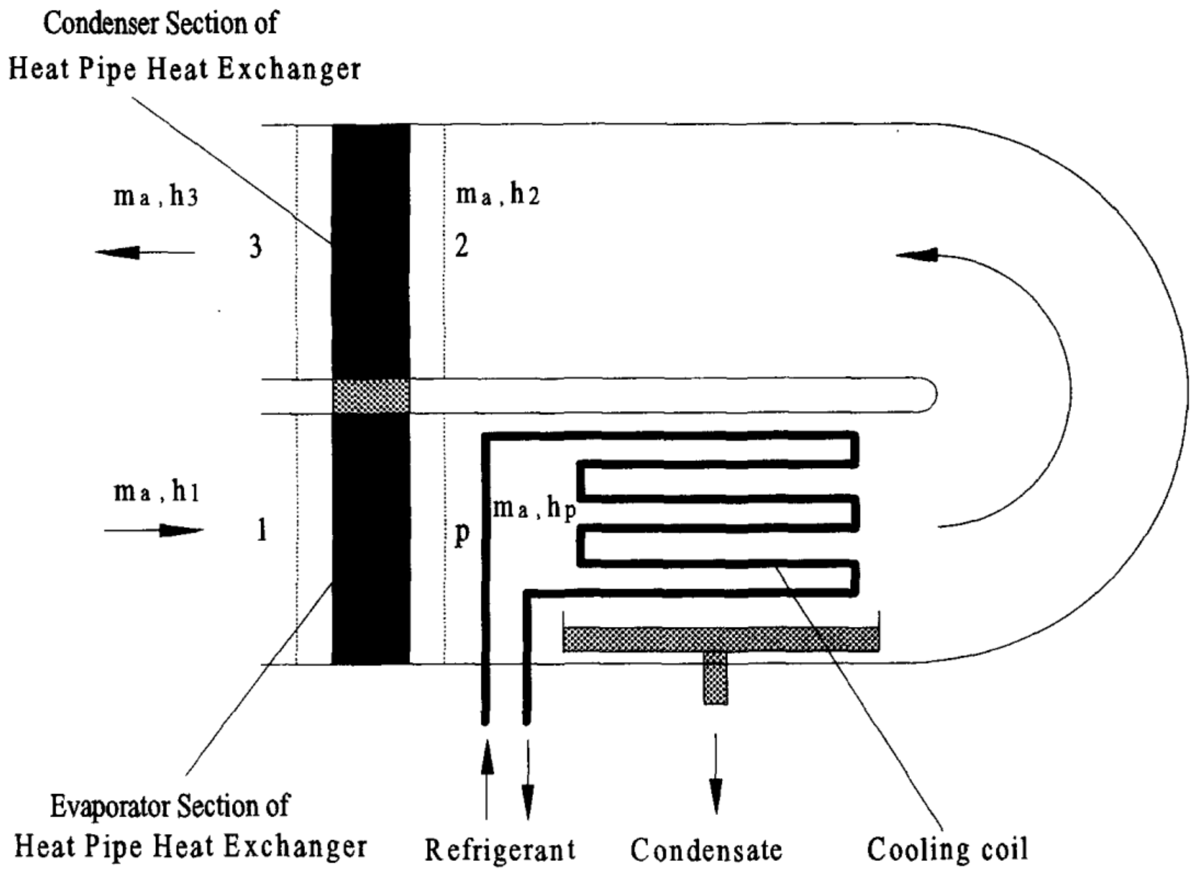

Figure 25. Schematic diagram of an AHU integrated with the HPHE [100].

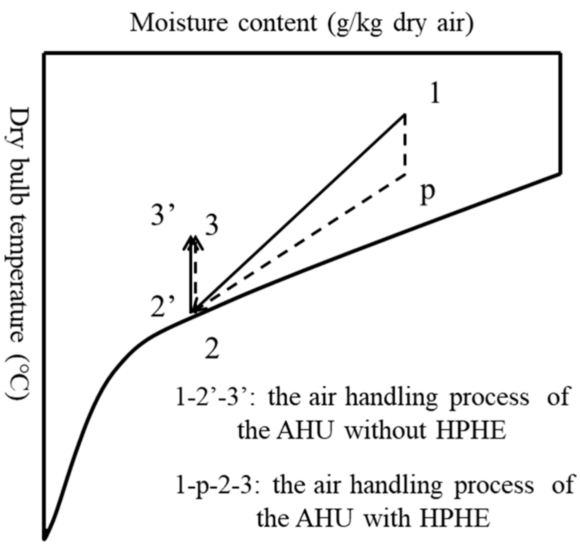

Figure 26. Psychrometric plots of air handling processes through the conventional AHU and AHU integrated with HPHE (solid line represents processes of air passed through the conventional AHU, while dash line represents air passed through the AHU owning the HPHE).

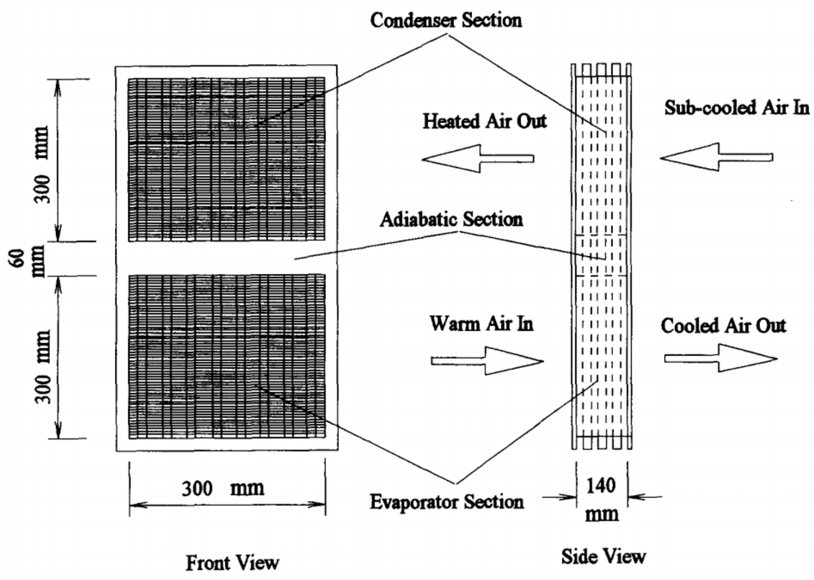

Figure 27. Schematic of the vertical HPHE [100].

Yau [104,105] further conducted experimental research on the performance of vertical HPHE applied to ACS in high humid tropical areas. The results implied that the dehumidification capability of the HPHE increased with the dry bulb temperature and relative humidity increases of the inlet air. However, the influence of the inlet dry bulb temperature on the sensible heat ratio was not as significant compared to the inlet relative humidity. In other research, Yau and Ahmadzadehtalatapeh [106] gave an overview of the application of the horizontal HPHE in HVAC systems in tropical climates. It was revealed that both vertical and horizontal HPHE configurations could be used to improve the performance of ACSs. Although there were many valuable studies on the effect of the vertical HPHE on the energy consumption and dehumidification improvement of ACSs in the tropics, there was limited research work on the utilization of horizontal configuration HPHEs in these regions. Subsequently, Yau and Ahmadzadehtalatapeh [24,107] conducted a series of simulation and experimental studies to investigate the dehumidification and energy savings of ACSs coupled with the horizontal HPHE in tropics. The schematic of the horizontal HPHE is shown in Figure 28. A transient system simulation program was employed to analyze the hourly effects of the ACSs integrated with the HPHE. The results showed that the performances of the ACS integrated with the HPHE were improved and a considerable amount of energy and power was saved.

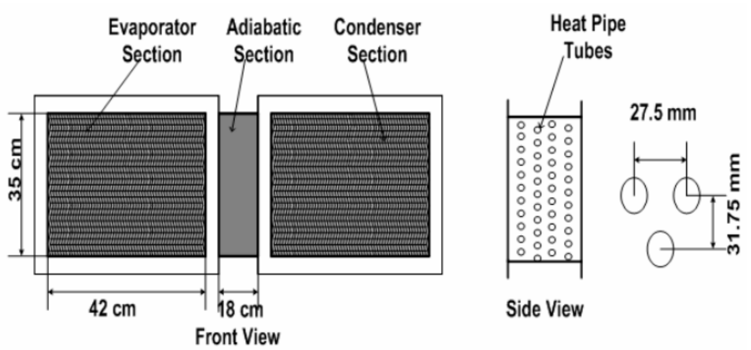

Figure 28. Schematic of the horizontal HPHE [24].

Barrak et al. [102] studied the dehumidification capability of AHU integrated with vertical PHP HE (PHPHE). As shown in Figure 29, the PHPHE was comprised of an 8-row staggered PHP. Each PHP was made by closed loop copper (with an outer diameter of 4.7 mm and tube thickness of 0.6 mm) bent into 7 turns. Distilled water, methanol, and methanol and water mixture fluid were charged into PHP with a filling ratio of 50% of the total volume. Wire fins with equal distances apart were added to the PHPHE to provide an additional heat exchange area. The performances of the ACS under different working fluids, supply air velocity, inlet air dry bulb temperature and relative humidity were analyzed. The results indicated that the dehumidification capacity of the ACS could be enhanced by using PHPHE with ratios of 25, 21 and 17% for methanol, mixture fluid and water, respectively. The total energy saving increased with the increase in the air velocity. The maximum total energy saving reached 1645, 1849 and 1932 W for water, mixture fluid and methanol, respectively. The increase in inlet temperature and inlet relative humidity would enhance the dehumidification capability of the CC. The inlet relative humidity had a more significant effect on the sensible heat ratio than the inlet air temperature.

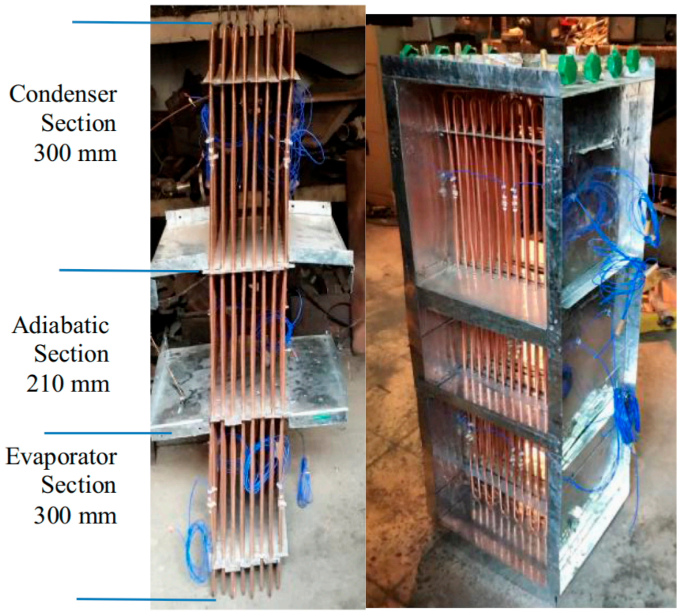

Figure 29. Photograph of the PHPHE [102].

Wan et al. [108] used LHP to enhance the performance of the AHU. The LHP was circuited before and after the CC, as shown in Figure 30. The results showed that the cooling and total energy savings were 23.5–25.7% and 38.1–40.9%, respectively, in the room design temperature of 22–26.8 °C and relative humidity of 50% for the case office building. The indoor relative humidity had a much greater effect on energy saving than the indoor design temperature.

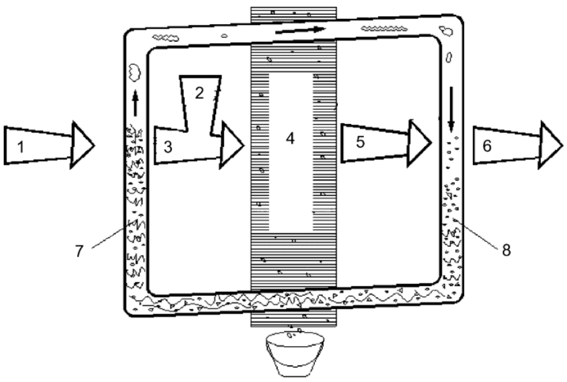

Figure 30. Schematic of the air-handling coil-based HP [108]: (1) Outdoor air, (2) Return Air, (3) Pre-cooled air, (4) CC, (5) Cooled and dehumidified air, (6) Reheated air, (7) Evaporating section of the HP, (8) Condensing section of the HP.

Guo et al. [57] carried out a study to analyze the influence of pump-assist SHP (PASHP) on energy consumption and dehumidifying improvement in the ACS. Four PASHP sets were installed on the CC to recover the cooling energy and reheat the cool and dehumidified air. As shown in Figure 31, the PASHP set consisted of a magnetic pump, a ball valve, a needle valve, an evaporator and a condenser. The evaporator and the condenser of the PASHP were mounted before and after the evaporator of the air conditioner. Every PASHP was charged with R134a. The experimental results showed that the supply air temperature of the proposed system increased from 11.7 to 24.1 °C, while the dehumidification capacity increased by 29.5%. The energy saving and dehumidification capacity improvement were obvious for the ACS coupled with the PASHP. The results were consistent with those of Ref. [108].

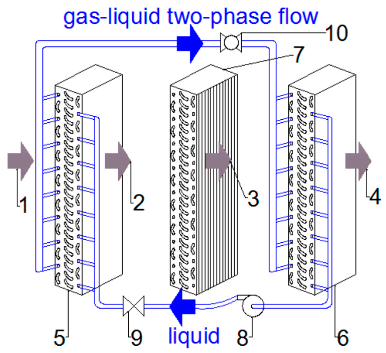

Figure 31. Schematic and combination of PASHP [57]: (1) Inlet air, (2) precooled air, (3) cooled and dehumidified air, (4) reheated air, (5) evaporator of PASHP, (6) condenser of PASHP, (7) evaporator of the air conditioner, (8) pump, (9) needle valve, (10) ball valve.

Supirattanakul et al. [109] designed a precooling and reheating set based on the PHP with check valves for improving the performance of the ACS. They also investigated the effects of working fluids on the heat flux of the PHP. The schematic of PHP is shown in Figure 32. The whole copper tube was bent into 56 turns. Check valves were installed on the PHP. R143a, R22 and R502 were employed to evaluate the performance of the ACS coupling with the PHP. The results indicated that the energy consumption of the novel ACS could be reduced effectively. Compared with the conventional system, the cooling load of the proposed ACS increased by 3.6%. The peak values of the COP and EER of the proposed ACS were increased by 14.9 and 17.6%, respectively.

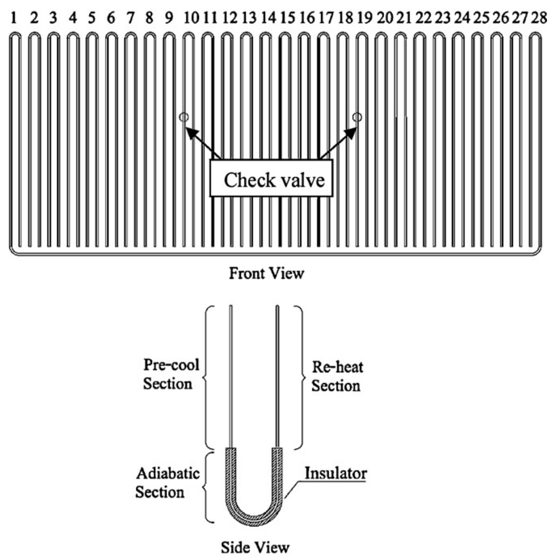

Figure 32. Schematic of PHP [109].

Kusumah et al. [110] applied a U-shaped HPHE to enhance the dehumidification performance of the ACS. The HPHE consisting of THPs was vertically placed in AHU (shown in Figure 33a). Water was encapsulated into the HPHE, which served as the working fluid. The thermal effectiveness and the heat recovery of the HPHE were evaluated by varying the inlet air temperature, air speed and the number of HPs. The results showed that the heat recovery of the HPHE increased with the increase in the inlet air temperature and speed. The thermal effectiveness of the HPHE increased with the increasing inlet air temperature, while it decreased with the increasing inlet air speed. The HPHE performed best when the maximum number of HPs was achieved. The energy saving and the maximum effectiveness of the HPHE were 608.45 W and 7.64%, respectively. In other research, Hakim et al. [111] changed the arrangement of the U-shaped HPs and added fins on the HPHE (shown in Figure 33b), as displayed in Ref. [110]. They found that the COP of the ACS improved by 39.9% compared with the system without the HPHE. The maximum energy saving of the two-row HPHE for precooling and reheating were 288.1 and 340.2 W, respectively, under the conditions of the inlet air temperature of 45 °C and the inlet air speed of 2.5 m/s. The highest effectiveness of the two-row HPHE reached 12.4% under the conditions of the minimum inlet air speed of 1.5 m/s and inlet air temperature of 35 °C rather than the maximum temperature of 45 °C, which was inconsistent with the conclusion in Ref. [110].

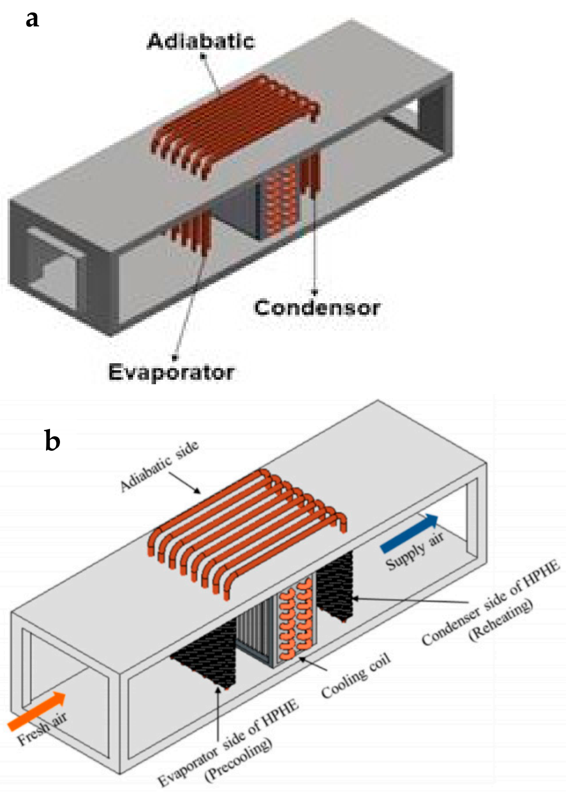

Figure 33. Placement of U-shaped HPHE in the AHU ((**a**) Without fins [110] and (**b**) With fins [111]).

Jouhara and Meskimmon [101,112] replaced the conventional HP with the LHP to make up the U-shaped LHP HE (LHPHE). And they set the LHPHE horizontally (with a slope) around the CC rather than vertically, as shown in Figure 34. Water and R134a were charged as the working fluid. Through tests and analysis, they found that the performance of the U-shaped LHPHE filling with water was better than filling with R134a. The effectiveness decreased with the increase in the inlet air velocity, which agreed with that of Ref. [110]. These papers also confirmed that the performance of the U-shaped LHPHE increased with the increasing HP number, which was consistent with the conclusion in [110,111]. Li and Ju [113] studied similar setups. The total and sensible effectiveness were selected to evaluate the performance of the U-shaped LHPHE. They confirmed that sensible and total effectiveness increased with the increase in the inlet air temperature and filling rate. However, these values would decrease when the inlet air temperature and filling rate exceeded 38 °C and 88%, respectively. The effect of the inlet air temperature on the effectiveness was similar to that of Ref. [111]. The effect of face velocity on the effectiveness was consistent with that of Refs. [101,110–112]. The dehumidification enhancement and energy saving of the HPHE employed in the ACS have been demonstrated by many scholars. However, the best performance obtained from previous research is restricted by the actual working conditions. In fact, very few studies have actually reported any control strategies based on the climatic condition applicable over a full year for the ACS coupled with the HPHE. Therefore, Sarkar [114] proposed an entire year operation control methodology applicable for enhancing the dehumidification of the ACS integrated with the HPHE. In order to allow this system to operate in varying environmental conditions throughout the year, a number of ancillary components, such as steam humidifier, precool and preheat coils were incorporated into the system to meet the off-design conditions, as shown in Figure 35. Based on the energy simulation study of two DOE prototype office-building models, the results indicated that the annual cooling energy savings of the proposed system were 1.5–19% for the six climate zones and the indoor temperature and relative humidity unmet hours were below 300, compared with the similar ACS integrated with wrap around HPHE without climatic controls and ancillary components.

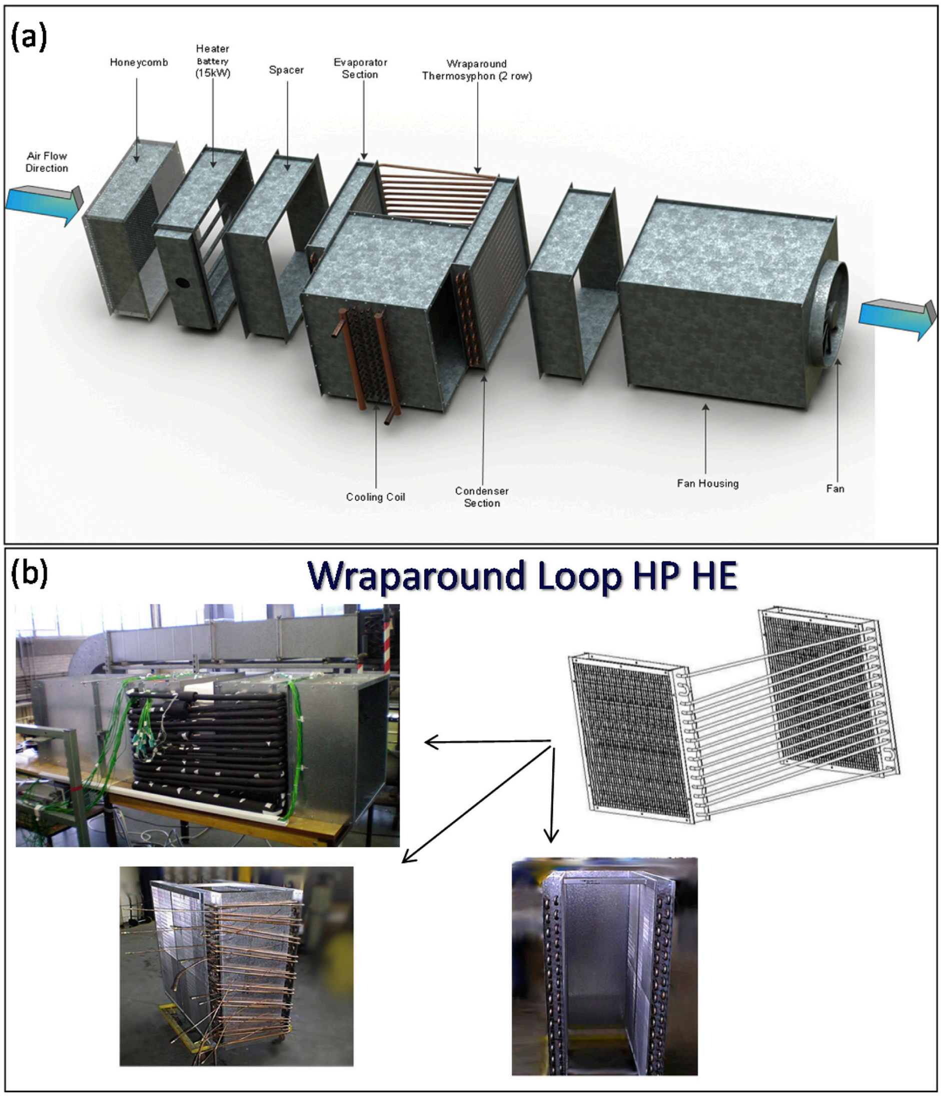

Figure 34. (**a**) Exploded assembly details, (**b**) Actual mechanical design of the wraparound HPHE [101].

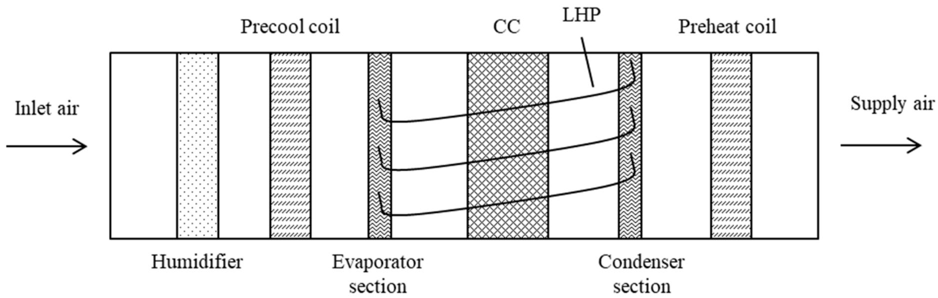

Figure 35. Schematic of the ACS integrated with HPHE for climatic control.

3.4.2. Exhaust Heat Recovery System Based on HPHE

Noie-Baghban and Majideian [115] carried out research with respect to waste heat recovery using HPHE for the hospital building. The schematic of the vertical HPHE is shown in Figure 36. They theoretically analyzed the influence of the working liquid in the design process of a single HP first and found that methanol had the larger merit compared to water and acetone. Then, they used eight staggered HPs to form a vertical HPHE apparatus. In the test conditions, the flow ratio of the evaporator and condenser sections was 1, and the working temperature was 15–55 °C. The effectiveness (calculated by Formula (3)) was used to investigate the performance of the HPHE in the heat recovery system. The results reflected that the maximum effectiveness of the HPHE was only 0.16. They attributed the low efficiency of the HPHE to lack of fins, high pitch to diameter and high air face velocity. Jadhav and Lele [116] theoretically analyzed the energy saving of the ACS integrated with the HPHE for 25 Indian cities representing different climatic areas. A 6-row HPHE was selected to realize the heat recovery of the ACS. The results showed that the maximum energy saving potential was for hot and dry, warm and humid, and composite Indian climatic zones.

$$\varepsilon_{\mathrm{r}} = \frac{T_{\mathrm{e,in}} - T_{\mathrm{e,out}}}{T_{\mathrm{e,in}} - T_{\mathrm{c,in}}} \quad (3)$$

where ε_{r} represents the effectiveness of the HPHE; $T_{\mathrm{e,in}}$ is the inlet air temperature of the evaporator section of the HPHE, °C; $T_{\mathrm{e,out}}$ is the out air temperature of the evaporator section of the HPHE, °C; $T_{\mathrm{c,in}}$ is the inlet air temperature of the condenser section of the HPHE.

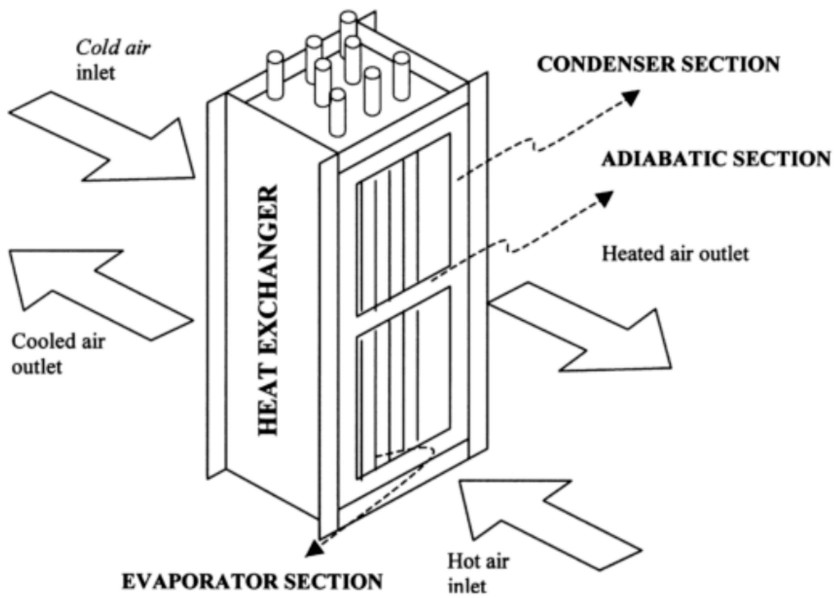

Figure 36. Schematic and working principle of the vertical HPHE [115].

Danielewicz et al. [117] added fins to the HPHE (shown in Figure 37) and explored a prediction model for an air to air HPHE using the ε-NTU (effectiveness-Number of Transfer Unit) and test methods. The variables including effectiveness, pressure drop, heat recovery, and the number of rows were considered. As shown in Figure 38, the results reflected that the effectiveness and heat recovery of the HPHE increased with an increasing number of rows. The pressure loss of the HPHE increased with the increasing inlet air speed. But effectiveness decreased with the increase in the inlet air speed. The reason was that increasing the inlet air speed led to a reduction in the contact of the HPs with the airflow, resulting in the airflow not having enough time to take away the heat released by the HPs. In addition, Putra et al. [118], Muhammaddiyah et al. [119] and Sukarno et al. [120,121] also performed experimental studies to evaluate the characteristics of ACS integrated with heat recovery based on vertical HPHE equipped with fins. Water with a filling rate of 50% acted as the working medium for the HP. The results reflected that the higher the row number value of the HPHE, the inlet air temperature and speed, the more heat recovery of the system obtained. The effectiveness of the HPHE increased with the increasing of row numbers and inlet air temperature, while it decreased with the increasing of the fresh air speed. These conclusions were consistent with those of Ref. [117]. The highest effectiveness value was over 60%. In other research, Sukarno et al. [122] further performed performance analysis for the HPHE by using the Buckingham Pi theorem.

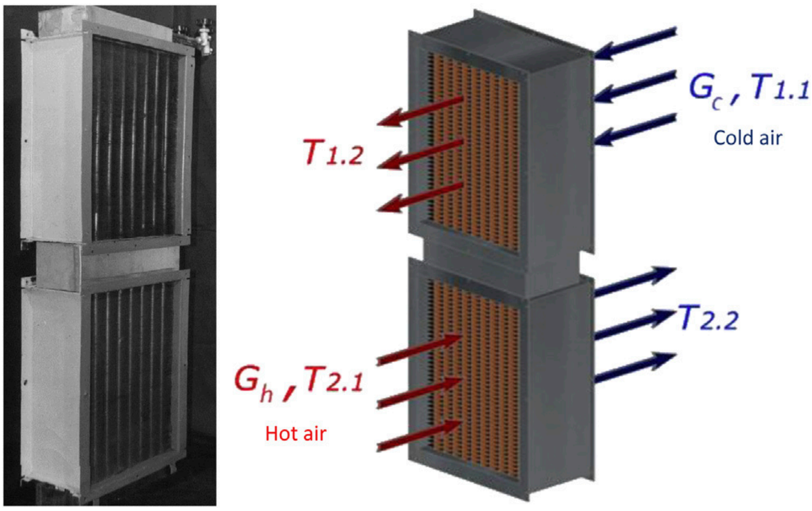

Figure 37. The photograph and illustration of the HPHE with fins [117].

a

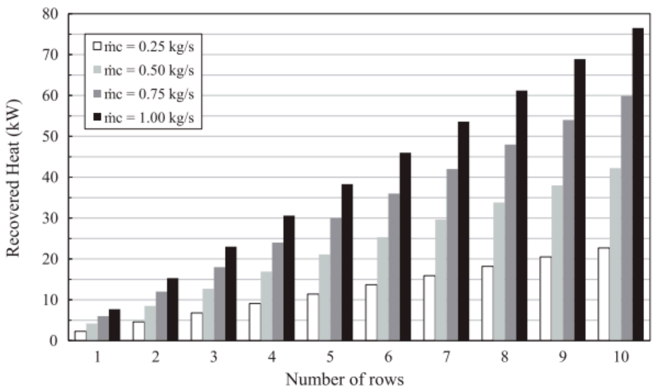

Figure 38. *Cont.*

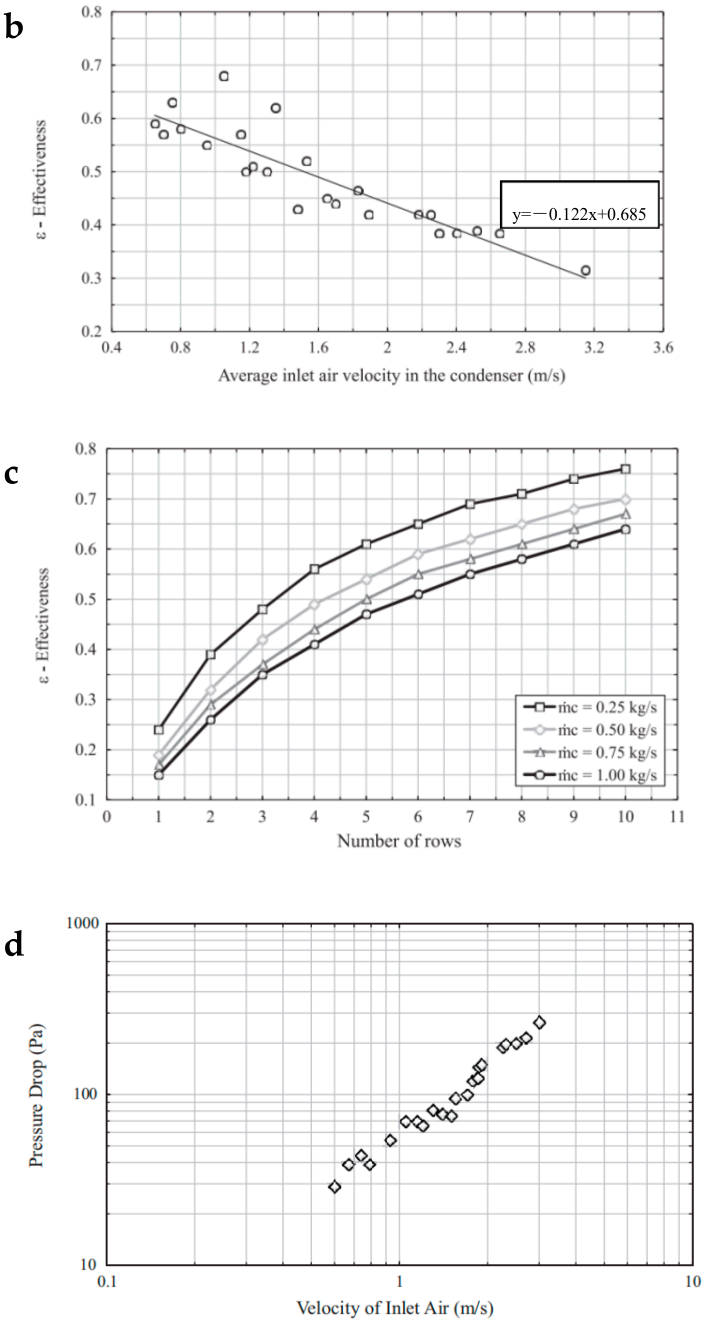

Figure 38. The performance of the HPHE test ((**a**) Heat recovery with respect to mass flow rate and number of rows, (**b**) Pressure drop with respect to inlet air velocity, (**c**) Effectiveness with respect to mass flow rate and number of rows and (**d**) Effectiveness with respect to the velocity of inlet air) [117].

Abd El-Baky and Mohamed [123] introduced the horizontal HPHE into the heat recovery application to reduce the cooling load caused by incoming fresh air from the ACS. They designed an experimental apparatus to evaluate the overall effectiveness of the HPHE. As shown in Figure 39, the HPHE consisted of 25 wick copper tubes and was finned with aluminum sheets. The HPs were horizontally arranged in staggered form. R11 with a saturation temperature of 30 °C was used as the working fluid. The ratio of the flowrate between return and fresh air ranged from 1 to 2.3. The inlet air temperature ranged from 32 to 40 °C. The results further confirmed that the effectiveness of the HPHE increased with an increase in the fresh air inlet temperature. The effect of airflow rate on effectiveness had a little positive correlation for the evaporator section and a largely negative correlation for the condenser section. Moreover, the maximum effectiveness and enthalpy ratio were about 48 and 85%, respectively, at an inlet air temperature of 40 °C. Subsequently, Abdelaziz et al. [124] further confirmed the above conclusions and found that the payback period of the proposed system was approximately 3 years.

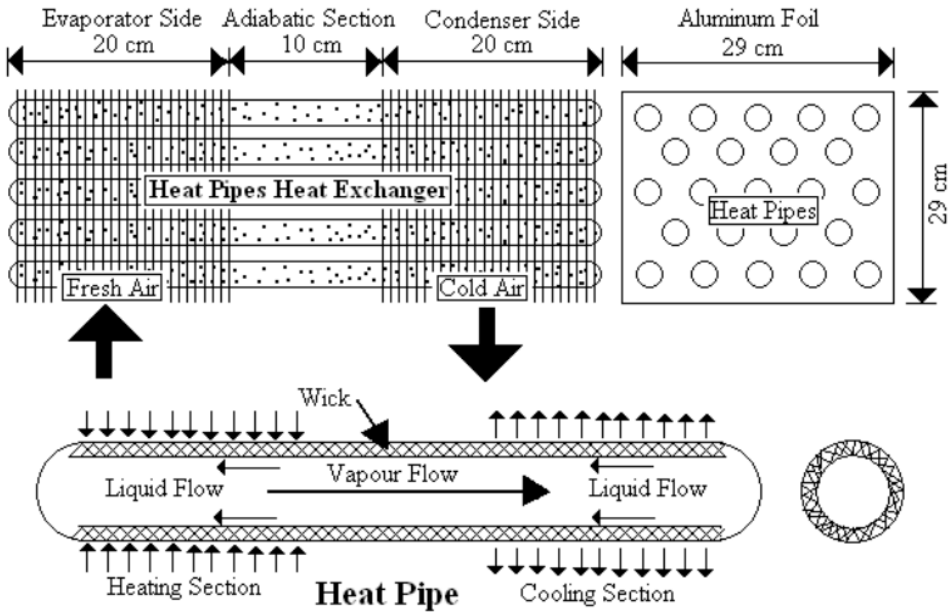

Figure 39. Schematic of the HPHE and wick HP [123].

Mahajan et al. [125] experimentally demonstrated the preheating and energy saving abilities of PHP with the working fluid of n-pentane. A copper capillary pipe was utilized to construct a 9-turn PHPHE, as shown in Figure 40. The behavior of PHPHE under different filling ratios was evaluated. The results reflected that the PHPHE with n-pentane could provide an average heat recovery of 225 W at a filling ratio of 70% while the pressure drop was less than 60 Pa. Under this working condition, an effectiveness of 0.05 and an effective thermal resistance of 0.11 °C/W were obtained. The reason for the low energy efficiency of PHPHE was that only a single PHP without fins was used in this study. In other research, Mahajan et al. [126] focused on modeling and predicting the heat transfer and aerodynamic performance of a 15-row PHPHE in a typical ACS. The single-finned PHP is shown in Figure 41. The ε-NTU method was employed to estimate the heat recovery of PHPHE. Energy and cost savings for typical ACS were also estimated. They found that the pressure drops of the evaporator and condenser section of the PHPHE consisting of 15-row of 20-turn were reasonable, with values of 36.4 and 39.8 Pa, respectively. PHPHE had the potential to precool inlet air by 8.0 °C. The effectiveness of the PHPHE reached 0.48. The total average annual energy consumption and running costs could be reduced by 16% and USD 700 for the proposed system in the commercial building.

Yang et al. [127] designed a PHPHE to recover energy from exhausted air in the ACS. As shown in Figure 42, the PHPHE consisted of 40 PHPs, with each having 40 turns. The working fluid was R134a, with the filling rate about 50% of the total volume. Under the variations of the outdoor air temperature (30–45 °C), wind velocity (1.0–3.5 m/s) and tilt angle (0–90°) of the PHPHE, the thermal performance of the PHPHE was studied. The results showed that with the increase in inlet air temperature, the recovery effectiveness of the PHPHE improved greatly. With the increase in the tilt angle, the recovery effectiveness of the PHPHE increased initially and then decreased. At the installation angle of 60 degrees, the recovery effectiveness of the PHPHE reached the largest value of 0.5. With increasing wind velocity, the recovery capacity increased while the recovery effectiveness decreased. The pressure loss of PHPHE was below 50 Pa.

Shen et al. [128] experimentally studied a novel parallel-flow HPHE (as shown in Figure 43), which consisted of a series of FHPs set in parallel. The R600A was used as the working fluid, with a filling rate of 26%. The experiments were conducted with different cooling airflow rates. The results showed that the cooling airflow rate had an important impact on heat transfer in the condenser section of the parallel-flow HPHE. The heat transfer efficiency of the parallel-flow HPHE increased with the increasing airflow rate, while the thermal resistance decreased.

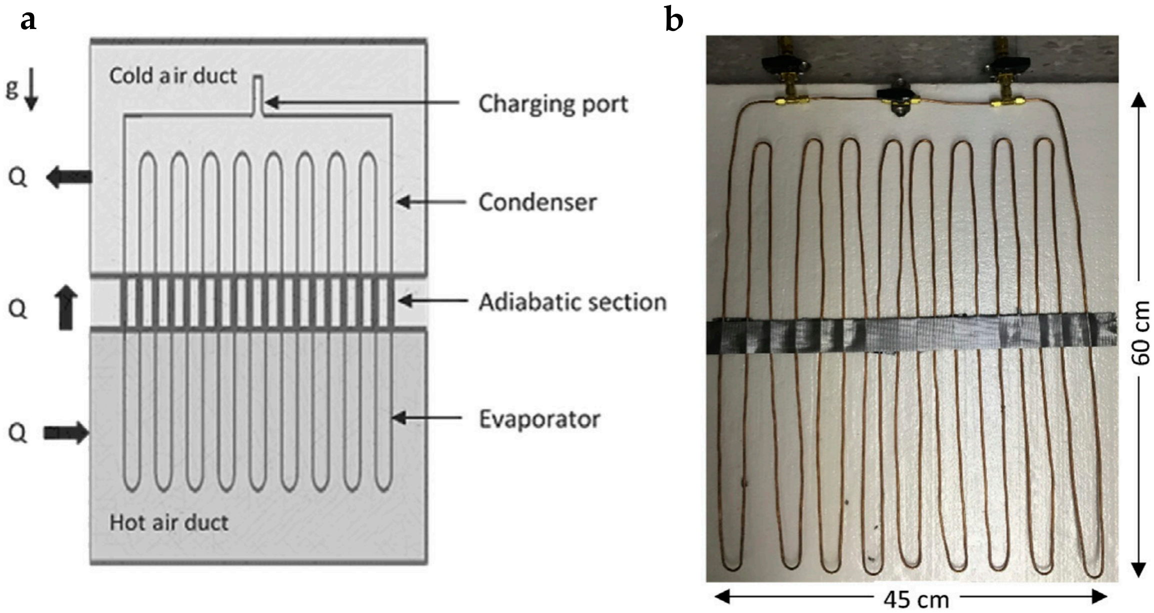

Figure 40. Installation schematic of the PHPHE and photograph of a single PHPHE ((**a**) PHPHE installation in the air duct and (**b**) Photograph of the PHPHE) [125].

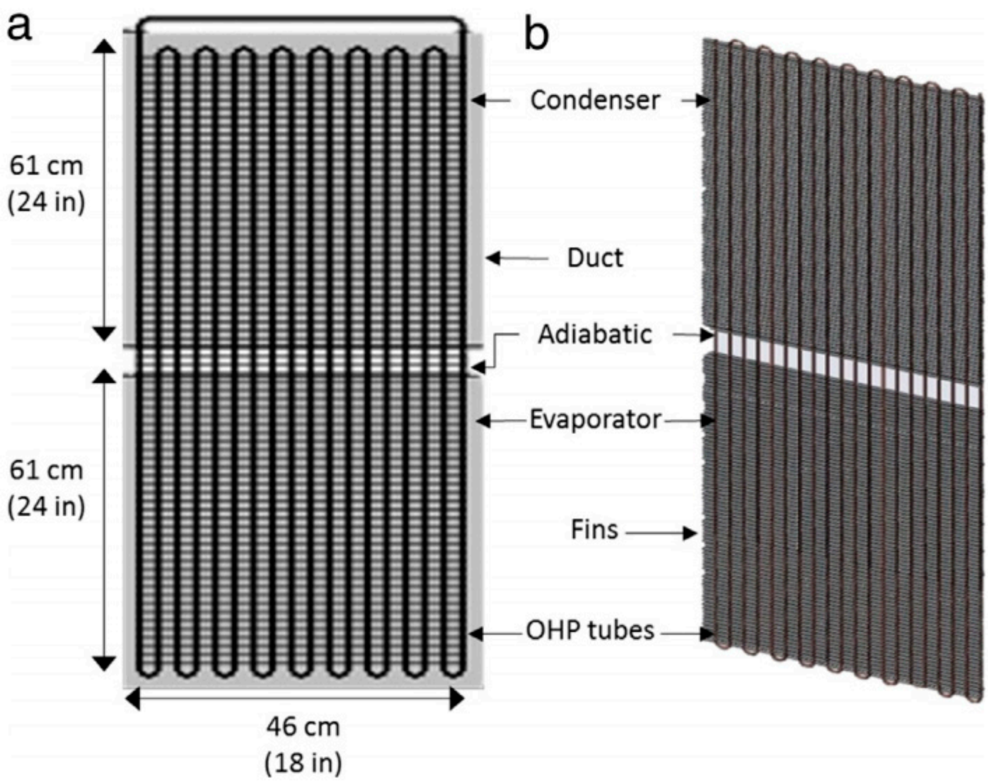

Figure 41. Schematic of a unit-row PHPHE ((**a**) Front dimensioned view and (**b**) Isometric view) [126].

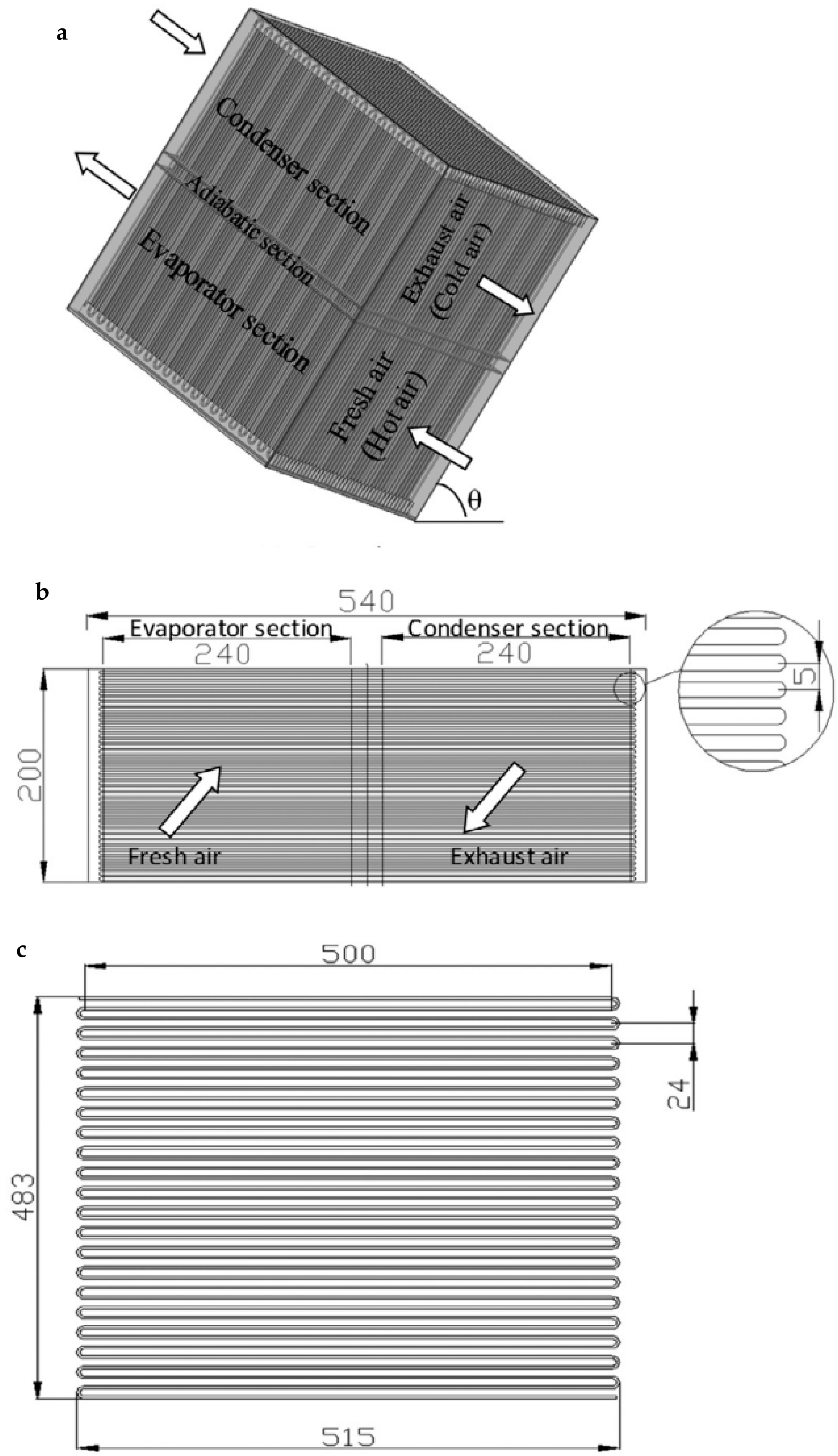

Figure 42. Schematic structure of PHPHE ((**a**) Overview of the PHPHE, (**b**) Front view and (**c**) A single PHP with 40 turns) [127].

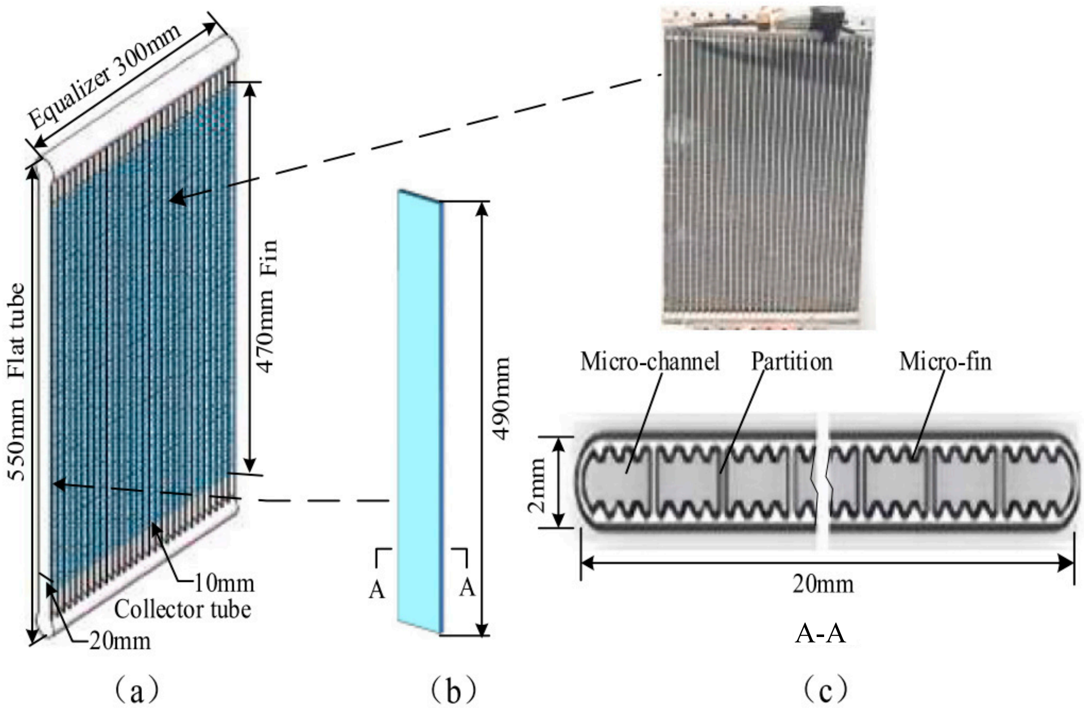

Figure 43. Schematic diagram of FHP-HE ((**a**) The FHP-HE, (**b**) A single flat plate unit and (**c**) A-A section view of the unit) [128].

Liu et al. [129] introduced the LHP heat recovery system into ACS (as shown in Figure 44). They established a one-dimensional steady-state model to investigate the characteristics of the heat recovery system. Water and methanol were charged into the LHP. The results indicated that the length of the evaporator had almost no impact on the upper boundary but had a significant effect on the lower boundary. The operation ranges of the LHP varied with the working fluids.

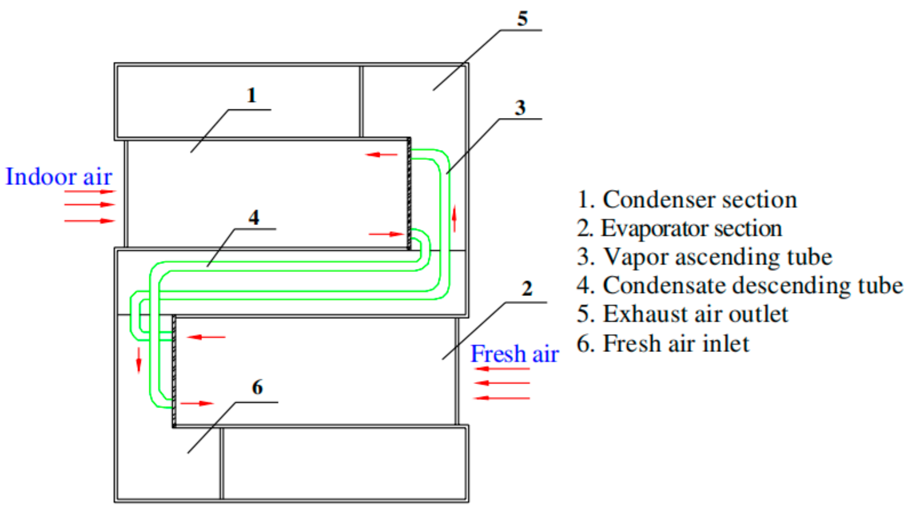

Figure 44. Schematic configuration of the LHP [129].

Xue et al. [130] evaluated the behavior of a novel LHP heat recovery system in a standard psychrometric laboratory. The schematic and working principle of the LHPHE is shown in Figure 45. The experimental apparatus is shown in Figure 46. R32 and R134a were charged into the LHP with a filling rate of 40%. The temperature effectiveness, heat transfer rate, and EER were evaluated by the experimental method. They found that the heat transfer rate and EER of the LHPHE increased with an increasing indoor-outdoor temperature difference. The highest temperature effectiveness was 62 and 70% for winter and summer working conditions, respectively. The average annual EER of the LHPHE employed in Harbin, Beijing, Shanghai and Guangzhou in China were about 12.7, 7.70, 5.8 and 3.7, respectively.

Zhou et al. [131,132] designed and developed a pump-driven LHP (PLHP) heat recovery system in order to satisfy the heat recovery demand in heating and cooling seasons. The principle diagram of the PLHP heat recovery system is shown in Figure 47. The PLHP heat recovery system could be operated in both winter and summer by switching different valves on and off. A pump was used to provide circulation power for the working fluid instead of relying on the pressure difference between the evaporator and condenser sections. This would enhance the heat transfer of the LHP. The authors experimentally analyzed the heat recovery performance of the PLHP under different working conditions. The results reflected that the heat transfer capacity and COP of the PLHP heat recovery system increased with the indoor-outdoor temperature difference. However, the temperature effectiveness showed an opposite trend. The PLHP performed better with R32 as the working fluid than with R22 and R152a. Under optimal operating conditions, the heat transfer capacity, temperature effectiveness and COP were 4.09 kW, 52.3% and 9.26, respectively, for summer working conditions and 6.63 kW, 33.8% and 14.20, respectively, for winter working conditions. They also confirmed that the heat recovery performance of the multi-loop PLHP system was better than that of the single-loop system.

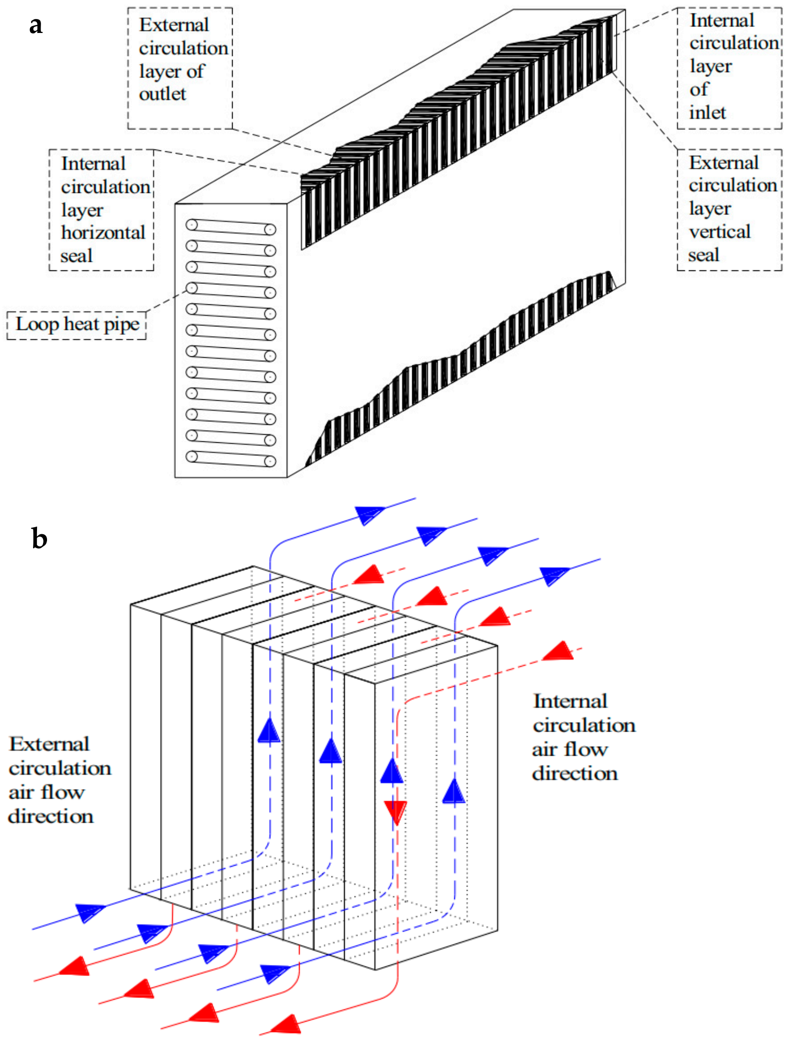

Figure 45. Schematic and working principle of the LHPHE ((**a**) Schematic diagram and (**b**) Working principle) [130].

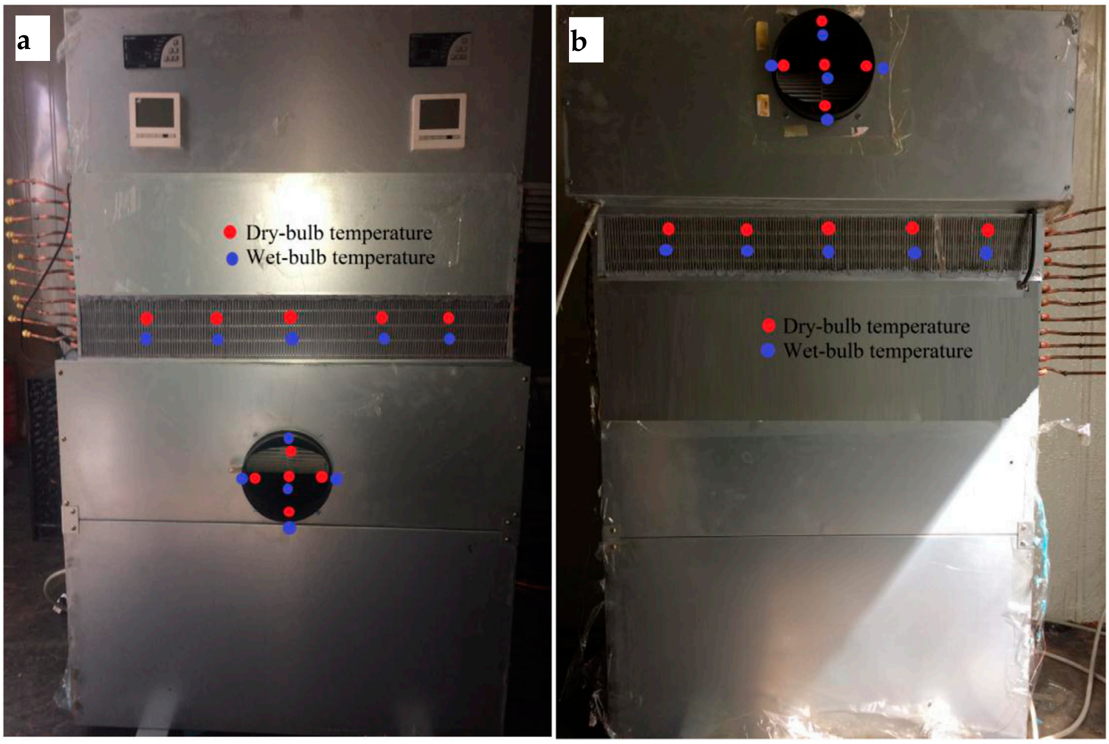

Figure 46. Schematic of temperature measurement point layout ((**a**) Indoor side of experimental device and (**b**) Outdoor side of experimental device) [130].

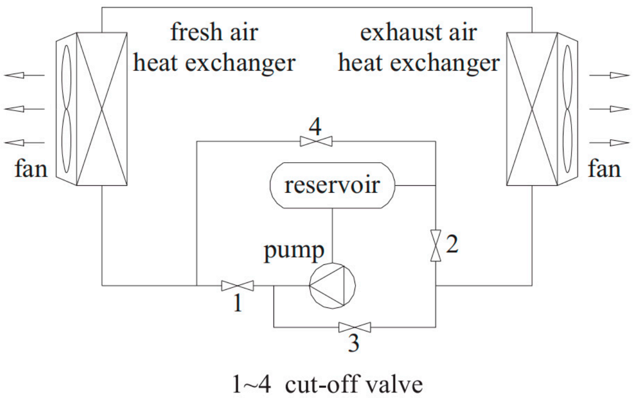

Figure 47. Principle diagram of the PLHP heat recovery system [131].

Liu et al. [133,134] proposed a composite LHP recovery system driven by the booster combined with the refrigerant pump (as shown in Figure 48). They did a series of experiments to analyze the performances of the PLHP, booster-driven LHP (BLHP) and composite-driven (booster combining with pump) LHP (CLHP) heat recovery system. The authors found that the CLHP heat recovery system had a better performance in all years compared with other systems, especially when it ran in cold climates. When the outdoor temperature was −15 °C, the temperature effectiveness of the CLHP heat recovery system was 68.3–78.0% and 52.5–52.9% larger than that of PLHP and BLHP, respectively. The outlet temperature of the CLHP heat recovery system increased by 7.8–8.7 °C and 6.6–7.2 °C compared to that of PLHP and BLHP, respectively. The heating capacity of CLHP was 67.7–78.0% and 51.2–52.5% larger than that of PLHP and BLHP, respectively. When the outdoor temperature was 40 °C, the temperature effectiveness of the CLHP heat recovery system was 19.5–24.6% larger than that of BLHP. The outlet temperature of the CLHP heat recovery system decreased by 6.3–6.6 °C and 1.7–2.1 °C compared to that of PLHP and

BLHP, respectively. The cooling capacity of CLHP was 176.2–188.7% and 30.3–33.6% larger than that of PLHP and BLHP, respectively.

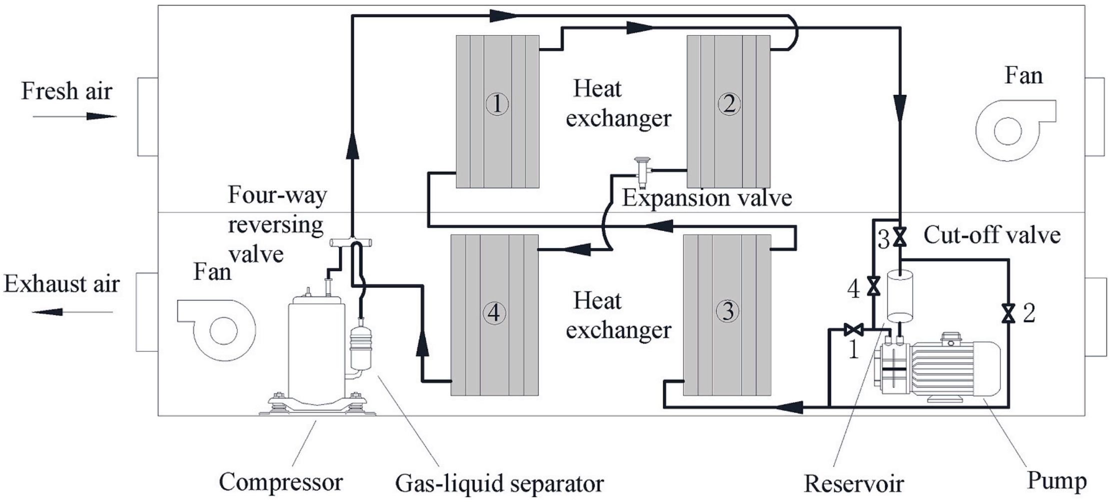

Figure 48. Principle diagram of the dual-drive LHP heat recovery system [133].

3.4.3. Dehumidification and Heat Recovery Systems Based on the Multi-HPHE

Ahmadzadehtalatapeh and Yau [135] and Yau [136] proposed a double HPHE system for reducing the energy consumption of the ACS. Outdoor air was pre-cooled twice before entering the CC, as shown in Figure 49. The processes of exhaust heat recovery and AHU dehumidification could be carried out simultaneously. According to the analysis, they found that the energy consumption level and air conditions provided by the ACS could be improved significantly.

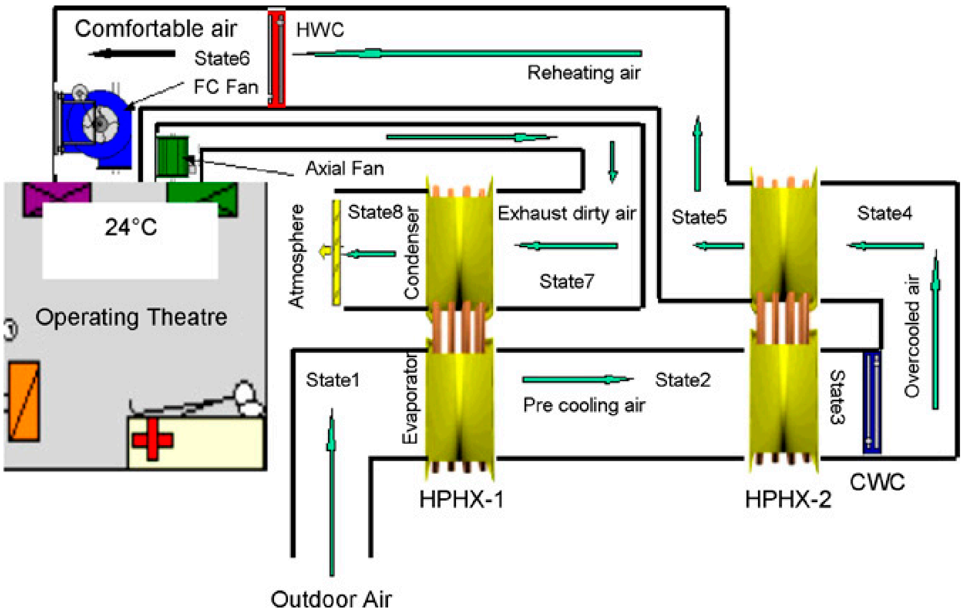

Figure 49. Schematic of the ACS with a double HPHE [136].

Martínez et al. [137] designed a mixed energy recovery system integrated with the HPHE and the indirect evaporative equipment for the ACS. They aimed to improve ACS efficiency by reducing the energy consumption of handling outdoor fresh air with a two-stage cooling method in summer. Both of the heat recovery devices could reuse the residual heat from the cooling room in a way that the fresh air and return air were not at risk of contact. A schematic diagram of the experimental installation is shown in Figure 50. The HPHE was a super-conducting device comprising an array of finned tubes, each of which was filled with ammonia and sealed at both ends. Based on the analysis of the factorial design 1125 experimental tests, the heat recovery efficiency had a linear relationship with the outdoor temperature and airflow factors and an extreme COP value of 9.83 of the study system was obtained. The percentage factor of the recirculated air towards each of the heat recovery devices had the greatest influence on the overall results of the experimental installation.

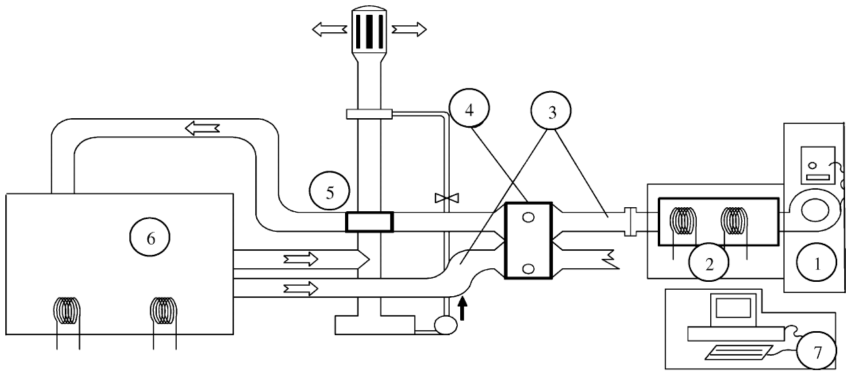

Figure 50. Schematic diagram of the mixed energy recovery system [137]: (1) Variable frequency fan, (2) AHU with variable flow air, (3) Air distribution ducts, (4) HPHE, (5) Indirect evaporative recuperator, (6) Test room, (7) Data acquisition computer.

Wang et al. [138] designed a secondary heat recovery ACS coupled with two sets of HPHEs. A primary HE consisting of horizontal wick HPs was utilized to realize the heat transfer between the exhaust air and the fresh air during the heating and cooling season. A secondary HE consisting of the capillary pump loop (CPL) HP was used to realize the heat exchange between the return air and the supply air during the cooling season. Primary HE could be used in winter and summer. The secondary HE was out of service in winter. The working medium in HP was ammonia. The HP physical diagram and the design drawing of HPHE are shown in Figures 51 and 52, respectively. The results revealed that the average heat recovery efficiency of the proposed system was 21.08 and 39.2% in winter and summer, respectively. The energy saving advantage of the novel system was outstanding compared to that of the common heat recovery system.

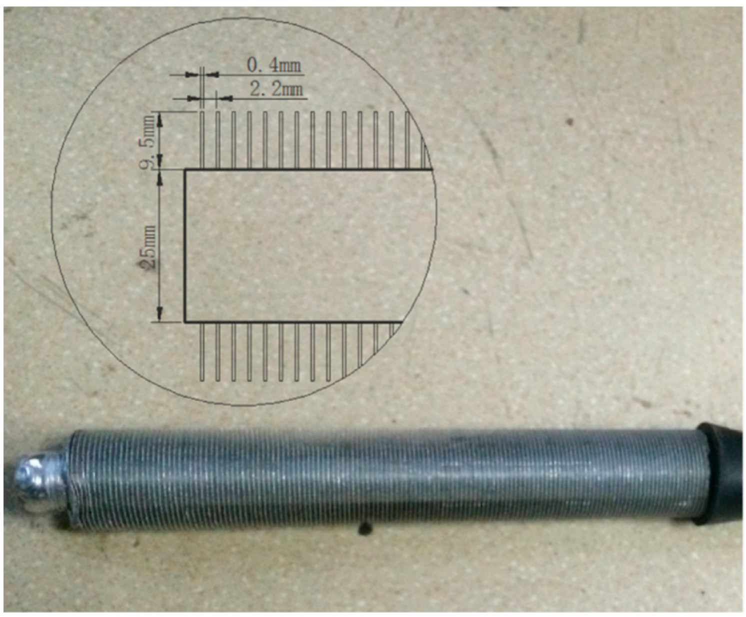

Figure 51. Physical diagram of the HP [138].

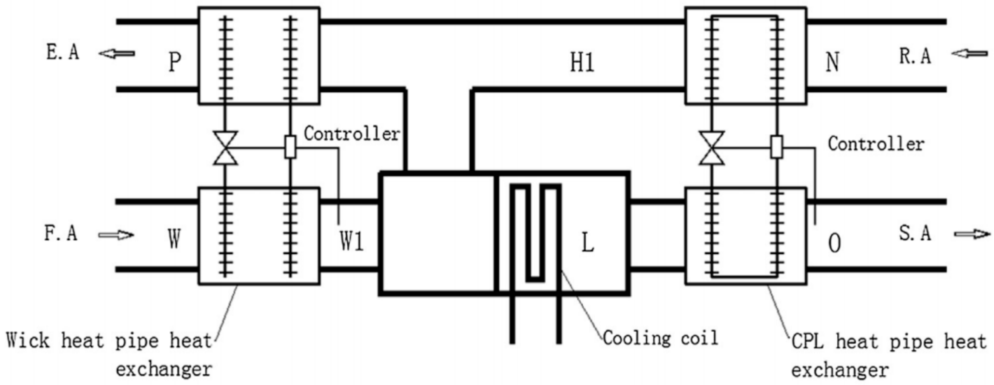

Figure 52. Schematic diagram of the secondary heat recovery ACS coupled with the HPHE [138].

3.5. Cooling Radiator Integrated with HP

Sun et al. [68] designed a novel cooling radiator coupled with an FHP. The FHP radiator consisted of 10 pieces of FHPs, as shown in Figure 53. Each FHP contained several microchannels separated by partitions (shown in Figure 54). Acetone was sealed into the microchannel and acted as the working medium with a filling rate of 15%. The thermal response speed, heating capacity and thermal uniformity were employed to investigate the performance of the FHP radiator under different flow modes, flow rate and cold source temperature. The cooling capacity of the cooling radiator was calculated using Formula (4). The experimental test indicated that the FHP radiator had a speed start-up time with a value of 245–385 s. The cooling capacity of the FHP radiator varied from 40.1 to 75.8 W/m^{-2}. The flow mode and the flow rate of the FHP radiator were not the major considerations that determined the cooling performance. Only the cold source temperature had an important impact on the thermal performance of the FHP radiator.

$$Q_c = \frac{QA_c}{A} \tag{4}$$

$$Q = \frac{Gc\Delta T}{3600} \tag{5}$$

where Q_c represents the effective heat dissipation of the FHP cooling radiator, W; Q is the total heat dissipation of the FHP cooling radiator, W; c is the heat capacity of water, J·kg^{-1}K^{-1}; G is the flow rate of the circulation system, kg·h^{-1}; A is the total area of the FHP cooling radiator, m^{-2}; A_c is the heat dissipation area of the FHP cooling radiator, m^{-2}; ΔT is the temperature difference between the two thermal resistances, K.

Wu et al. [139] proposed a new radiant cooling terminal integrated with the HE and the FHP (shown in Figure 55). To decouple the condensation prevention and cooling capacity improvement, the running strategy in which the FHP was only used for removing the sensible heat load while the HE was used for removing the sensible and latent heat load simultaneously was proposed. The total size of the FHP was 980 mm × 880 mm (L × H). And the working fluid of the FHP was acetone with a filling rate of 20%. The contact area between the HE and FHP was 980 mm × 180 mm (L × H). The results showed that the thermal response speed of the radiant terminal was 360 s, and the surface temperature was relatively uniform with the fluctuation of ±3 °C under the proposed running strategy. The cooling capacity and heat transfer coefficient were 185.5 W and 16.8 W/K, respectively. The latent heat transfer proportion of the FHP was 12.1%. When fans and sealing air ducts were added to the FHP, the surface temperature and cooling capacity of the FHP simultaneously increased by 4–6 °C and 75.7%, respectively, under the force convection running strategy.

Zhao et al. [140] developed a novel direct-expansion terminal by combining the FHP and ASHP for improving the cooling and dehumidification of the traditional radiant cooling terminals (as shown in Figure 56). Experimental tests were conducted to evaluate the performance of the new cooling terminal. They found that the cooling capacity of the proposed cooling radiator ranged from 1160 to 2600 W. When the cross flow fan was open and ran at the highest velocity, the cooling capacity was 2.24 times that of the pure radiation mode. The variation in the indoor humidity ratio was from 2.8 to 7.9 g/kg after dehumidification, and the indoor relative humidity could reach a comfortable zone within 30 min.

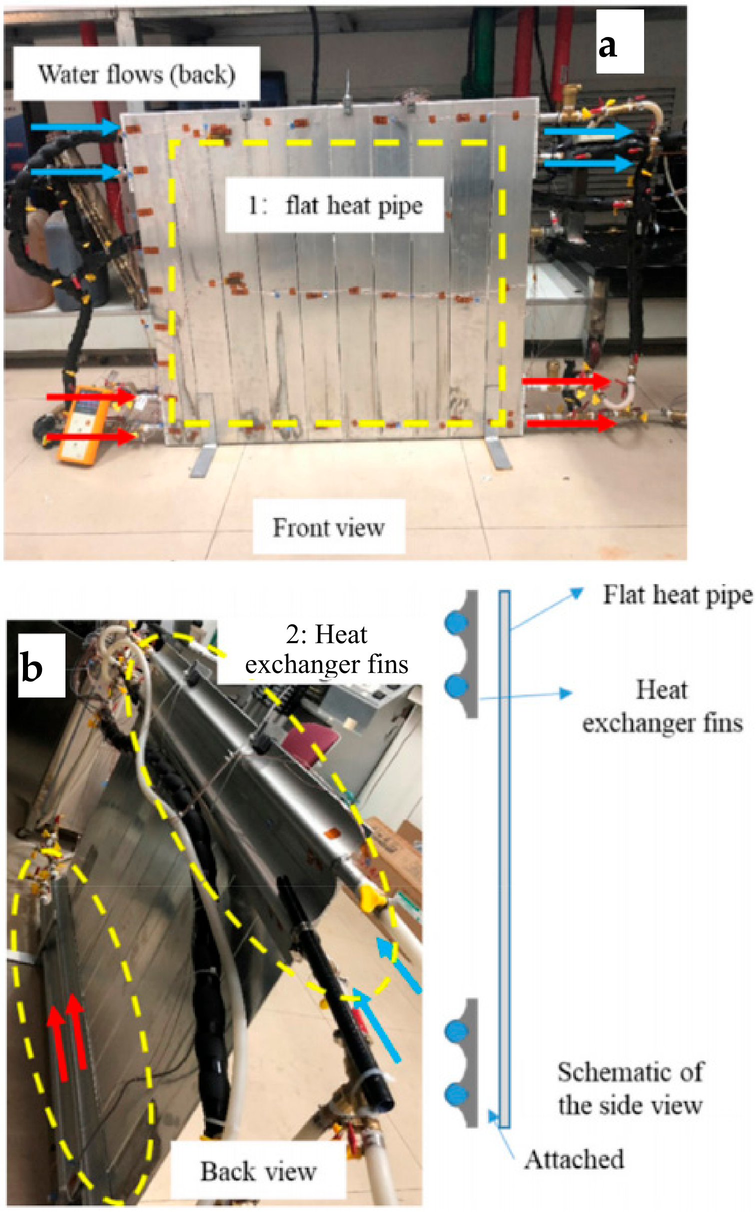

Figure 53. The photograph of the test heating radiator ((**a**) Front view and (**b**) Back view. Note: Red arrows represent the water flows in the heating mode) [68].

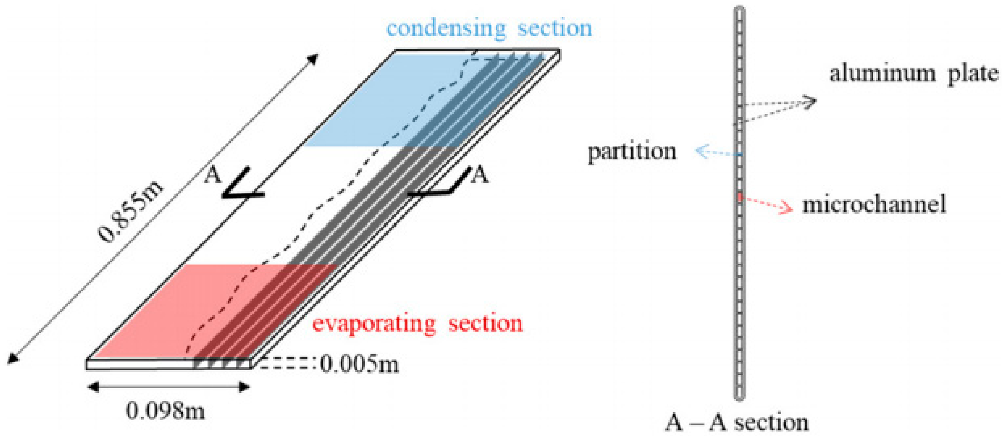

Figure 54. Schematic of a piece of FHP [68].

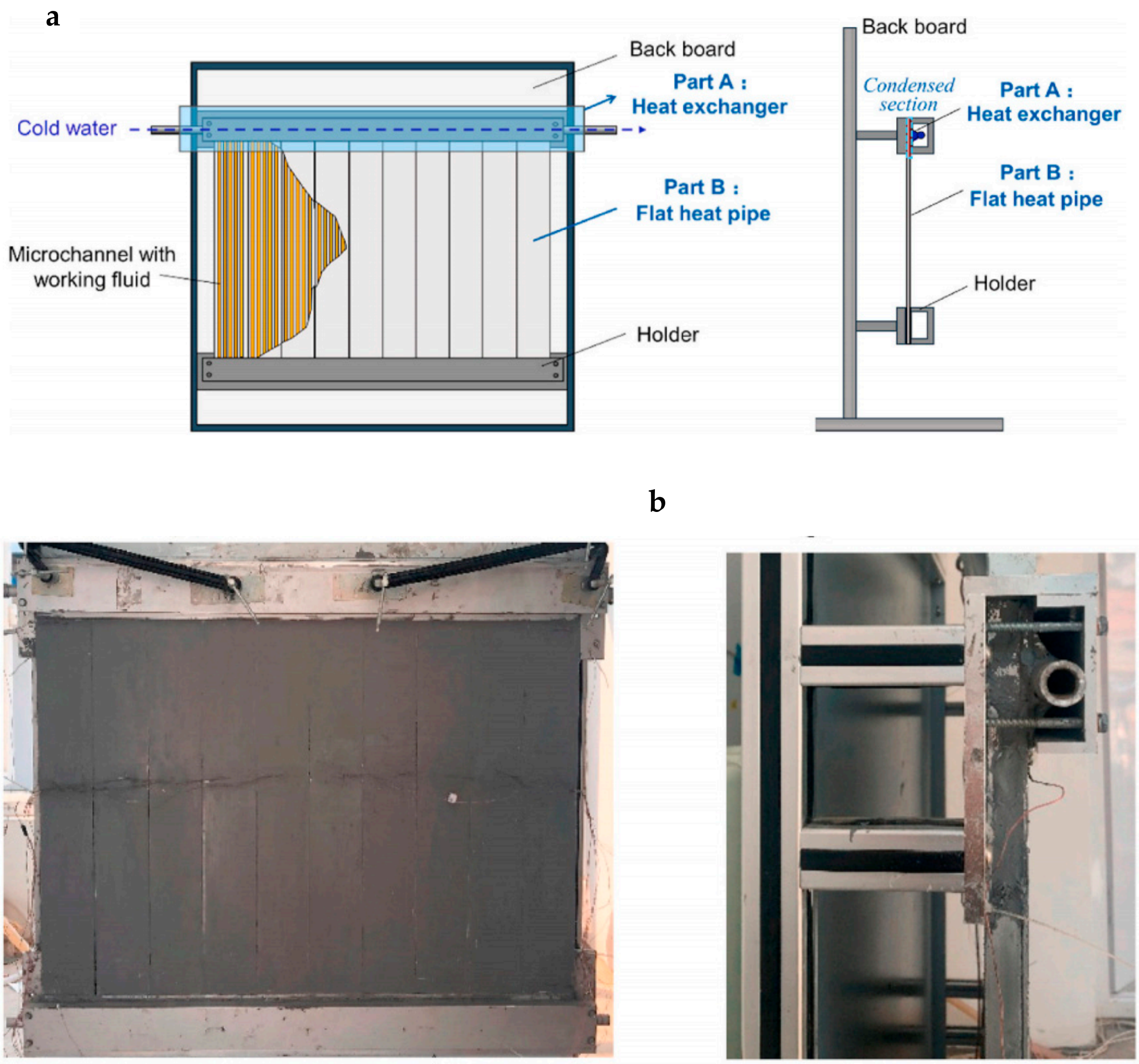

Figure 55. Schematic and test rig of the cooling terminal ((**a**) Schematic of the FHP cooling terminal and (**b**) Photograph of the FHP cooling terminal) [139].

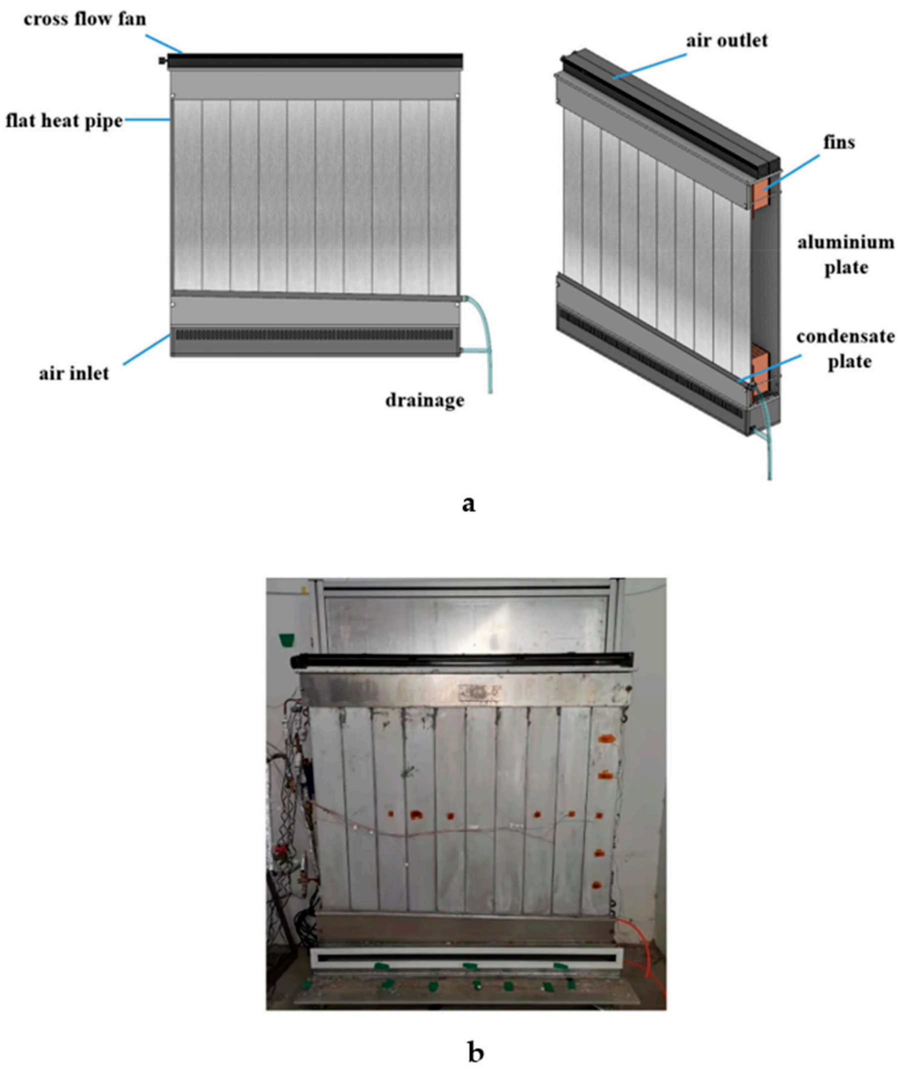

Figure 56. Photograph of the direct-expansion terminal integrated with FHP ((**a**) Modeling diagram of the novel terminal and (**b**) Actual novel terminal) [140].

A summary of the ACS integrated with HP is shown in Table 1.

Table 1. The summary of the ACS integrated with HP.

References	Research Methods	Purpose	HP Types	Installation Direction	HP Working Fluid	Filling Ratio /Volume	Fins	Wick Structure	Core Conclusions
Saw et al. [69]	Experiment	Design an active cool roof system	PHP	Horizontal	Methanol	80%	N	N	The PHP cool roof system could effectively decrease the attic temperature with a reduction of nearly 12.9%.
Li and Zhang [70]	Experiment and simulation	Utilizing air energy and sky radiation energy for cooling	GHP	Vertical	-	28%	N	N	The heat transfer capacity of the WIHP was 50.7 kW/m^2. The average temperature of the inner surface of the north WIHP was about 2 °C lower than that of the conventional wall.

Table 1. *Cont.*

References	Research Methods	Purpose	HP Types	Installation Direction	HP Working Fluid	Filling Ratio /Volume	Fins	Wick Structure	Core Conclusions
Turnpenny et al. [71]	Experiment and simulation	Utilizing air energy for cooling storage	Wicked HP	Horizontal	Methanol	-	Y	Y	The heat transfer rate of the PCM unit was about 40 W during the melt period.
Singh et al. [72]	Experiment and simulation	Utilizing air energy for cooling storage	GHP	Vertical	R134a	-	Y	N	The proposed cooling system could handle 60% of the heat load for the datacenter every year. Its payback period was about 3.5 years.
Yan et al. [73]	Experiment and simulation	Utilizing air energy for cooling storage	SHP	Vertical	R22	100%	Y	N	The proposed system had an annual cooling storage capacity of approximately 31,500 kW and a cooling release capacity of approximately 28,350 kW. The payback period of the seasonal cold storage system was about 8–10 years.
Chotivisarut et al. [74,75]	Experiment and simulation	Utilizing sky radiation energy for cooling storage	GHP	Vertical	R134a	60%	N	N	The proposed system had a great potential in reducing cooling load in low temperature and humidity areas.
He et al. [76]	Experiment and simulation	Utilizing sky radiation energy for cooling storage	FHP	Vertical	-	-	N	N	The peak inner surface temperature reduction of the MHP-RC-PCM wall was about 8 °C compared with that of the traditional brick wall. The average time lag of the traditional brick wall, the PCM wall and the MHP-RC-PCM was about 3.1, 4.1 and 4.5 h, respectively.
Yu et al. [77,78]	Experiment and simulation	Utilizing sky radiation energy for cooling storage	FHP	Vertical	-	-	N	N	The cooling load and the energy saving efficiency of the MHP-RC-PCM wall were about 22–28% and 18%, respectively, compared with that of the traditional brick wall.
Shen et al. [79]	Experiment and simulation	Utilizing sky radiation energy for cooling storage	FHP	Vertical	-	-	N	N	The cooling loads of the south wall were decreased by over 40% under some conditions compared to the traditional brick wall. The low wind speeds favored a lower cooling load, while reducing the emissivity of the radiative plate exhibited the opposite trend.

Table 1. *Cont.*

References	Research Methods	Purpose	HP Types	Installation Direction	HP Working Fluid	Filling Ratio /Volume	Fins	Wick Structure	Core Conclusions
Yan et al. [80–84]	Experiment and simulation	Utilizing sky radiation energy for cooling storage	GHP	Vertical	R245fa	20%	N	N	The pipe encapsulated PCM wall system could improve the thermal insulation effect of the wall in the daytime and remove a lot of the indoor heat gain during the nighttime. The cooling loads of buildings with the proposed system in Hong Kong, Wuhan, Beijing, Harbin and Kunming could be reduced by 11.7, 16.1, 21.1, 28.6 and 44.2%, respectively, compared to that of the traditional wall.
Fikri et al. [87,88]	Experiment	Enhancing the evaporative cooling performance	GHP	Vertical	Water	50%	[87]: N [88]: Y	N	The saturation efficiency of the proposed direct-indirect evaporative cooler increased with the increase of the inlet temperature but decreased with the increase of the relative humidity and air velocity. The three-stage combined evaporative cooler provided a suitable relative humidity.
Riffat and Zhu [89,90]	Experiment and simulation	Enhancing the evaporative cooling performance	Wicked HP	Horizontal	[89]: - [90]: Distilled water	-	Y	Y	The cooling capacity of the IEC increased as the outdoor air velocity increased. However, it decreased as the outdoor air humidity increased. The indoor air temperature reduction was 3.8 °C per square meter of ceramic surface area for the room equipped with a chilled ceiling using the horizontal IEC.
Amer [91]	Experiment and simulation	Enhancing the evaporative cooling performance	Wicked HP	Vertical	Deionised water	-	Y	Y	The cooling capacity of the proposed IEC decreased with the decrease in the inlet air flowrate. In contrast, the wet bulb effectiveness and COP increased as the inlet air flowrate decreased.

Table 1. *Cont.*

References	Research Methods	Purpose	HP Types	Installation Direction	HP Working Fluid	Filling Ratio /Volume	Fins	Wick Structure	Core Conclusions
Boukhanouf et al. [92]	Experiment and simulation	Enhancing the evaporative cooling performance	Wicked HP	Vertical	Deionised water	-	Y	Y	When the inlet air flowrate was 150 m^3/s, the wet bulb effectiveness of the proposed system increased from 0.7 to 0.84 with the inlet air temperature increasing from 30 to 40 °C, meanwhile the in- and out-let temperature difference of the supply air increased from about 7.5 to 10.7 °C. An increase in relative humidity would also cause an increase in wet bulb efficiency, but the cooling capacity would be reduced.
Rajski et al. [93]	Simulation	Enhancing the evaporative cooling performance	GHP	Vertical	Deionised water	-	Y	N	The wet bulb effectiveness increased as the inlet air temperature and relative humidity increased. The pressure loss increased as the inlet air velocity increased.
Alharbi et al. [94]	Experiment and simulation	Enhancing the evaporative cooling performance	Wicked HP	Vertical	Deionised water	-	Y	Y	The cooling capacity increased as the inlet air temperature increased. However, it decreased with an increase in relative humidity.
Naphon [95]	Experiment	Enhancing the performance of the SAC	GHP	Vertical	R134a	50%	N	N	Compared with a conventional SAC, the proposed SAC coupling with the HP cooling device provided the highest COP and energy efficiency ratio (EER) with an increase of 6.4 and 17.5%, respectively.
Alklaibi [95]	Simulation	Enhancing the performance of the SAC	LHP	-	-	-	-	-	Both configurations had the same COP, and the COP could be improved by reducing the compressor energy demand when LHP was used instead of the heating component under a low sensible heat coefficient working condition.

Table 1. *Cont.*

References	Research Methods	Purpose	HP Types	Installation Direction	HP Working Fluid	Filling Ratio /Volume	Fins	Wick Structure	Core Conclusions
Nethaji and Tharves Mohideen [97]	Experiment	Enhancing the performance of the SAC	LHP	Horizontal	Ethanol	51%	N	-	Under the indoor temperature of 22–26 °C and relative humidity of 50%, they found that the COP of the SAC improved by 18–20%. The dehumidification capability was enhanced by 30%. The latent heat recovery was 482 W.
Eidan et al. [56]	Experiment	Enhancing the performance of the SAC	GHP	Vertical	Distilled water, acetone and R134a	50–100%	N	Y	The refrigeration effect was enhanced by 3.5, 6.03 and 3.97% for a 100% filling ratio of R134a, acetone, and water, compared to the window-type air conditioner without the HPHE. The consumed power saving of the window-type air conditioner with the HPHE were 2.01, 2.195 and 1.33% for water, acetone and R134a, respectively.
Xia et al. [98]	Experiment and simulation	Enhancing the performance of the SAC	-	Vertical	Water	-	Y	-	L-type HPHS was more advantageous in terms of thermal management and had average temperature reductions of 10.0 °C and 5.9 °C for small power chips and large power chips, respectively.
Nakkaew et al. [99]	Experiment	Enhancing the performance of the SAC	Wicked HP	Horizontal	Deionized water	1.21–1.31 cc	Y	Y	The maximum heat transfer rate obtained from the HPHE was about 240 W. The EER of the proposed SAC increased by about 3% and was fractionally higher than that of the traditional SAC.
Wu et al. [100]	Experiment	Air supply dehumidification	GHP	Vertical	R22	60%	Y	-	The relative humidity of the air stream passing through the condenser of the HPHE could be reduced to 70–74% from 92–100%. The heat recovery of 1920–2504.5 kJ/h was obtained. A cooling capability improvement by 20–32.7% was also discovered for the CC.

Table 1. *Cont.*

References	Research Methods	Purpose	HP Types	Installation Direction	HP Working Fluid	Filling Ratio /Volume	Fins	Wick Structure	Core Conclusions
Jouhara and Meskimmon [101,112]	Experiment	Air supply dehumidification	LHP	Horizontal	Water and R134a	-	Y	Y	The effectiveness of the HP decreased with the increase of the supply air velocity. The performance of the water HP was better than that of the R134a HP with an increase of about 18%.
Barrak et al. [102]	Experiment	Air supply dehumidification	PHP	Vertical	Distilled water, methanol and mixture fluid	50%	Y	N	The total energy saving was increased with the increase in the air velocity. The maximum total energy saving reached 1645, 1849 and 1932 W for water, mixture fluid and methanol, respectively.
Firouzfar et al. [103]	Experiment	Air supply dehumidification	GHP	Vertical	Methanol, methanol-silver nanofluid	50%	Y	N	The inlet relative humidity had a more significant effect on the sensible heat ratio HPHE using methanol-silver nanofluid had a better performance than that of using pure methanol.
Sarkar [114]	Simulation	Air supply dehumidification	-	Horizontal	-	-	-	-	Annual cooling energy savings of the proposed system were 1.5–19% for the six climate zones. The indoor temperature and relative humidity unmet hours were below 300.
Yau [104,105]	Experiment	Air supply dehumidification	GHP	Vertical	-	-	Y	N	The influence of the inlet dry bulb temperature on the sensible heat ratio was not so significant compared to the inlet relative humidity.
Ahmadzadehtalatapeh and Yau [24]	Experiment and simulation	Air supply dehumidification	-	Horizontal	-	-	Y	-	Performances of the ACS integrated with the HPHE were improved, and a considerable amount of energy and power was saved when the 8-row HPHE was used.
Yau and Ahmadzadehtalatapeh [107]	Experiment and simulation	Air supply dehumidification	Wicked HP	Horizontal	R134a	110%	Y	Y	The dehumidification of the CC coupled with the HPHE was improved by 6%. The payback period for the proposed system was about 1.9 years.

Table 1. *Cont.*

References	Research Methods	Purpose	HP Types	Installation Direction	HP Working Fluid	Filling Ratio /Volume	Fins	Wick Structure	Core Conclusions
Wan et al. [108]	Experiment	Air supply dehumidification	LHP	-	-	-	-	-	The cooling and total energy savings were 23.5–25.7% and 38.1–40.9%, respectively, in the room design temperature of 22–26.8 °C and relative humidity of 50% for the case office building.
Guo et al. [57]	Experiment	Air supply dehumidification	LHP	-	R134a	-	Y	-	The energy saving and the dehumidification capacity improvement were obvious for the ACS coupled with the PASHP.
Supirattanakul et al. [109]	Experiment	Air supply dehumidification	PHP	Vertical	R134a, R22 and R502	-	N	N	The highest peak value of the COP and EER of the proposed ACS were increased by 14.9% and 17.6%, respectively.
Kusumah et al. [110]	Experiment	Air supply dehumidification	Wicked HP	Vertical	Water	-	N	Y	HPHE performed best when a maximum number of HPs was achieved. The energy saving and the maximum effectiveness of the HPHE were 608.45 W and 7.64%, respectively.
Hakim et al. [111]	Experiment	Air supply dehumidification	Wicked HP	Vertical	Water	50%	Y	Y	The highest effectiveness of the two-row HPHE reached 12.4% under conditions of the inlet air speed of 1.5 m/s and inlet air temperature of 35 °C.
Li and Ju [113]	Experiment and simulation	Air supply dehumidification	LHP	Horizontal	R22	52–97%	Y	-	The sensible and total effectiveness increased with the increasing inlet air temperature and filling rate. However, these values would decrease when the inlet air temperature and filling rate exceeded 38 °C and 88%, respectively.
Noie-Baghban and Majideian [115]	Experiment and simulation	Waste heat recovery	Wicked HP	Vertical	Methanol, acetone and water	-	N	Y	Methanol had the larger merit compared to water and acetone. The maximum effectiveness of the HPHE was 0.16.
Jadhav and Lele [116]	Simulation	Waste heat recovery	-	-	-	-	-	-	The maximum energy saving potential was for hot and dry, warm and humid, and composite Indian climatic zones.

Table 1. *Cont.*

References	Research Methods	Purpose	HP Types	Installation Direction	HP Working Fluid	Filling Ratio /Volume	Fins	Wick Structure	Core Conclusions
Danielewicz et al. [117]	Experiment and simulation	Waste heat recovery	GHP	Vertical	Methanol	-	Y	N	The effectiveness and heat recovery of the HPHE increased with an increasing number of rows. The pressure loss of the HPHE increased with the increase in the inlet air speed. The effectiveness decreased with the increase in the inlet air speed.
Putra et al. [118]	Experiment	Waste heat recovery	THP	Vertical	Water	50%	Y	-	When the inlet air temperature and velocity were 45 °C and 2 m/s, the maximum heat recovery capacity of HPHE was 1404.29 kJ/h.
Muhamm-addiyah et al. [119]	Experiment	Waste heat recovery	Wicked HP	Vertical	Water	50%	Y	Y	The maximum effectiveness was approximately 54% under the conditions of minimum air speed and maximum air temperature.
Sukarno et al. [120–122]	Experiment	Waste heat recovery	Wicked HP	Vertical	Water	50%	Y	Y	The maximum effectiveness was over 60% under the conditions of air speed of 2 m/s and maximum air temperature. When the Reynold number increased, the Sp number increased. However, when the effectiveness increased, the Sp number had the opposite variation tendency.
Abd El-Baky and Mohamed [123]	Experiment	Waste heat recovery	Wicked HP	Horizontal	R134a	-	Y	Y	The effect of airflow rate on effectiveness had a little positive correlation for the evaporator section and a largely negative correlation for the condenser section. The maximum effectiveness and the enthalpy ratio were about 48 and 85%, respectively.
Abdelaziz et al. [124]	Experiment	Waste heat recovery	GHP	Horizontal	R123	-	Y	N	The energy consumption reduced by approximately 30% for the ACS coupled with the HPHE. The payback period of the proposed system was approximately 3 years.

Table 1. *Cont.*

References	Research Methods	Purpose	HP Types	Installation Direction	HP Working Fluid	Filling Ratio /Volume	Fins	Wick Structure	Core Conclusions
Mahajan et al. [125]	Experiment	Waste heat recovery	PHP	Vertical	n-pentane	0–70%	N	N	The effectiveness of 0.05 and the effective thermal resistance of 0.11 °C/W were obtained at a filling ratio of 70%.
Mahajan et al. [126]	Simulation	Waste heat recovery	PHP	Vertical	Acetone	-	Y	N	The effectiveness of the PHPHE reached 0.48. The total average annual energy consumption and running cost could be reduced by 16% and USD 700 for the proposed system in the commercial building.
Yang et al. [127]	Experiment	Waste heat recovery	PHP	Vertical	R134a	50%	N	N	An installation angle of 60 degree was a maximum value for the PHPHE. The recovery effectiveness of the PHPHE increased with the increasing inlet air temperature. However, it decreased with the increasing wind velocity.
Shen et al. [128]	Experiment	Waste heat recovery	FHP	Vertical	R600A	26%	Y	N	The heat transfer efficiency of the parallel-flow HPHE increased with the increasing airflow rate, while the thermal resistance decreased.
Liu et al. [129]	Experiment and simulation	Waste heat recovery	LHP	Horizontal	Water and methanol	-	Y	N	The length of the evaporator had almost no impact on the upper boundary but had a significant effect on the lower boundary. The operation ranges of the LHP varied with the working fluids.
Xue et al. [130]	Experiment	Waste heat recovery	LHP	Horizontal	R32 and R134a	40%	Y	N	The highest temperature effectiveness was 62 and 70% for winter and summer working conditions, respectively.
Zhou et al. [131,132]	Experiment	Waste heat recovery	LHP	Horizontal	R32, R22 and R152a	-	Y	N	The heat transfer capacity and COP of the PLHP heat recovery system increased with the indoor-outdoor temperature difference. However, the temperature effectiveness showed an opposite trend. PLHP performed better with R32 as the working fluid than with R22 and R152a.

Table 1. *Cont.*

References	Research Methods	Purpose	HP Types	Installation Direction	HP Working Fluid	Filling Ratio /Volume	Fins	Wick Structure	Core Conclusions
Liu et al. [133,134]	Experiment	Waste heat recovery	LHP	Horizontal	R32	-	Y	N	The CLHP heat recovery system performed better than that of PLHP and BLHP when the ambient temperature exceeded about 35 °C or was below 8 °C.
Ahmadzadeh-talatapeh and Yau [135], Yau [136]	Experiment and simulation	Air supply dehumidification and waste heat recovery	GHP	Vertical	-	-	Y	N	When the ACS was integrated with HPHE, the annual energy saving could reach to 27.48 MWh. The payback period of the ACS coupled with the HPHE was about 4 years.
Martínez et al. [137]	Experiment	Air supply dehumidification and waste heat recovery	Wicked HP	Horizontal	Ammonia	3.04 g	Y	Y	The heat recovery efficiency had a linear relationship with the outdoor temperature and airflow factors, and an extreme COP value 9.83 of the study system was obtained.
Wang et al. [138]	Experiment and simulation	Air supply dehumidification and waste heat recovery	Wicked HP	Horizontal	Ammonia	-	Y	Y	The average heat recovery efficiency of the proposed system was 21.08% and 39.2% in winter and summer, respectively. The energy saving advantage of the novel system was outstanding compared to the common heat recovery system.
Sun et al. [68]	Experiment	Design a cooling radiator	FHP	Vertical	Acetone	15%	Y	N	The FHP radiator had a speed start-up time with a value of 245–385 s. The cooling capacity of the FHP radiator varied from 40.1 W/m^2 to 75.8 W/m^2. Cold source temperature had an important impact on the thermal performance of the FHP radiator.
Wu et al. [139]	Experiment	Design a cooling radiator	FHP	Vertical	Acetone	20%	Y	N	The cooling radiator had a uniform surface temperature and a faster thermal response time with a value of about 360 s. The surface temperature and cooling capacity of the FHP simultaneously increased by 4–6 °C and 75.7%, respectively, under the force convection running strategy.

Table 1. *Cont.*

References	Research Methods	Purpose	HP Types	Installation Direction	HP Working Fluid	Filling Ratio /Volume	Fins	Wick Structure	Core Conclusions
Zhao et al. [140]	Experiment	Design a cooling radiator	FHP	Vertical	Acetone	20%	Y	N	When the cross flow fan was open and ran at the highest velocity, the cooling capacity was 2.24 times that of pure radiation mode. The indoor relative humidity could be controlled quickly.

4. Conclusions and Future Works

As a passive heat transfer device with a high effective thermal conductivity, an HP is widely used to enhance the performance of the ACS and improve the building's thermal environment. This paper focuses on summarizing the different HP types applied in the ACS and providing brief insight into the enhancement of ACS integrated with HP. The energy saving of the ACS coupled with HP is 3–40.9%. The payback period of this system ranges from 1.9–10 years. In addition, the major conclusions drawn from the present study are as follows.

(1) HP can start well at lower temperatures and store natural cold sources in water, ice, PCM and building envelope. When HP is embedded into the building envelope, it changes the heat transfer characteristics of traditional walls and effectively reduces the cooling and heating demands in the building.

(2) The evaporation cooling system is constrained by the surrounding wet bulb temperature. However, the supply air temperature can be handled below the dew point temperature when the evaporative cooling system is running with the HP. This means that the wet bulb efficiency will exceed 1.

(3) The energy saving of the SAC is 3–20% when the HP is installed on the indoor or outdoor unit of the SAC. The thermal environment of the room will also be improved by increasing the supply air temperature and decreasing the relative humidity of the supply air when the HP is installed in the indoor unit.

(4) When the HP is installed on the AHU, it can replace the conventional reheater and also have the function of heat recovery. The impacts of inlet air temperature and number of HP on the dehumidification and heat recovery of the ACS are positive, while the face velocity is negative.

(5) The cooling radiator integrated with the HP has a fast thermal response speed. And the surface temperature of the cooling radiator is relatively uniform.

The heat transfer characteristics of the HP are greatly affected by its structure, working fluid and external environmental conditions. Although the improvement in energy efficiency of the ACS by HPs has been confirmed, the improvement is very small under some operating conditions. Pressure loss is still an inevitable problem for HPHE. At present, there is already a considerable amount of literature focusing on the difference between the ACS coupled with and without the HP. However, there is little literature focusing on the building envelope cooling system integrated with the HP. The characteristics of these active and passive cooling systems need to be further studied. Moreover, the use of sustainable materials, such as nanofluid and graphene, will further improve the performance of the HP applied in the ACS. There is also a need to focus on more innovative ways and cheaper systems with respect to the improvement of the ACS integrated with HP. The performance of different HPs working in the same conditions has not been comprehensively analyzed. It is also necessary to improve the heat transfer performance of HPs at a low temperature to expand the application of the ACS waste heat and low-grade natural energies.

Author Contributions: Conceptualization, T.Y. and L.Z.; methodology, T.Y. and S.D.; formal analysis, T.Y. and L.Z.; data curation, S.D. and J.Z.; writing—original draft preparation, T.Y. and Z.L.; writing—review and editing, Z.L. and L.Z.; visualization, S.D.; supervision, J.Z.; project administration, L.Z.; funding acquisition, T.Y. All authors have read and agreed to the published version of the manuscript.

Funding: This work was funded by the Program of Science and Technology Research of Henan Province in China (232102320214) and the Plan Project of Housing and Urban Rural Construction Science and Technology of Henan Province in China (HNJS-2022-K58).

Data Availability Statement: Not available.

Conflicts of Interest: The authors declare no conflict of interest. The funders had no role in the design of the study; in the collection, analyses, or interpretation of data; in the writing of the manuscript; or in the decision to publish the results.

References

1. IEA. *Energy Technology Perspective 2017*; Catalysing Energy Technology Transformations: Paris, France, 2017.
2. Casals, X.G. Analysis of building energy regulation and certification in Europe: Their role, limitations and differences. *Energy Build.* **2006**, *38*, 381–392. [CrossRef]
3. Liu, Z.; Liu, Y.; He, B.-J.; Xu, W.; Jin, G.; Zhang, X. Application and suitability analysis of the key technologies in nearly zero energy buildings in China. *Renew. Sustain. Energy Rev.* **2019**, *101*, 329–345. [CrossRef]
4. Al-Shargabi, A.A.; Almhafdy, A.; Ibrahim, D.M.; Alghieth, M.; Chiclana, F. Buildings' energy consumption prediction models based on buildings' characteristics: Research trends, taxonomy, and performance measures. *J. Build. Eng.* **2022**, *54*, 104577. [CrossRef]
5. Yuan, T.; Ding, Y.; Zhang, Q.; Zhu, N.; Yang, K.; He, Q. Thermodynamic and economic analysis for ground-source heat pump system coupled with borehole free cooling. *Energy Build.* **2017**, *155*, 185–197. [CrossRef]
6. Solano, J.; Caamaño-Martín, E.; Olivieri, L.; Almeida-Galárraga, D. HVAC systems and thermal comfort in buildings climate control: An experimental case study. *Energy Rep.* **2021**, *7*, 269–277. [CrossRef]
7. Zhang, Z.; Zhang, Y.; Khan, A. Thermal comfort of people in a super high-rise building with central air-conditioning system in the hot-humid area of China. *Energy Build.* **2020**, *209*, 109727. [CrossRef]
8. Kokogiannakis, G.; Daly, D.; McDowell, C.; Roth, J.; Tibbs, M.; Cooper, P. In-situ comparison between the energy performance of an in-slab gas heating system and a split system air conditioning in classrooms. *Energy Build.* **2023**, *279*, 112713. [CrossRef]
9. Yang, H.; Pei, N.; Liu, L.; Fan, M.; Qin, Y. Experimental study on the effect of condensate water on the performance of split air conditioning system. *Energy Rep.* **2021**, *7*, 840–851. [CrossRef]
10. Yau, Y.; Pean, H. The performance study of a split type air conditioning system in the tropics, as affected by weather. *Energy Build.* **2014**, *72*, 1–7. [CrossRef]
11. Deng, X.; Shen, Y.; Yang, S.; Feng, J.; Wang, S.; Li, D.; Li, Y. Feasibility of condensate water recycle of split air handling unit in Chinese University buildings. *Energy Built Environ.* **2022**, *5*, 309–315. [CrossRef]
12. Li, X.; Zhang, C.; Zhao, T.; Han, Z. Adaptive predictive control method for improving control stability of air-conditioning terminal in public buildings. *Energy Build.* **2021**, *249*, 111261. [CrossRef]
13. Zhou, F.; Liu, Y.; Zhao, Y.; Ma, G. Dehumidifying characteristics of air conditioner with reheating coil under mild and humid conditions. *Appl. Therm. Eng.* **2021**, *196*, 117338. [CrossRef]
14. Shafieian, A.; Khiadani, M. A multipurpose desalination, cooling, and air-conditioning system powered by waste heat recovery from diesel exhaust fumes and cooling water. *Case Stud. Therm. Eng.* **2020**, *21*, 100702. [CrossRef]
15. Filipsson, P.; Trüschel, A.; Gräslund, J.; Dalenbäck, J.-O. Performance evaluation of a direct ground-coupled self-regulating active chilled beam system. *Energy Build.* **2020**, *209*, 109691. [CrossRef]
16. Arumugam, P.; Ramalingam, V.; Vellaichamy, P. Effective PCM, insulation, natural and/or night ventilation techniques to enhance the thermal performance of buildings located in various climates—A review. *Energy Build.* **2022**, *258*, 111840. [CrossRef]
17. Vidrih, B.; Arkar, C.; Medved, S. Generalized model-based predictive weather control for the control of free cooling by enhanced night-time ventilation. *Appl. Energy* **2016**, *168*, 482–492. [CrossRef]
18. Aili, A.; Zhao, D.; Lu, J.; Zhai, Y.; Yin, X.; Tan, G.; Yang, R. A kW-scale, 24-hour continuously operational, radiative sky cooling system: Experimental demonstration and predictive modeling. *Energy Convers. Manag.* **2019**, *186*, 586–596. [CrossRef]
19. Jia, L.; Lu, L.; Chen, J.; Han, J. A novel radiative sky cooling-assisted ground-coupled heat exchanger system to improve thermal and energy efficiency for buildings in hot and humid regions. *Appl. Energy* **2022**, *322*, 119422. [CrossRef]
20. Gratia, E.; Bruyere, I.; De Herde, A. How to use natural ventilation to cool narrow office buildings. *Build. Environ.* **2004**, *39*, 1157–1170. [CrossRef]
21. Nwaji, G.; Okoronkwo, C.; Ogueke, N.; Anyanwu, E. Hybrid solar water heating/nocturnal radiation cooling system I: A review of the progress, prospects and challenges. *Energy Build.* **2019**, *198*, 412–430. [CrossRef]

22. Delgado, M.G.; Ramos, J.S.; Domínguez, S. Using the sky as heat sink: Climatic applicability of night-sky based natural cooling techniques in Europe. *Energy Convers. Manag.* **2020**, *225*, 113424. [CrossRef]
23. Shuxue, X.; Jianhui, N.; Hongxia, M.; Guoyuan, M. Cooling and dehumidification performance study of a new air conditioning system with double evaporation temperature. *Energy Build.* **2023**, *295*, 113294. [CrossRef]
24. Ahmadzadehtalatapeh, M.; Yau, Y. The application of heat pipe heat exchangers to improve the air quality and reduce the energy consumption of the air conditioning system in a hospital ward—A full year model simulation. *Energy Build.* **2011**, *43*, 2344–2355. [CrossRef]
25. Korpela, T.; Kuosa, M.; Sarvelainen, H.; Tuliniemi, E.; Kiviranta, P.; Tallinen, K.; Koponen, H.K. Waste heat recovery potential in residential apartment buildings in Finland's Kymenlaakso region by using mechanical exhaust air ventilation and heat pumps. *Int. J. Thermofluids* **2022**, *13*, 100127. [CrossRef]
26. Hesaraki, A.; Huda, N. A comparative review on the application of radiant low-temperature heating and high-temperature cooling for energy, thermal comfort, indoor air quality, design and control. *Sustain. Energy Technol. Assess.* **2022**, *49*, 101661. [CrossRef]
27. Liao, W.; Luo, Y.; Peng, J.; Wang, D.; Yuan, C.; Yin, R.; Li, N. Experimental study on energy consumption and thermal environment of radiant ceiling heating system for different types of rooms. *Energy* **2022**, *244*, 122555. [CrossRef]
28. González-Cruz, E.M.; Krüger, E.L. Experimental study on a low energy radiant-capacitive heating and cooling system. *Energy Build.* **2022**, *255*, 111674. [CrossRef]
29. Chen, Y.; Wang, D.; Liu, Y.; Wang, Y.; Liu, Y. Experimental investigation on the thermal performance of an enhanced convection-radiant heating wall panel with orifices. *Int. J. Therm. Sci.* **2022**, *181*, 107704. [CrossRef]
30. Anand, R.; Jawahar, C.; Solomon, A.B.; Bellos, E. A review of experimental studies on cylindrical two-phase closed thermosyphon using refrigerant for low-temperature applications. *Int. J. Refrig.* **2020**, *120*, 296–313. [CrossRef]
31. Qian, N.; Marengo, M.; Chen, J.; Fu, Y.; Zhang, J.; Xu, J. Heat transfer and temperature characteristics of single-loop oscillating heat pipe under axial-rotation conditions. *Int. J. Heat Mass Transf.* **2022**, *197*, 123308. [CrossRef]
32. Xu, Q.; Yang, G.; Wang, C.; Liu, Z.; Zhang, X.; Li, Z.; Lohani, S.P.; Zhao, Y.; Xiong, Y.; Ding, Y. Experimental study on the reinforcement of a gravity heat pipe based on a latent thermal functionally fluid. *Energy* **2023**, *278*, 127782. [CrossRef]
33. Maydanik, Y.F. Loop heat pipes. *Appl. Therm. Eng.* **2005**, *25*, 635–657. [CrossRef]
34. Zhao, Y.H.; Zhang, K.R.; Diao, Y.H. Heat Pipe with Micro-Pore Tubes Array and Making Method Thereof and Heat Exchanging System. U.S. Patent, US20110203777 A1, 25 August 2011.
35. Jouhara, H.; Bertrand, D.; Axcell, B.; Montorsi, L.; Venturelli, M.; Almahmoud, S.; Milani, M.; Ahmad, L.; Chauhan, A. Investigation on a full-scale heat pipe heat exchanger in the ceramics industry for waste heat recovery. *Energy* **2021**, *223*, 120037. [CrossRef]
36. Deng, Z.; Zheng, Y.; Liu, X.; Zhu, B.; Chen, Y. Experimental study on thermal performance of an anti-gravity pulsating heat pipe and its application on heat recovery utilization. *Appl. Therm. Eng.* **2017**, *125*, 1368–1378. [CrossRef]
37. Liu, X.; Han, X.; Wang, Z.; Hao, G.; Zhang, Z.; Chen, Y. Application of an anti-gravity oscillating heat pipe on enhancement of waste heat recovery. *Energy Convers. Manag.* **2020**, *205*, 112404. [CrossRef]
38. Abdelkareem, M.A.; Maghrabie, H.M.; Sayed, E.T.; Kais, E.-C.A.; Abo-Khalil, A.G.; Al Radi, M.; Baroutaji, A.; Olabi, A. Heat pipe-based waste heat recovery systems: Background and applications. *Therm. Sci. Eng. Prog.* **2022**, *29*, 101221. [CrossRef]
39. Veerasamy, A.; Balakrishnan, K.; Razack, S.A. Performance of heat pipe with nanorefrigerant in electronic cooling applications. *Mater. Today Proc.* **2022**, *65*, 375–379. [CrossRef]
40. Chen, A.; Jiang, F.; Dong, J.; Chen, J.; Zhu, Y. Design, fabrication and thermal performance of a novel ultra-thin loop heat pipe with printed wick structure for mobile electronics cooling. *Appl. Therm. Eng.* **2022**, *200*, 117683. [CrossRef]
41. Phan, N.; Nagano, H. Novel hybrid structures to improve performance of miniature flat evaporator loop heat pipes for electronics cooling. *Int. J. Heat Mass Transf.* **2022**, *195*, 123187. [CrossRef]
42. Gudeta, M.S.; Atnaw, S.M.; Shibeshi, M.; Gardie, E. Performance analysis of solar water heater system with heat pipe evacuated tube collector on Moha soft drink industries in Ethiopia. *Case Stud. Therm. Eng.* **2022**, *36*, 102211. [CrossRef]
43. Li, H.; Liu, H.; Li, M. Review on heat pipe based solar collectors: Classifications, performance evaluation and optimization, and effectiveness improvements. *Energy* **2022**, *244*, 122582. [CrossRef]
44. Tamuli, B.R.; Nath, S.; Bhanja, D. Performance enhancement of a dual heat pipe array based evacuated tube solar water heater for north eastern India climatic condition: A numerical approach. *Appl. Therm. Eng.* **2022**, *213*, 118597. [CrossRef]
45. Wang, Z.; Diao, Y.; Liang, L.; Zhao, Y.; Zhu, T.; Bai, F. Experimental study on an integrated collector storage solar air heater based on flat micro-heat pipe arrays. *Energy Build.* **2017**, *152*, 615–628. [CrossRef]
46. Li, H.; Sun, Y. Operational performance study on a photovoltaic loop heat pipe/solar assisted heat pump water heating system. *Energy Build.* **2018**, *158*, 861–872. [CrossRef]
47. Wang, G.; Yang, Y.; Yu, W.; Wang, T.; Zhu, T. Performance of an air-cooled photovoltaic/thermal system using micro heat pipe array. *Appl. Therm. Eng.* **2022**, *217*, 119184. [CrossRef]
48. Song, Z.; Ji, J.; Li, Z. Comparison analyses of three photovoltaic solar-assisted heat pumps based on different concentrators. *Energy Build.* **2021**, *251*, 111348. [CrossRef]
49. Zhao, Y.; Fan, Y.; Li, W.; Li, Y.; Ge, M.; Xie, L. Experimental investigation of heat pipe thermoelectric generator. *Energy Convers. Manag.* **2022**, *252*, 115123. [CrossRef]

50. Sun, X.; Ling, L.; Liao, S.; Chu, Y.; Fan, S.; Mo, Y. A thermoelectric cooler coupled with a gravity-assisted heat pipe: An analysis from heat pipe perspective. *Energy Convers. Manag.* **2018**, *155*, 230–242. [CrossRef]
51. Liu, Z.; Cheng, K.; Wang, Z.; Wang, Y.; Ha, C.; Qin, J. Performance analysis of the heat pipe-based thermoelectric generator (HP-TEG) energy system using in-situ resource for heat storage applied to the early-period lunar base. *Appl. Therm. Eng.* **2023**, *218*, 119303. [CrossRef]
52. Wang, X.; Wen, Q.; Yang, J.; Xiang, J.; Wang, Z.; Weng, C.; Chen, F.; Zheng, S. A review on data centre cooling system using heat pipe technology. *Sustain. Comput. Informatics Syst.* **2022**, *35*, 100774. [CrossRef]
53. Sun, Y.; Wang, T.; Yang, L.; Hu, L.; Zeng, X. Research of an integrated cooling system consisted of compression refrigeration and pump-driven heat pipe for data centers. *Energy Build.* **2019**, *187*, 16–23. [CrossRef]
54. He, Z.; Xi, H.; Ding, T.; Wang, J.; Li, Z. Energy efficiency optimization of an integrated heat pipe cooling system in data center based on genetic algorithm. *Appl. Therm. Eng.* **2021**, *182*, 115800. [CrossRef]
55. Chaudhry, H.N.; Hughes, B.R.; Ghani, S.A. A review of heat pipe systems for heat recovery and renewable energy applications. *Renew. Sustain. Energy Rev.* **2012**, *16*, 2249–2259. [CrossRef]
56. Eidan, A.A.; Alshukri, M.J.; Al-Fahham, M.; AlSahlani, A.; Abdulridha, D.M. Optimizing the performance of the air conditioning system using an innovative heat pipe heat exchanger. *Case Stud. Therm. Eng.* **2021**, *26*, 101075. [CrossRef]
57. Guo, Z.; Shao, J.; Li, X.; Liu, R.; Wang, W.; Tian, X. Application of pump-assisted separate heat pipe on dehumidifying enhancement in air conditioning system. *Appl. Therm. Eng.* **2016**, *98*, 374–379. [CrossRef]
58. Wang, Y.; Wang, X.; Wang, J.; Liu, Y.; Chen, J. Heat transfer performance of a two-phase closed thermosyphon with different inclination angles based on the core-tube monitoring. *Case Stud. Therm. Eng.* **2023**, *42*, 102738. [CrossRef]
59. Kafeel, K.; Turan, A. Simulation of the response of a thermosyphon under pulsed heat input conditions. *Int. J. Therm. Sci.* **2014**, *80*, 33–40. [CrossRef]
60. Jose, J.; Hotta, T.K. A comprehensive review of heat pipe: Its types, incorporation techniques, methods of analysis and applications. *Therm. Sci. Eng. Prog.* **2023**, *42*, 101860. [CrossRef]
61. Zhang, J.; Song, G.; Qiu, Z.; Li, H. Thermal analysis and effects study of evaporator exit vapor quality in a separate heat pipe. *Appl. Therm. Eng.* **2020**, *181*, 115716. [CrossRef]
62. Deng, W.; Wang, X.; Ye, Q.; Zhao, H.; Xu, J. Development of the double two-phase thermosyphon loops used in low temperature Stirling refrigerator. *Int. J. Refrig.* **2023**, *155*, 173–183. [CrossRef]
63. Li, C.; Liu, Z.; Zhang, X. Steady-state operating characteristics analysis of loop heat pipes with flat-plate evaporator. *Therm. Sci. Eng. Prog.* **2022**, *28*, 101070. [CrossRef]
64. Bai, L.; Guo, J.; Lin, G.; He, J.; Wen, D. Steady-state modeling and analysis of a loop heat pipe under gravity-assisted operation. *Appl. Therm. Eng.* **2015**, *83*, 88–97. [CrossRef]
65. Akachi, H. Structure of a Heat Pipe. U.S. Patent 4,921,041, 1 May 1990.
66. Feng, C.; Wan, Z.; Mo, H.; Tang, H.; Lu, L.; Tang, Y. Heat transfer characteristics of a novel closed-loop pulsating heat pipe with a check valve. *Appl. Therm. Eng.* **2018**, *141*, 558–564. [CrossRef]
67. Ando, M.; Okamoto, A.; Nagai, H. Start-up and heat transfer characteristics of oscillating heat pipe with different check valve layouts. *Appl. Therm. Eng.* **2021**, *196*, 117286. [CrossRef]
68. Sun, H.; Wu, Y.; Lin, B.; Duan, M.; Lin, Z.; Li, H. Experimental investigation on the thermal performance of a novel radiant heating and cooling terminal integrated with a flat heat pipe. *Energy Build.* **2020**, *208*, 109646. [CrossRef]
69. Saw, L.; Yew, M.; Chong, W.; Poon, H.; Liew, W.; Yeo, W. Development of the closed loop pulsating heat pipe cool roof system for residential buildings. *Case Stud. Therm. Eng.* **2021**, *28*, 101487. [CrossRef]
70. Li, Z.; Zhang, Z. Dynamic heat transfer characteristics of wall implanted with heat pipes in summer. *Energy Build.* **2018**, *170*, 40–46. [CrossRef]
71. Turnpenny, J.; Etheridge, D.; Reay, D. Novel ventilation cooling system for reducing air conditioning in buildings.: Part I: Testing and theoretical modelling. *Appl. Therm. Eng.* **2000**, *20*, 1019–1037. [CrossRef]
72. Singh, R.; Mochizuki, M.; Mashiko, K.; Nguyen, T. Heat pipe based cold energy storage systems for datacenter energy conservation. *Energy* **2011**, *36*, 2802–2811. [CrossRef]
73. Yan, C.; Shi, W.; Li, X.; Wang, S. A seasonal cold storage system based on separate type heat pipe for sustainable building cooling. *Renew. Energy* **2016**, *85*, 880–889. [CrossRef]
74. Chotivisarut, N.; Nuntaphan, A.; Kiatsiriroat, T. Seasonal cooling load reduction of building by thermosyphon heat pipe radiator in different climate areas. *Renew. Energy* **2012**, *38*, 188–194. [CrossRef]
75. Chotivisarut, N.; Kiatsiriroat, T. Cooling load reduction of building by seasonal nocturnal cooling water from thermosyphon heat pipe radiator. *Int. J. Energy Res.* **2009**, *33*, 1089–1098. [CrossRef]
76. He, W.; Yu, C.; Yang, J.; Yu, B.; Hu, Z.; Shen, D.; Liu, X.; Qin, M.; Chen, H. Experimental study on the performance of a novel RC-PCM-wall. *Energy Build.* **2019**, *199*, 297–310. [CrossRef]
77. Yu, C.; Shen, D.; He, W.; Hu, Z.; Zhang, S.; Chu, W. Parametric analysis of the phase change material wall combining with micro-channel heat pipe and sky radiative cooling technology. *Renew. Energy* **2021**, *178*, 1057–1069. [CrossRef]
78. Yu, C.; Shen, D.; Wang, W.; Song, X.; Xin, J.; Cai, L.; Tu, J. Numerical study on the thermal performance of phase change materials wall by radiative cooling. *Appl. Therm. Eng.* **2022**, *215*, 119013. [CrossRef]

79. Shen, D.; Yu, C.; Wang, W. Investigation on the thermal performance of the novel phase change materials wall with radiative cooling. *Appl. Therm. Eng.* **2020**, *176*, 115479. [CrossRef]
80. Yan, T.; Li, J.; Gao, J.; Xu, X.; Yu, J. Model validation and application of the coupled system of pipe-encapsulated PCM wall and nocturnal sky radiator. *Appl. Therm. Eng.* **2021**, *194*, 117057. [CrossRef]
81. Yan, T.; Zhou, X.; Xu, X.; Yu, J.; Li, X. Parametric analysis on performances of the pipe-encapsulated PCM (PenPCM) wall system coupled with gravity heat-pipe and nocturnal radiant cooler. *Renew. Energy* **2022**, *196*, 161–180. [CrossRef]
82. Yan, T.; Luo, Y.; Xu, T.; Wu, H.; Xu, X.; Li, J. Experimental study of the coupled wall system of pipe-encapsulated PCM wall and nocturnal sky radiator for self-activated heat removal. *Energy Build.* **2021**, *241*, 110964. [CrossRef]
83. Yan, T.; Sun, Z.; Gao, J.; Xu, X.; Yu, J.; Gang, W. Simulation study of a pipe-encapsulated PCM wall system with self-activated heat removal by nocturnal sky radiation. *Renew. Energy* **2020**, *146*, 1451–1464. [CrossRef]
84. Yan, T.; Gao, J.; Xu, X.; Xu, T.; Ling, Z.; Yu, J. Dynamic simplified PCM models for the pipe-encapsulated PCM wall system for self-activated heat removal. *Int. J. Therm. Sci.* **2019**, *144*, 27–41. [CrossRef]
85. Amer, O.; Boukhanouf, R.; Ibrahim, H.G. A review of evaporative cooling technologies. *Int. J. Environ. Sci. Dev.* **2015**, *6*, 111–117. [CrossRef]
86. Abdullah, S.; Zubir, M.N.B.M.; Bin Muhamad, M.R.; Newaz, K.M.S.; Öztop, H.F.; Alam, S.; Shaikh, K. Technological development of evaporative cooling systems and its integration with air dehumidification processes: A review. *Energy Build.* **2023**, *283*, 112805. [CrossRef]
87. Fikri, B.; Putra NS, D.; Winarta, A.; AAbdullah, N.; Ariantara, B. Experimental investigation of modified direct evaporative cooler using heat pipe. *J. Adv. Res. Fluid Mech. Therm. Sci.* **2019**, *55*, 209–217.
88. Fikri, B.; Sofia, E.; Putra, N. Experimental analysis of a multistage direct-indirect evaporative cooler using a straight heat pipe. *Appl. Therm. Eng.* **2020**, *171*, 115133. [CrossRef]
89. Riffat, S.; Zhu, J. Mathematical model of indirect evaporative cooler using porous ceramic and heat pipe. *Appl. Therm. Eng.* **2004**, *24*, 457–470. [CrossRef]
90. Riffat, S.; Zhu, J. Experimental Investigation of an Indirect Evaporative Cooler Consisting of a Heat Pipe Embedded in Porous Ceramic. *J. Eng. Res.* **2004**, *1*, 46–52. [CrossRef]
91. Amer, O. A Heat Pipe and Porous Ceramic Based Sub Wet-Bulb Temperature Evaporative Cooler: A Theoretical and Experimental Study. Ph.D. Thesis, University of Nottingham, Nottingham, UK, 2017.
92. Boukhanouf, R.; Amer, O.; Ibrahim, H.; Calautit, J. Design and performance analysis of a regenerative evaporative cooler for cooling of buildings in arid climates. *J. Affect. Disord.* **2018**, *142*, 1–10. [CrossRef]
93. Rajski, K.; Danielewicz, J.; Brychcy, E. Performance Evaluation of a Gravity-Assisted Heat Pipe-Based Indirect Evaporative Cooler. *Energies* **2020**, *13*, 200. [CrossRef]
94. Alharbi, A.; Almaneea, A.; Boukhanouf, R. Integrated hollow porous ceramic cuboids-finned heat pipes evaporative cooling system: Numerical modelling and experimental validation. *Energy Build.* **2019**, *196*, 61–70. [CrossRef]
95. Naphon, P. On the performance of air conditioner with heat pipe for cooling air in the condenser. *Energy Convers. Manag.* **2010**, *51*, 2362–2366. [CrossRef]
96. Alklaibi, A. Evaluating the possible configurations of incorporating the loop heat pipe into the air-conditioning systems. *Int. J. Refrig.* **2008**, *31*, 807–815. [CrossRef]
97. Nethaji, N.; Mohideen, S.T. Energy conservation studies on a split air conditioner using loop heat pipes. *Energy Build.* **2017**, *155*, 215–224. [CrossRef]
98. Xia, G.; Zhuang, D.; Ding, G. Thermal management solution for enclosed controller used in inverter air conditioner based on heat pipe heat sink. *Int. J. Refrig.* **2019**, *99*, 69–79. [CrossRef]
99. Nakkaew, S.; Chitipalungsri, T.; Ahn, H.S.; Jerng, D.-W.; Asirvatham, L.G.; Dalkılıç, A.S.; Mahian, O.; Wongwises, S. Application of the heat pipe to enhance the performance of the vapor compression refrigeration system. *Case Stud. Therm. Eng.* **2019**, *15*, 100531. [CrossRef]
100. Wu, X.P.; Johnson, P.; Akbarzadeh, A. Application of heat pipe heat exchangers to humidity control in air-conditioning systems. *Appl. Therm. Eng.* **1997**, *17*, 561–568. [CrossRef]
101. Jouhara, H.; Meskimmon, R. An investigation into the use of water as a working fluid in wraparound loop heat pipe heat exchanger for applications in energy efficient HVAC systems. *Energy* **2018**, *156*, 597–605. [CrossRef]
102. Barrak, A.S.; Saleh, A.A.; Naji, Z.H. An experimental study of using water, methanol, and binary fluids in oscillating heat pipe heat exchanger. *Eng. Sci. Technol. Int. J.* **2020**, *23*, 357–364. [CrossRef]
103. Firouzfar, E.; Soltanieh, M.; Noie, S.H.; Saidi, M.H. Investigation of heat pipe heat exchanger effectiveness and energy saving in air conditioning systems using silver nanofluid. *Int. J. Environ. Sci. Technol.* **2012**, *9*, 587–594. [CrossRef]
104. Yau, Y.H. Application of a heat pipe heat exchanger to dehumidification enhancement in a HVAC system for tropical climates—A baseline performance characteristics study. *Int. J. Therm. Sci.* **2007**, *46*, 164–171. [CrossRef]
105. Yau, Y. Experimental thermal performance study of an inclined heat pipe heat exchanger operating in high humid tropical HVAC systems. *Int. J. Refrig.* **2007**, *30*, 1143–1152. [CrossRef]
106. Yau, Y.; Ahmadzadehtalatapeh, M. A review on the application of horizontal heat pipe heat exchangers in air conditioning systems in the tropics. *Appl. Therm. Eng.* **2010**, *30*, 77–84. [CrossRef]

107. Yau, Y.H.; Ahmadzadehtalatapeh, M. Predicting yearly energy recovery and dehumidification enhancement with a heat pipe heat exchanger using typical meteorological year data in the tropics. *J. Mech. Sci. Technol.* **2011**, *25*, 847–853. [CrossRef]
108. Wan, J.; Zhang, J.; Zhang, W. The effect of heat-pipe air-handling coil on energy consumption in central air-conditioning system. *Energy Build.* **2007**, *39*, 1035–1040. [CrossRef]
109. Supirattanakul, P.; Rittidech, S.; Bubphachot, B. Application of a closed-loop oscillating heat pipe with check valves (CLOHP/CV) on performance enhancement in air conditioning system. *Energy Build.* **2011**, *43*, 1531–1535. [CrossRef]
110. Kusumah, A.S.; Hakim, I.I.; Sukarno, R.; Rachman, F.F.; Putra, N. The Application of U-shape Heat Pipe Heat Exchanger to Reduce Relative Humidity for Energy Conservation in Heating, Ventilation, and Air Conditioning (HVAC) Systems. *Int. J. Technol.* **2019**, *10*, 1202–1210. [CrossRef]
111. Hakim, I.I.; Sukarno, R.; Putra, N. Utilization of U-shaped finned heat pipe heat exchanger in energy-efficient HVAC systems. *Therm. Sci. Eng. Prog.* **2021**, *25*, 100984. [CrossRef]
112. Jouhara, H.; Meskimmon, R. Experimental investigation of wraparound loop heat pipe heat exchanger used in energy efficient air handling units. *Energy* **2010**, *35*, 4592–4599. [CrossRef]
113. Li, M.; Ju, Y. Experimental investigation on the thermal performance of wraparound loop heat pipe heat exchanger for heat recovery in air handling units. *Heat Transf. Res.* **2017**, *48*, 1313–1326. [CrossRef]
114. Sarkar, M. On Climatic Control of Wrap-Around Heat Pipe (WAHP) Enhanced Dehumidifier in Outdoor Air Systems. *Int. J. Air-Cond. Refrig.* **2019**, *27*, 1950013. [CrossRef]
115. Noie-Baghban, S.H.; Majideian, G.R. Waste heat recovery using heat pipe heat exchanger (HPHE) for surgery rooms in hospitals. *Appl. Therm. Eng.* **2000**, *20*, 1271–1282. [CrossRef]
116. Jadhav, T.; Lele, M. Theoretical energy saving analysis of air conditioning system using heat pipe heat exchanger for Indian climatic zones. *Eng. Sci. Technol. Int. J.* **2015**, *18*, 669–673. [CrossRef]
117. Danielewicz, J.; Sayegh, M.; Śniechowska, B.; Szulgowska-Zgrzywa, M.; Jouhara, H. Experimental and analytical performance investigation of air to air two phase closed thermosyphon based heat exchangers. *Energy* **2014**, *77*, 82–87. [CrossRef]
118. Putra, N.S.D.; Anggoro, T.; Winarta, A. Experimental Study of Heat Pipe Heat Exchanger in Hospital HVAC System for Energy Conservation. *Int. J. Adv. Sci. Eng. Inf. Technol.* **2017**, *7*, 871. [CrossRef]
119. Muhammaddiyah, S.; Winarta, A.; Putra, N. Experimental Study of Heat Pipe Heat Exchanger Multi Fin for Energy Efficiency Effort in Operating Room Air System. *Int. J. Technol.* **2018**, *9*, 422–429. [CrossRef]
120. Sukarno, R.; Putra, N.; Hakim, I.I.; Rachman, F.F.; Mahlia, T.M.I. Utilizing heat pipe heat exchanger to reduce the energy consumption of airborne infection isolation hospital room HVAC system. *J. Build. Eng.* **2021**, *35*, 102116. [CrossRef]
121. Sukarno, R.; Putra, N.; Hakim, I.I.; Rachman, F.F.; Mahlia, T.M.I. Multi-stage heat-pipe heat exchanger for improving energy efficiency of the HVAC system in a hospital operating room 1. *Int. J. Low-Carbon Technol.* **2021**, *16*, 259–267. [CrossRef]
122. Sukarno, R.; Putra, N.; Hakim, I.I. Non-dimensional analysis for heat pipe characteristics in the heat pipe heat exchanger as energy recovery device in the HVAC systems. *Therm. Sci. Eng. Prog.* **2021**, *26*, 101122. [CrossRef]
123. Abd El-Baky, M.A.; Mohamed, M.M. Heat pipe heat exchanger for heat recovery in air conditioning. *Appl. Therm. Eng.* **2007**, *27*, 795–801. [CrossRef]
124. Abdelaziz, G.B.; Abdelbaky, M.; Halim, M.; Omara, M.; Elkhaldy, I.; Abdullah, A.; Omara, Z.; Essa, F.; Ali, A.; Sharshir, S.W.; et al. Energy saving via Heat Pipe Heat Exchanger in air conditioning applications "experimental study and economic analysis". *J. Build. Eng.* **2021**, *35*, 102053. [CrossRef]
125. Mahajan, G.; Thompson, S.M.; Cho, H. Experimental characterization of an n-pentane oscillating heat pipe for waste heat recovery in ventilation systems. *Heliyon* **2018**, *4*, e00922. [CrossRef] [PubMed]
126. Mahajan, G.; Thompson, S.M.; Cho, H. Energy and cost savings potential of oscillating heat pipes for waste heat recovery ventilation. *Energy Rep.* **2017**, *3*, 46–53. [CrossRef]
127. Yang, H.; Wang, J.; Wang, N.; Yang, F. Experimental study on a pulsating heat pipe heat exchanger for energy saving in air-conditioning system in summer. *Energy Build.* **2019**, *197*, 1–6. [CrossRef]
128. Shen, C.; Zhang, B.; Zhang, D.; Zhang, Y.; Wei, S.; Yang, S. Experimental study on the parallel-flow heat pipe heat exchanger for energy saving in air conditioning. *J. Build. Eng.* **2023**, *75*, 106842. [CrossRef]
129. Liu, D.; Tang, G.-F.; Zhao, F.-Y.; Wang, H.-Q. Modeling and experimental investigation of looped separate heat pipe as waste heat recovery facility. *Appl. Therm. Eng.* **2006**, *26*, 2433–2441. [CrossRef]
130. Xue, L.; Ma, G.; Zhou, F.; Wang, L. Operation characteristics of air–air heat pipe inserted plate heat exchanger for heat recovery. *Energy Build.* **2019**, *185*, 66–75. [CrossRef]
131. Zhou, F.; Duan, W.; Ma, G. Thermal performance of a pump-driven loop heat pipe as an air-to-air energy recovery device. *Energy Build.* **2017**, *151*, 206–216. [CrossRef]
132. Zhou, F.; Duan, W.; Ma, G. Thermal performance of a multi-loop pump-driven heat pipe as an energy recovery ventilator for buildings. *Appl. Therm. Eng.* **2018**, *138*, 648–656. [CrossRef]
133. Liu, S.; Ma, G.; Xu, S.; Jia, X.; Wu, G. Experimental study of ventilation system with heat recovery integrated by pump-driven loop heat pipe and heat pump. *J. Build. Eng.* **2022**, *52*, 104404. [CrossRef]
134. Shuailing, L.; Guoyuan, M.; Xiaoya, J.; Shuxue, X.; Guoqiang, W. Performance of a mechanically-driven loop heat pipe heat recovery system. *Appl. Therm. Eng.* **2022**, *207*, 118066. [CrossRef]

135. Ahmadzadehtalatapeh, M.; Yat Huang, Y. Fully fresh air air-conditioning system equipped with double heat pipe based heat recovery technology. *Int. J. Eng.* **2013**, *26*, 51–57. [CrossRef]
136. Yau, Y. The use of a double heat pipe heat exchanger system for reducing energy consumption of treating ventilation air in an operating theatre—A full year energy consumption model simulation. *Energy Build.* **2008**, *40*, 917–925. [CrossRef]
137. Martinez, F.J.R.; Plasencia, M.A.-G.; Gómez, E.V.; Diez, F.V.; Martin, R.H. Design and experimental study of a mixed energy recovery system, heat pipes and indirect evaporative equipment for air conditioning. *Energy Build.* **2003**, *35*, 1021–1030. [CrossRef]
138. Wang, H.; Zhou, S.; Wei, Z.; Wang, R. A study of secondary heat recovery efficiency of a heat pipe heat exchanger air conditioning system. *Energy Build.* **2016**, *133*, 206–216. [CrossRef]
139. Wu, Y.; Sun, H.; Duan, M.; Lin, B.; Zhao, H. Dehumidification-adjustable cooling of radiant cooling terminals based on a flat heat pipe. *J. Affect. Disord.* **2021**, *194*, 107716. [CrossRef]
140. Zhao, H.; Wu, Y.; Lin, B.; Sun, H. Experimental investigation on the improvement of cooling and dehumidification of a direct-expansion terminal integrated with flat heat pipe. *Energy Build.* **2022**, *260*, 111922. [CrossRef]